A PRACTICAL BURN RATE ANALYSIS FOR USE IN ENGINE DEVELOPMENT AND DESIGN

by

Hon Man Cheung

Bachelor of Science in Mechanical Engineering
Columbia University
School of Engineering and Applied Science
(1991)

Submitted to the
Department of Mechanical Engineering
in Partial Fulfillment of the Requirements for the
Degree of

MASTER OF SCIENCE IN MECHANICAL ENGINEERING

at the

MASSACHUSETTS INSTITUTE OF TECHNOLOGY

February 1993

Signature of Author _____
Department of Mechanical Engineering
January 15, 1993

Certified by _____
John B. Heywood
Professor, Department of Mechanical Engineering
Thesis Supervisor

Accepted by _____
Ain A. Sonin
Chairman, Department Graduate Program

A PRACTICAL BURN RATE ANALYSIS FOR USE IN ENGINE DEVELOPMENT AND DESIGN

by

Hon Man Cheung

Submitted to the Department of Mechanical Engineering
on January 15, 1993 in partial fulfillment of the requirements for
the Degree of Master of Science in Mechanical Engineering

ABSTRACT

A single zone burn rate analysis for cylinder pressure data proposed by Gatowski et al in 1984 and Chun in 1987 was implemented and evaluated in this work. The analysis, which uses the heat release approach based on the First Law of Thermodynamics, included sub-models for the effects of residual fraction, heat transfer, and crevice. One of the important parameter in the analysis, the ratio of specific heats, γ, was estimated at various equivalence ratios and initial burned fractions by matching the burning profile of the one-zone procedure to that of the two-zone engine simulations. Since a two-zone analysis usually is more complex and time-consuming, this approach allowed the use of the simpler one-zone analysis with a more accurate thermodynamic properties.

Each of these sub-models were assessed and recalibrated, if necessary. Sensitivity checks were done on parameters like wall temperature, heat transfer calibration constants, swirl ratio, motoring polytropic constant, initial mass, heat transfer exponent, and uncertainty in pressure data. In addition, new ratios of specific heats was computed by the matching process for alternative fuel including propane, methanol, and methanol-gasoline mixtures. The burn rate analysis also incorporated several other computations. suggested by the engineers at Chrysler because of their usefulness. These included the effective compression ratio, polytropic constants, specific fuel consumption, and energy losses due to blowdown and throttling.

Cylinder pressure at various engine operating conditions obtained from the Sloan Lab. and Chrysler were used to evaluate the accuracy and compatibility of the analysis to real data. The results showed that the analysis performed better at moderate operating conditions than at wide open throttle due to inaccuracies in pressure data. Subsequent use of the burn rate analysis on alternative fuels and engine hydrocarbon emissions studies at the Sloan Laboratory indicated that it could be used as a useful tool in engine development activities.

Thesis Advisor:
John B. Heywood
Sun Jae Professor of Mechanical Engineering
Co-Director, Leaders for Manufacturing Program
Director, Sloan Automotive Laboratory

ACKNOWLEDGMENTS

Life is a highway. This work probably signified one of the intersections on this road where I turned onto another path. What lies ahead? Who knows? But I know that I would not have reached this part of the road without the following individuals. So, before I take the turn, I would like to spend a moment expressing my gratitude to them.

All these years, my family has always been there for me. Thank you very much for your support both financially and mentally. I appreciate that you are always behind my decisions. Knowing that I have you standing behind me, I will never be afraid to march forward. I love you.

Besides my family, I am also very fortunate to have wonderful friends with whom I had shared many good and bad times. I would like to extend special thanks to Neha Shah and her family, Jay Bar, Manish Sagar, Kaushal Majmudar, and Ginat Gutierrez for their friendships which have been invaluable to me, and for making my ride more enjoyable and colorful.

I also would like to thank the students from the Sloan Lab. for their assistance and companionship throughout my stay at MIT. Thanks Jon Fox, Serge Brussovansky, Christian Barranco and Kyoung Doug Min for the data, computing help, lifting, and the coffee maker along with Christophe Hochede, Pete Hinze, Serge Pinatel, Eric Deutch, Jim Ryan, Kristine Drobot, Koen DeWitte, and Mike Norris for all the fun time and help they had provided me.

My work was made easier by the cooperation of the engineers at Chrysler Corporation especially Peter Hartman and others who had provided me with a variety of data for my analysis. It had been a pleasure working with them and I appreciate very much their help.

Last but not least, I would like to extend my gratitude to my advisor, Professor John B. Heywood for his advises and directions on my research. He had not only taught me about automotive engine but also showed me the way to conduct research and study. I hope I will put his teaching into good use in the future.

The funding for this research was provided by the MIT Leaders for Manufacturing Program in which Chrysler Corporation is a member.

TABLE OF CONTENTS

LIST OF TABLES

LIST OF FIGURES

CHAPTER 1 - INTRODUCTION

1.1 Background

Cylinder pressure has always been an important measurement in studies of automotive engines because of its direct relation to the combustion process. In an internal combustion engine, chemical energy stored in fuel is released through combustion. The burning of fuel raises the cylinder pressure which, in turns, drives the piston to produce useful work. Thus, by knowing the time-history of the cylinder pressure, the amount of fuel burned can be estimated. This fuel mass burned expressed as a fraction of the total mass is the mass fraction burned. Mass fraction burned and mass burning rate curves (Figure 1-1) show how combustion progresses as a function of crank angle. The burn rate analysis provides researchers with valuable information about the quality of combustion. It can be used in many aspects of engine research and developments such as cycle-by-cycle variations and lean burning behaviors.

Because of its usefulness, many methods have been developed over the years to determine the mass fraction burned. One of the earlier models was proposed by Rassweiler and Withrow [1] in 1936. Although the model is over fifty-years old and several other new approaches have been proposed by others since then, it is still one of most widely used methods. One advantage of this approach is that it is simple to apply. It requires only the cylinder pressure along with the cylinder volume details. Due to its simplicity, data processing time is short which allows real-time processing with today's fast computers.

Despite its advantages, the Rassweiler and Withrow model also has its drawbacks. The polytropic constant (n) used in the calculation is assumed to be a constant throughout the analysis. However, the polytropic constant varies from compression to expansion and changes during the combustion process. Besides, it is not easy to select an appropriate polytropic constant because it varies with engine operating conditions. In addition, the

effect of heat transfer is not accounted for in the model. It is included only to the extent that the polytropic constant is different from the ratio of specific heats (γ) which is a thermodynamic property of the unburned and burned fuel. The model also does not account for the existence of crevices, small narrow volumes connected to the combustion chamber. Cylinder charge flows into the crevice during compression and returns to the combustion chamber during expansion. Some of the charge is not burned because the flame cannot propagate into these crevice regions.

Because of the limitations of the Rassweiler and Withrow model, more complete and sophisticated approaches have been proposed by others over recent years. Some utilize a two-zone combustion analysis which models the burned gas and unburned gas as two separate regions. This approach is complicated and time-consuming, thereby limit its use.

A simpler one-zone model was proposed by Gatowski et al. [2] at Massachusetts Institute of Technology in 1984. The single-zone analysis uses the energy release approach to determine the burn rate from measured cylinder pressure. During combustion, chemical energy of the reactants is converted into sensible energy of the products which increases the pressure inside the chamber. In addition to combustion, the change in cylinder chamber volume, heat transfer to the walls, and mass transfer between the chamber and crevices also influence the pressure. If these effects can be related to the pressure and be separated from the effect of combustion, the mass fraction burned can then be estimated. The approach uses the First Law of Thermodynamics and several sub-models to relate the overall energy balance to the measured pressure. One advantage of this method is that it calculates each effect explicitly. Therefore, additional information about the combustion process can be obtained if the pressure data is accurate. It is more complete than the Rassweiler and Withrow method but simpler than the two-zone model, thus greatly reduces data processing time.

1.2 Objective

The energy release burn rate analysis was first implemented by Chun [3] and later by Sztenderowicz [4] at the Sloan Automotive Laboratory of MIT. It had been used for various applications within the Sloan Laboratory. However, it is yet to be widely used in the industry. Different divisions of a company with various needs would implement their own versions of the burn rate analysis based on different models making communications among them difficult. Hence, a standardized pressure data analysis will be beneficial.

The goal of implementing the energy release burn rate into the automotive industry's engine development and design activities leads to the following objectives:

1. Assess and calibrate, if necessary, all the sub-models used in the analysis to ensure validity and accuracy.
2. Incorporate additional calculations into the burn rate analysis to satisfy the needs of different users.
3. Test the complete model with data from practical engines to ensure that the analysis is robust and compatible to commercial engines.

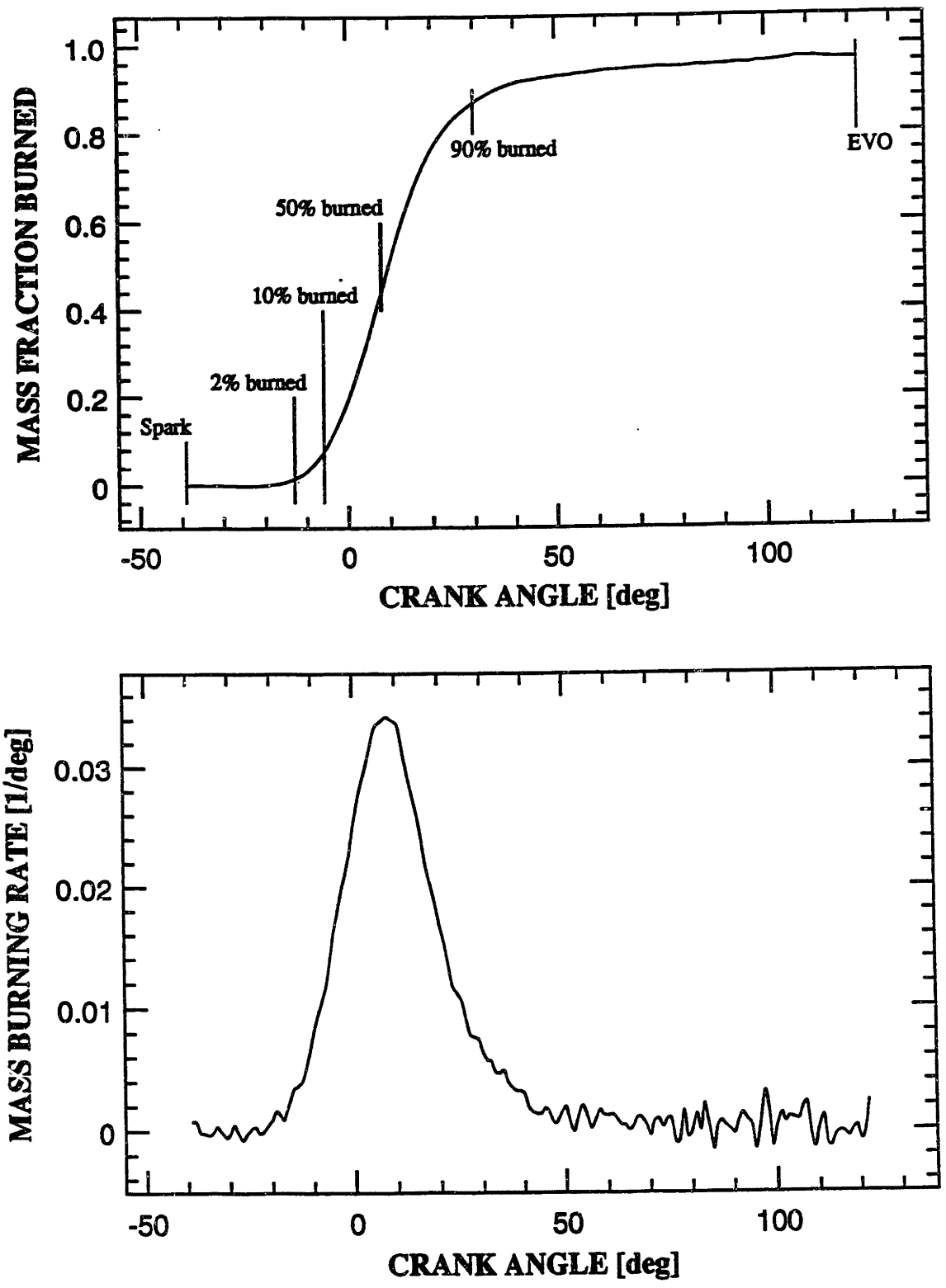

Figure 1-1. Sample mass fraction burned and burning rate profiles.

CHAPTER 2 - ENERGY RELEASE BURN-RATE MODEL

2.1 Energy Release Equation

To derive the energy release burn-rate relationship, consider the combustion chamber to be the control volume of a thermodynamic system with the cylinder wall, piston head, and the cylinder roof as the boundary. Figure 2-1 shows the schematic of the system. The First Law for this system is

$$\delta Q_{ch} = dU_s + \delta W + \sum h_i dm_i + \delta Q_{ht} \qquad (2.1)$$

where δQ_{ch} = chemical energy release by combustion,

dU_s = change in sensible energy from reactants to products,

δW = work done by piston,

$\Sigma h_i dm_i$ = mass flux across the system boundary,

δQ_{ht} = heat transfer to the chamber walls.

The First Law provides the basic framework of the model. Then each term of Eq. (2.1) is converted into expressions in terms of cylinder pressure, volume, and other convenient parameters.

The sensible energy can be represented by

$$U_s = mu(T) \qquad (2.2)$$

where m = mass of charge inside the control volume,

T = mean charge temperature determined by the Ideal Gas Law.

Differentiating both sides of Eq. (2.2) gives

$$dU_s = m\frac{\partial u}{\partial T}dT + udm$$

$$dU_s = mc_v(T)dT + u(T)dm \qquad (2.3)$$

where c_v is the specific heat at constant volume.

The piston work is simply given by pressure multiplied by the change of cylinder volume:

$$\delta W = pdV \tag{2.4}$$

The mass flux across the system boundary is given by two terms:

$$\sum h_i dm_i = h_{inj} dm_f + h' dm_{cr} \tag{2.5}$$

The first term describes the energy flow due to fuel injection whereas the second term accounts for the effect of flow into and out of crevices. All our analysis will be mainly for spark-ignition (SI) engine and will focus on the period between intake valve closing (IVC) and exhaust valve opening (EVO). During this period, there is no fuel injected into the chamber during this period. Hence, the fuel injection energy term is dropped. All the crevices inside the cylinder are aggregated into one single volume because of the overall effect is what is required. The crevice gas flow is at the same pressure as cylinder gas but different temperature. The temperature and enthalpy of crevice gas flow is evaluated at cylinder conditions if mixture is flowing into the crevice and at crevice conditions if mixture is returning into the combustion chamber. The crevice model will be discussed more fully in Chapter 2.2.2. Therefore, Eq. (2.5) becomes

$$\sum h_i dm_i = h' dm_{cr} = -h' dm_{cyl} \tag{2.6}$$

The Ideal Gas Law states

$$pV = mRT$$

or

$$Vdp + pdV = R(Tdm + mdT)$$

hence

$$mdT = \frac{Vdp + pdV}{R} - Tdm \tag{2.7}$$

In addition, the constant volume specific heat (c_v) can be expressed in terms of the ratio of specific heats (γ):

$$\gamma = \frac{c_p}{c_v}$$

where c_p is the specific heat at constant pressure.

and
$$\frac{c_v}{R} = \frac{1}{\gamma - 1} \tag{2.8}$$

In the burn rate analysis, γ is approximated by a function of temperature:

$$\gamma = a + bT \tag{2.9}$$

The method of obtaining this function will be presented in Chapter 2.3.

Substituting Eqs. (2.3) to (2.9) into Eq. (2.1) and expressing the energy release rate in terms of crank angle (θ) provides us with the functional form of the burn rate expression:

$$\frac{dQ_{ch}}{d\theta} = \frac{\gamma}{\gamma - 1} p \frac{dV}{d\theta} + \frac{1}{\gamma - 1} V \frac{dp}{d\theta} + V_{cr}\left[\frac{T'}{T_w} + \frac{T}{T_w(\gamma - 1)} + \frac{1}{bT_w} \ln\left(\frac{\gamma - 1}{\gamma' - 1}\right)\right] \frac{dp}{d\theta} + \frac{dQ_{ht}}{d\theta} \tag{2.10}$$

where V_{cr} = crevice volume,

T' = crevice gas temperature,

T_w = wall temperature,

γ = ratio of specific heats for cylinder gas,

γ' = ratio of specific heats for crevice gas.

Therefore, the mass fraction is given by the percentage of the integral of Eq. (2.10) over the total available energy, that is,

$$x_b = \frac{\int_{spark}^{EVO} \left(\frac{dQ_{ch}}{d\theta}\right) d\theta}{m_f Q_{LHV}} \tag{2.11}$$

where x_b = mass fraction burned,

m_f = mass of fuel,

Q_{LHV} = lower heating value of fuel.

The effect of heat transfer on the overall fraction burned is not directly measured. Thus, a model is employed to estimate the heat transfer effect which will be discussed in the following section.

2.2 Sub-models

As described in the previous section, there are several events occurred inside the chamber other than combustion that affect the cylinder pressure history. These events include heat transfer to the chamber walls, flow into and out of crevices, and residual fraction left over from the previous burning cycle. Since these effects on the overall burned fraction are not directly measured, models are used to relate them to the pressure history.

2.2.1 Heat Transfer

During engine operation, energy is translated from the in-cylinder gases by heat transfer to the chamber walls. The loss of energy lowers the pressure and shows up in the pressure history. If this pressure history is used to calculate the mass fraction burned without compensating for the heat loss, abnormally low burned fractions will be obtained. Thus, a model is needed to estimate the amount of energy lost in heat transfer.

The heat transfer model used in the burn rate analysis is based on Woschni's correlation for engine heat transfer coefficient (h_c) [5]. The convective heat transfer rate is given by

$$\frac{dQ_{ht}}{dt} = Ah_c(T - T_w) \qquad (2.12)$$

where A = heat transfer area,

h_c = convective heat transfer coefficient.

The heat transfer coefficient is given by Woschni's correlation with some minor modifications:

$$h_c = 3.26 c_1 B^{m-1} p^m T^{0.75-1.62 m_w m} \qquad (2.13)$$

where m = heat transfer exponent which equals 0.8,

B = bore,

p = cylinder pressure,

T = cylinder charge temperature,

c_1 = calibration constant that gives the correct dimension for h_c,

w = characteristic velocity contributed by piston movement, charge motion, and combustion,

$$w = 2.28(\bar{s}_p + u_{swirl}) + 3.24 * 10^{-3} c_2 T_{ivc} (\frac{V_d}{V_{ivc}})(\frac{p_f - p_m}{p_{ivc}}) \qquad (2.14)$$

where $\bar{s}_p$ = the mean piston speed,

u_{swirl} = swirl velocity due to charge motion,

V_d = displaced volume,

c_2 = calibration constant that gives the correct dimension,

p_f = firing pressure,

p_m = motoring pressure,

the subscript *ivc* refers to conditions at intake valve closing.

The swirl velocity (u_{swirl}) is given by a swirl ratio (R_{swirl}) that is input by the user depending on the charge motion of the engine.

$$u_{swirl} = \pi N B R_{swirl} \qquad (2.15)$$

where N = engine speed [rev/sec.],

B = bore,

R_{swirl} = swirl ratio which is defined as the ratio between the angular velocity of a solid-body rotating flow and the crankshaft angular rotational speed.

Unlike the Woschni correlation, Eq. (2.14) includes the movement of the mixture induced by charge motion in term of u_{swirl}. In addition, the calibration constant c_1 and c_2 are added to adjust the heat transfer effect.

2.2.2 Crevice Model

In an engine, there exist several crevices, for example, above the top ring between the piston and the cylinder, around the spark plug, and between the cylinder block and the head gasket (Figure 2-2) [6]. Gas flows into and out of the crevice as cylinder pressure rises and falls, thus, affecting the combustion process. The simplest way to model the crevice effect is to assume all crevices to be one single volume. The gas inside the crevice is at essentially the same pressure as the chamber, but at a different temperature. Since crevice volumes are narrow and the walls are cold, crevice gas is close to wall temperature. The mass in the crevice can be estimated using the Ideal Gas Law,

$$m_{cr} = \frac{pV_{cr}}{RT_w}$$

The volume and temperature are assumed to be constants which gives

$$dm_{cr} = \frac{V_{cr}}{RT_w} dp \qquad (2.16)$$

Eq. (2.16) confirms that the gas flows into or out of the crevice depending on the variations of the cylinder pressure. When the cylinder pressure rises ($dp > 0$), mass flows into the crevice. On the other hand, mass returns to the chamber when the pressure drops ($dp < 0$). When the cylinder mixture is pushed into the crevice because of the high cylinder pressure, the state of the crevice gas is evaluated at the cylinder condition. However, in the case of crevice gas returning to the chamber because the cylinder pressure drops, the crevice condition is used to evaluated the state of the returning mixture.

The total crevice volume for a warm-up engine is about 1% to 2%. In this model, the effect of blowby is not included because the significance of blowby is small in modern engines.

2.2.3 Residual Gas Fraction

At the end of combustion (EOC) and during exhaust, some burned gas stays in the chamber without being pushed out. This residual gas affects the combustion process by mixing with the fresh intake charge. Since the burned gas is hot, the mixing heats up and dilutes the fresh charge. Therefore, a model is needed to predict the amount of residual fraction (x_r).

The model used in the burn rate analysis was developed by Fox [7] of MIT in 1992. The model relates x_r to the engine speed, inlet pressure, valve overlap, and fuel-air equivalence ratio.

$$x_r = 1.266\sqrt{|p_{in} - p_{ex}|}\left(\frac{F_{overlap}}{N}\right)\left(\frac{p_{in}}{p_{ex}}\right)^{-0.87} + 0.632\frac{\phi}{R_c}\left(\frac{p_{in}}{p_{ex}}\right)^{-0.74} \qquad (2.17)$$

where N = engine speed,

ϕ = fuel-air equivalence ratio,

R_c = compression ratio,

$F_{overlap}$ = valve overlap factor.

The valve overlap factor is defined as

$$F_{overlap} = \frac{D_{iv}A_{iv} + D_{ev}A_{ev}}{V_d} \qquad (2.18)$$

where D is the diameters of the intake (iv) and exhaust (ex) valves. The quantities A_{iv} and A_{ex} are defined as,

$$A_{iv} = \int_{IVO}^{iv=ev} IV_{lift}\,d\theta \qquad \& \qquad A_{ex} = \int_{ev=iv}^{EVC} EV_{lift}\,d\theta \qquad (2.19)$$

Alternatively, the overlap factor can be estimated with a second order equation.

$$F_{overlap} = \frac{1.45*10^{-3}}{B}[107 + 7.8(EVC - IVO) + (EVC - IVO)^2](\frac{l_{\max}}{B})(\frac{d_{ave}}{B}) \quad (2.20)$$

where l_{max} = average maximum valve lift,

d_{ave} = average valve diameter.

Sometimes exhaust gas is intentionally circulated back to the cylinder (*%EGR*) to mix with fresh mixture along the residual gas for better fuel efficiency. Thus, the total initial burned gas fraction before combustion is

$$x_{b,0} = (\frac{EGR}{100})(1 - x_r) + x_r \quad (2.21)$$

Since by definition,

$$x_{b,0} = \frac{m_b}{m_i + m_b}$$

where m_i is the mass of fresh intake, the total mass of cylinder charge can be computed knowing the residual gas fraction and *%EGR*,

$$m_{total} = \frac{m_i}{1 - x_{b,0}} \quad (2.22)$$

With all sub-models established, Figure 2-3 shows the contribution of each effect on the overall mass fraction burned. Heat transfer has significant effect especially at the end of combustion whereas crevice effect is relatively small because of the small crevice volume.

2.3 Ratio of Specific Heats

The algorithm used to determine the ratio of specific heats (γ) was first proposed by Chun [3] in 1986. This approach improves the one-zone analysis by finding the $\gamma(T)$ which makes the one-zone burning rate predictions match closely with predictions made from the same pressure data with a two-zone model.

The flow chart in Figure 2-4 shows the steps used to determine γ. A pre-defined mass fraction burned profile is inputted into a two-zone engine cycle simulation program which was developed by Poulos and Heywood [8] in 1983. The effects of heat transfer and crevice are set to zero because they can only be modeled approximately. Mass fraction burned is specified by a Wiebe function:

$$x_b = 1 - e^{[-a(\frac{\theta-\theta_0}{\Delta\theta})^{m+1}]} \tag{2.23}$$

where θ_0 = start of combustion,

$\Delta\theta$ = total burn duration.

a = a constant equals to 5,

m = a constant equals to 2.

From the simulation program, a time-history of cylinder pressure can be generated. By rearranging the burn rate equation, Eq. (2.10) without heat transfer and crevice effects, an expression of γ in terms of fraction burned, pressure and volume can be obtained.

$$\gamma = \frac{\delta Q_{ch}/d\theta + V dp/d\theta}{\delta Q_{ch}/d\theta - p dV/d\theta} \tag{2.24}$$

The input for the simulation program were:

N = 1500 rpm,

θ_0 = 20 degBTC,

$\Delta\theta$ = 60 deg,

p_{in} = 0.5 atm.

Figures 2-5, 2-6 show γ from IVC to EVO calculated from the simulation program. Using these values, γ is approximated by a linear function of cylinder temperature during the compression and compression processes

$$\gamma(T) = a + bT \tag{2.25}$$

During combustion, γ is approximated by a constant value. As shown in the plot, Eq. (2.22) produces numerically unstable γ values near the end of combustion. In order to avoid this instability, the combustion γ is an average of gamma values from 7% to 93% burned. The approximated γ is put into the burn rate analysis, and Figure 2-7 shows the variation of γ from IVC to EVO. In order to ensure a smooth transitions from compression to combustion and from combustion to expansion, a 10 degrees transition region was added at the beginning and end of combustion.

In Figure 2-8, the pre-defined fraction burned profile was compared to the mass fraction burned profile obtained from the burn rate analysis using the estimated γ. The two profiles match reasonably well with a slight difference after spark. This difference may possibly due to that the simulation pressure is from a two-zone model whereas the burn rate analysis is one-zone. Besides, the combustion γ is assumed to be a constant in the burn rate analysis.

Since γ of the entire cylinder charge varied with the fuel-air equivalence ratio, residual fraction, and fuel types, a number of γ's were computed at different equivalence ratios and residual fractions for fuel types including iso-octane, propane, indolene, methanol, M10 (10% methanol and 90% indolene by volume), M60, and M85.

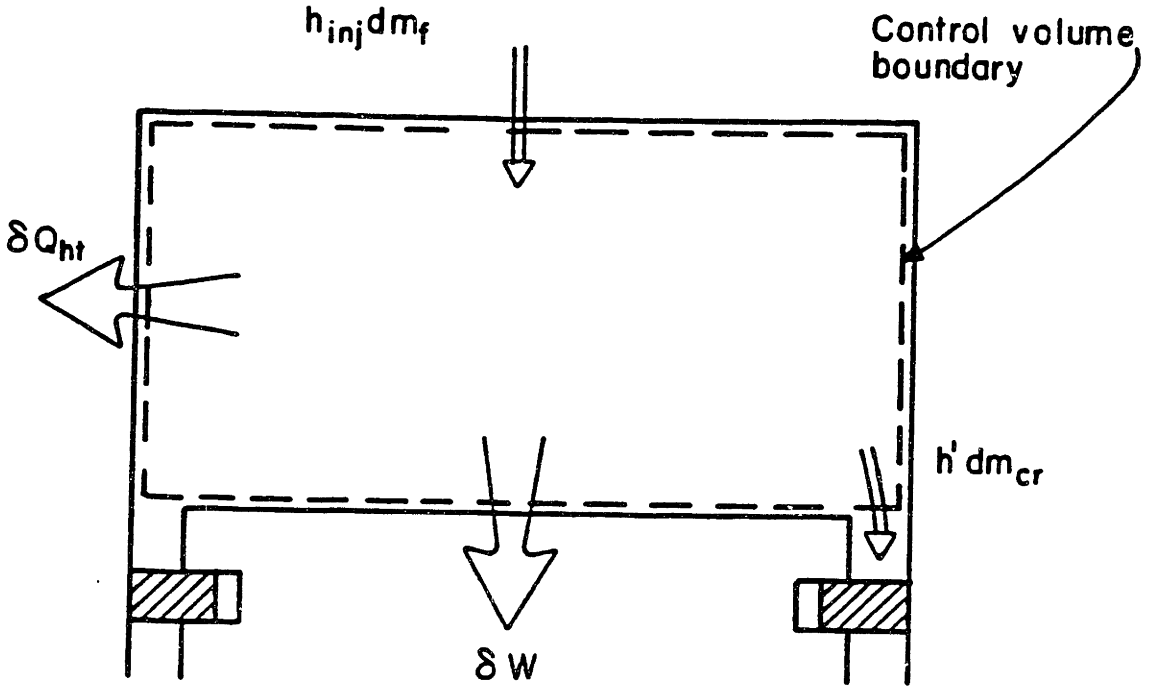

Figure 2-1. Schematic of thermodynamic system and sign convention of combustion chamber. [2]

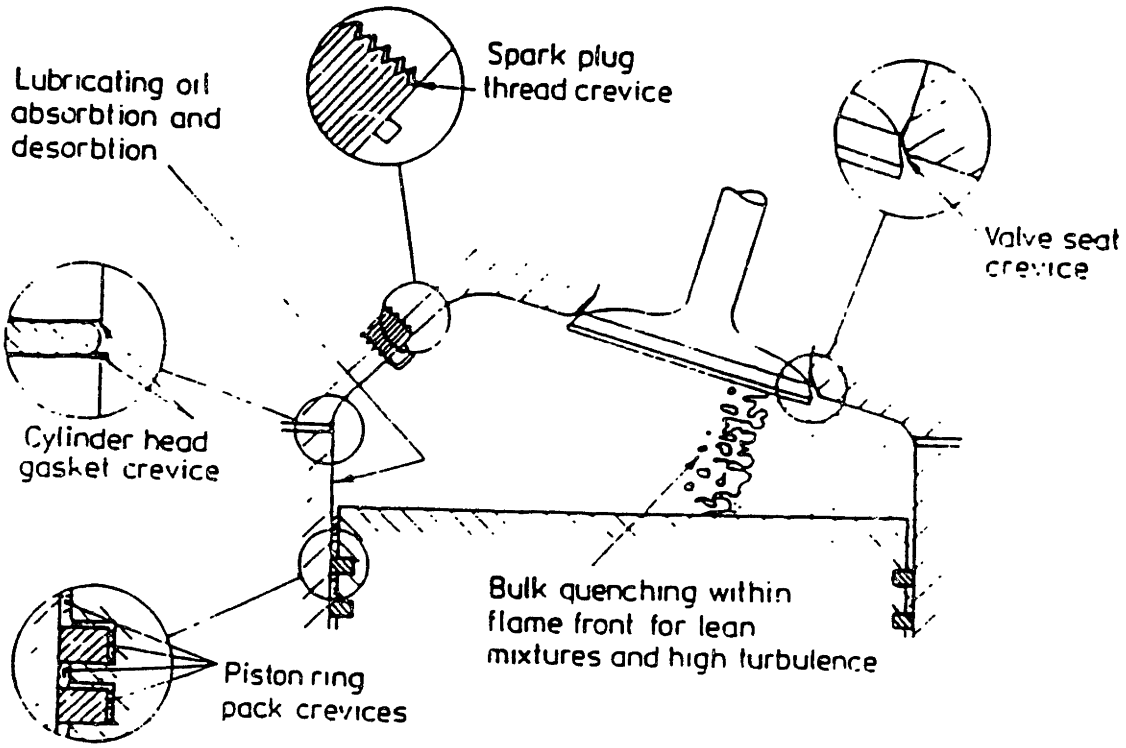

Figure 2-2. Possible sources of crevice region. [6]

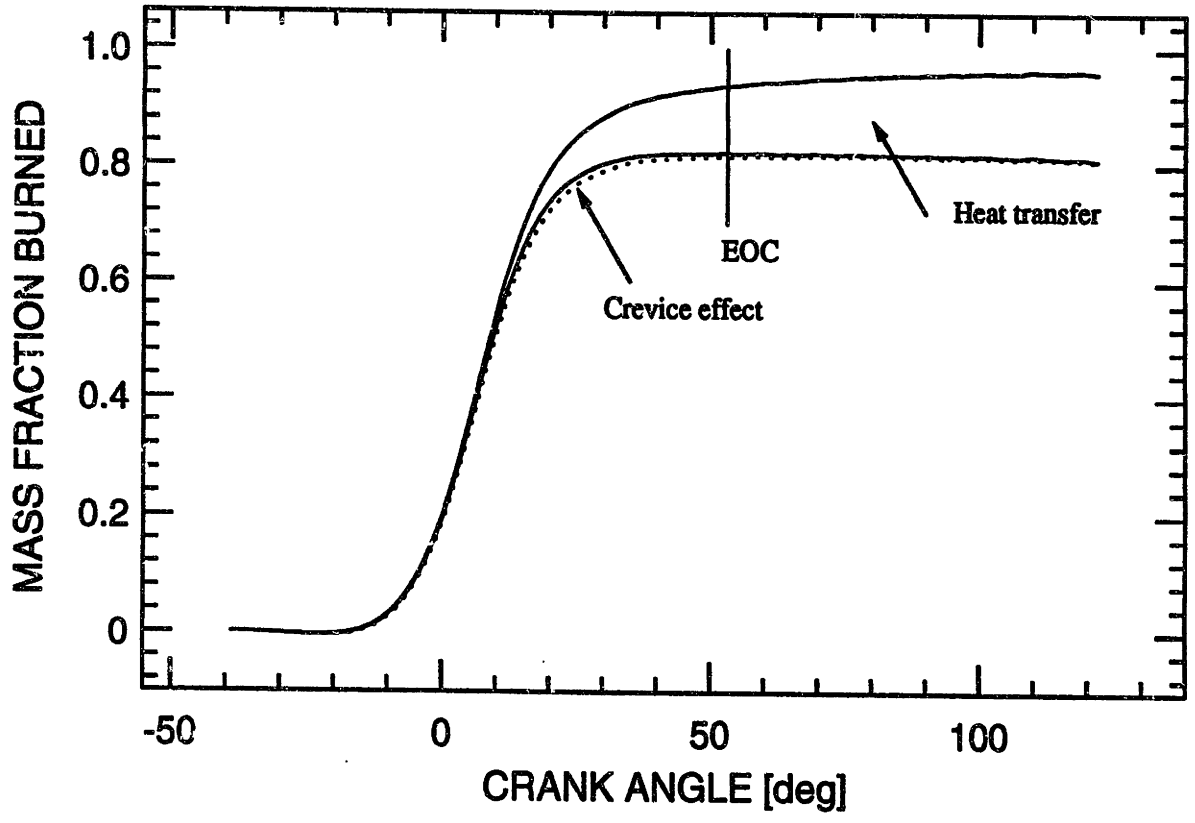

Figure 2-3. Relative contribution of each effect to overall burn rate analysis.

Ratio of Specific Heats:

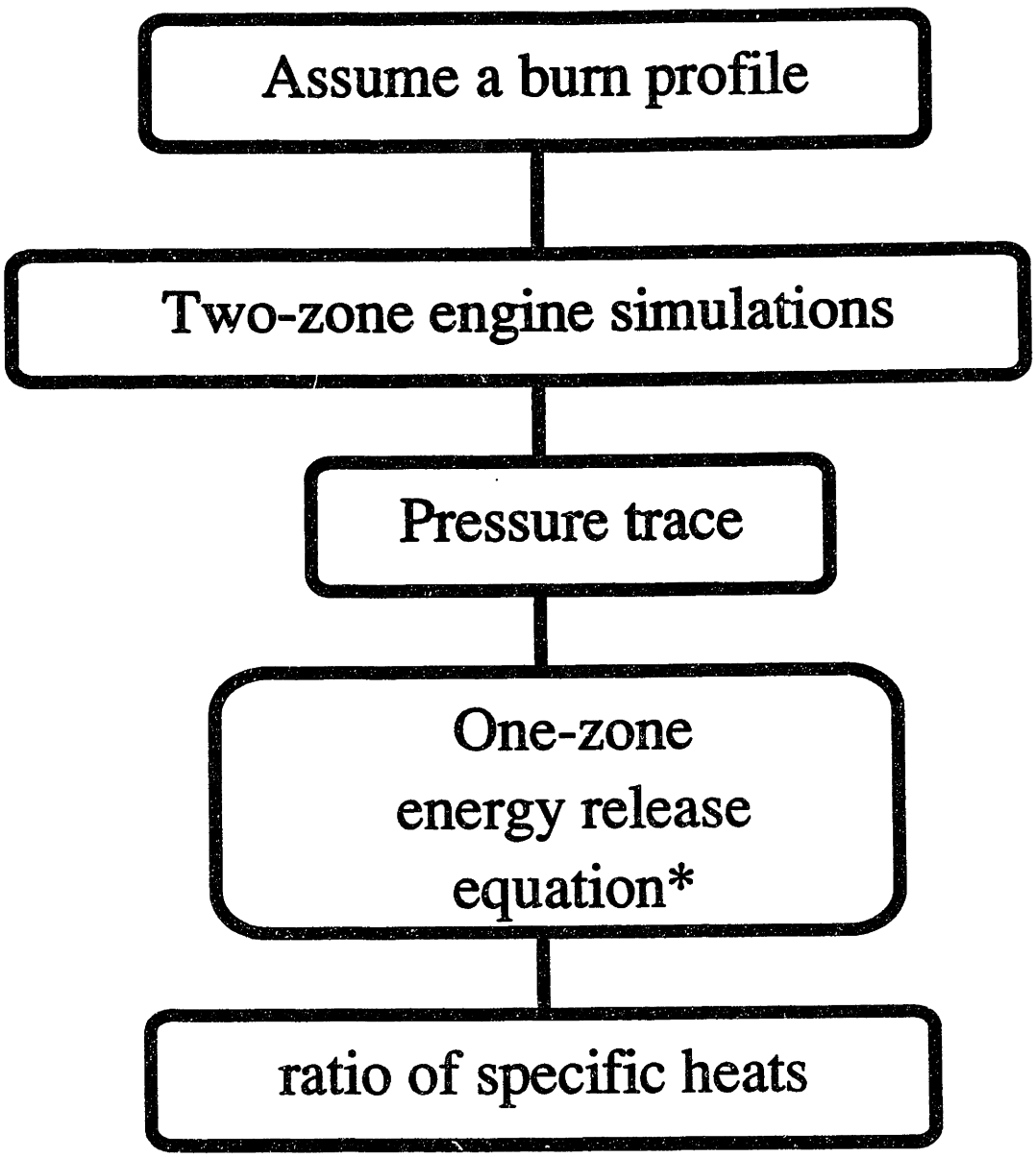

$$* \gamma = \frac{\delta Q_{ch}/d\theta + V\,dp/d\theta}{\delta Q_{ch}/d\theta - p\,dV/d\theta}$$

Figure 2-4. Procedure used to estimate the ratio of specific heats.

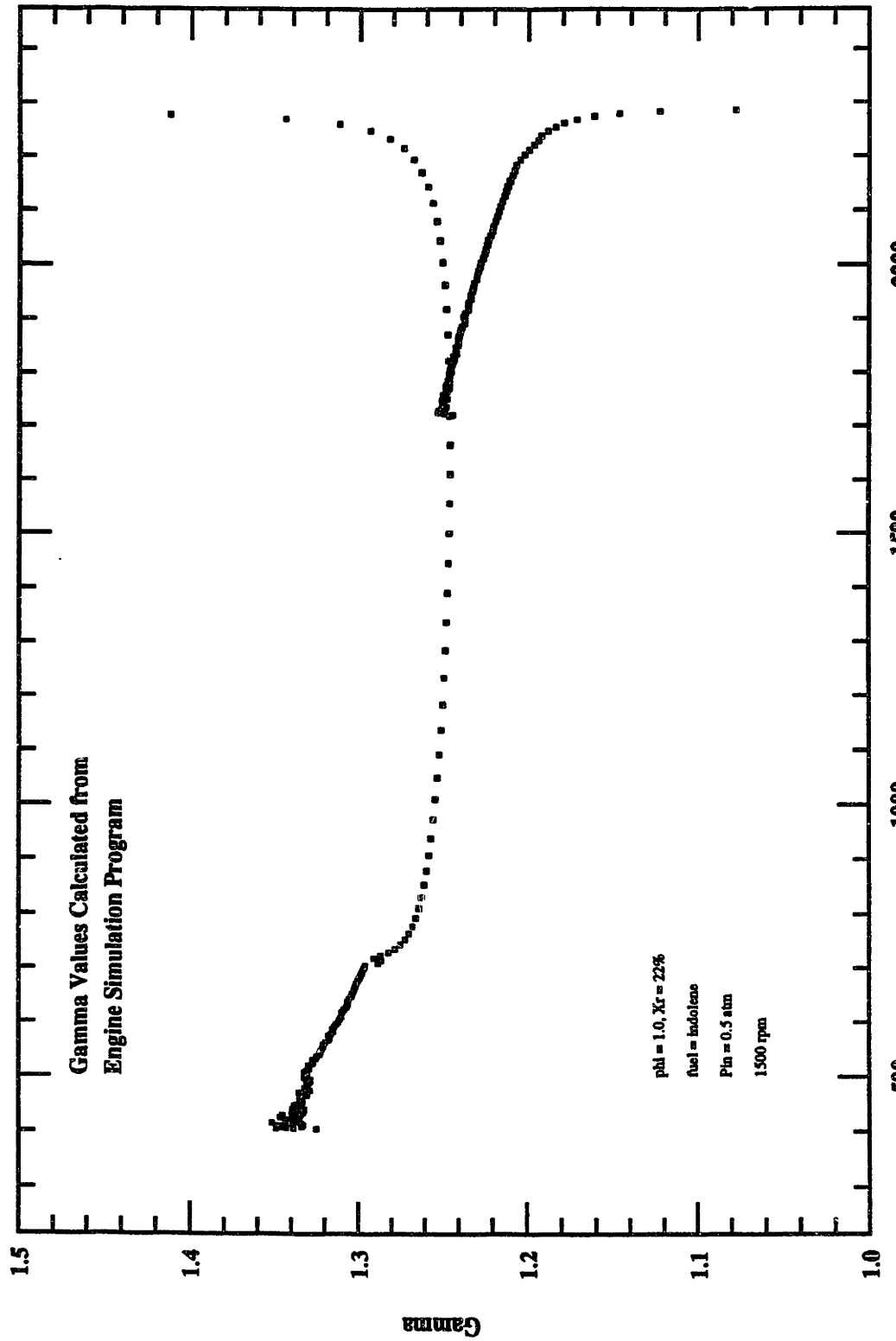

Figure 2-5. γ from engine simulation as a function of temperature.

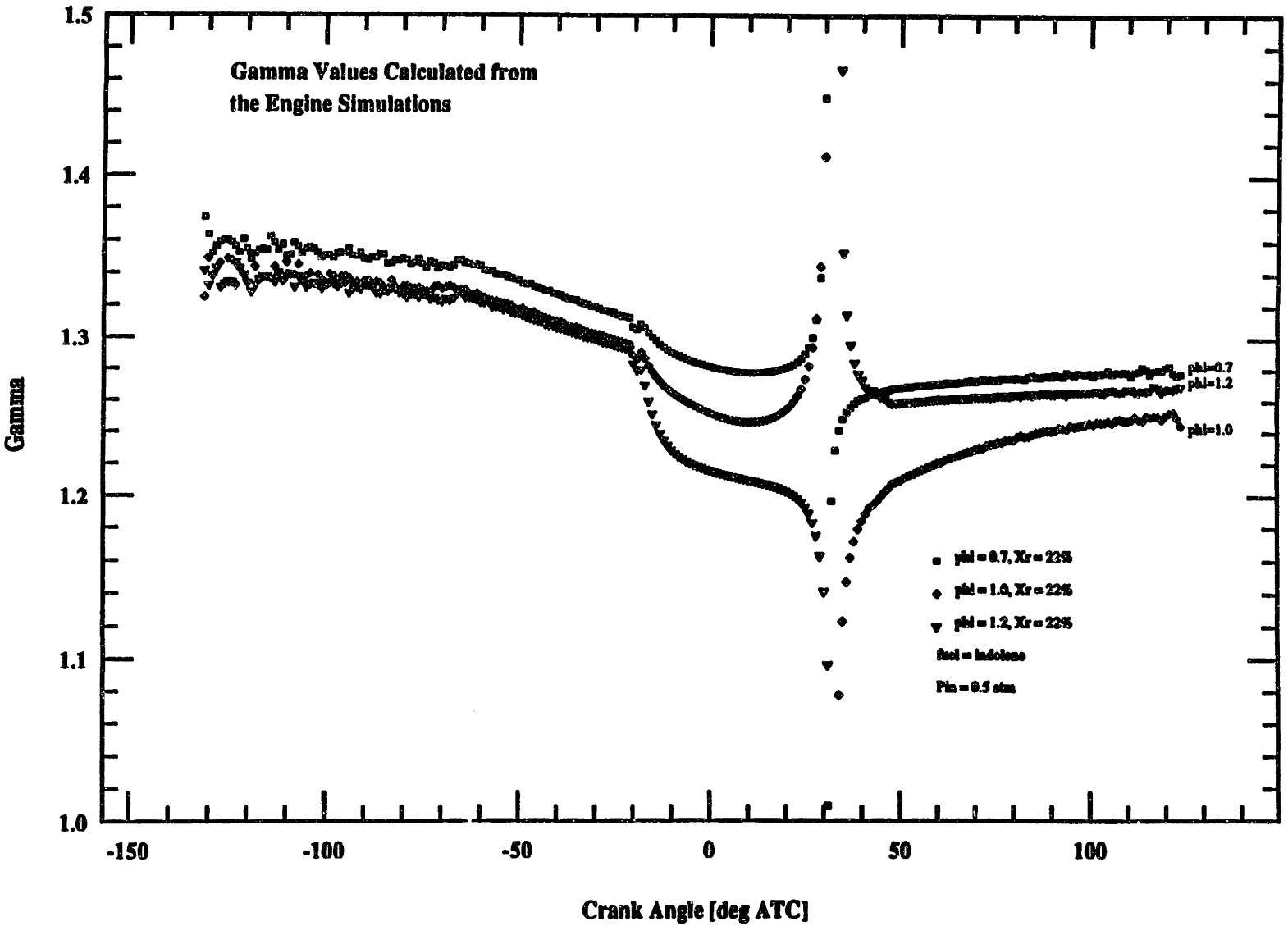

Figure 2-6. γ from engine simulation as a function of crank angle.

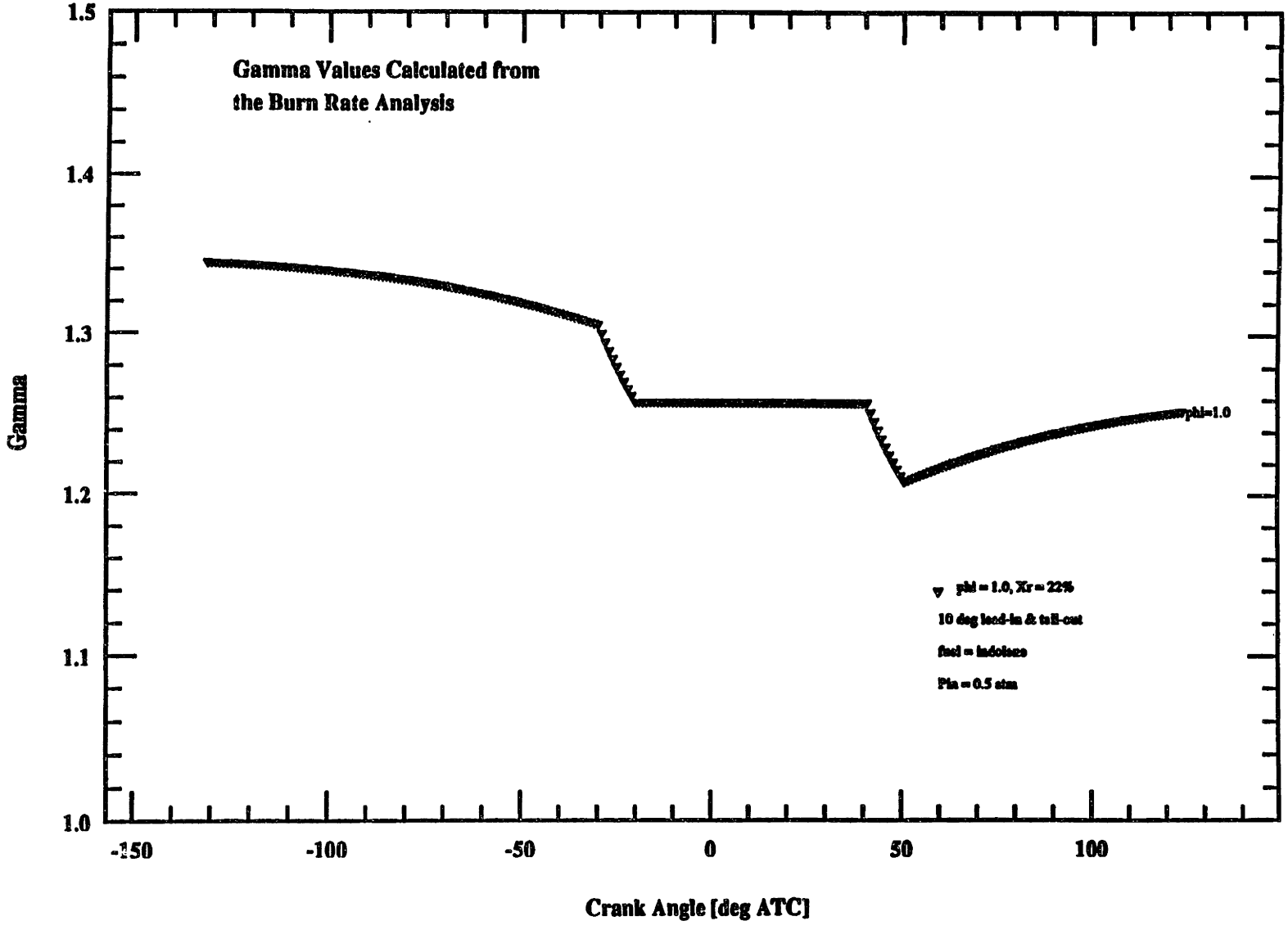

Figure 2-7. γ from burn rate analysis as a function of crank angle.

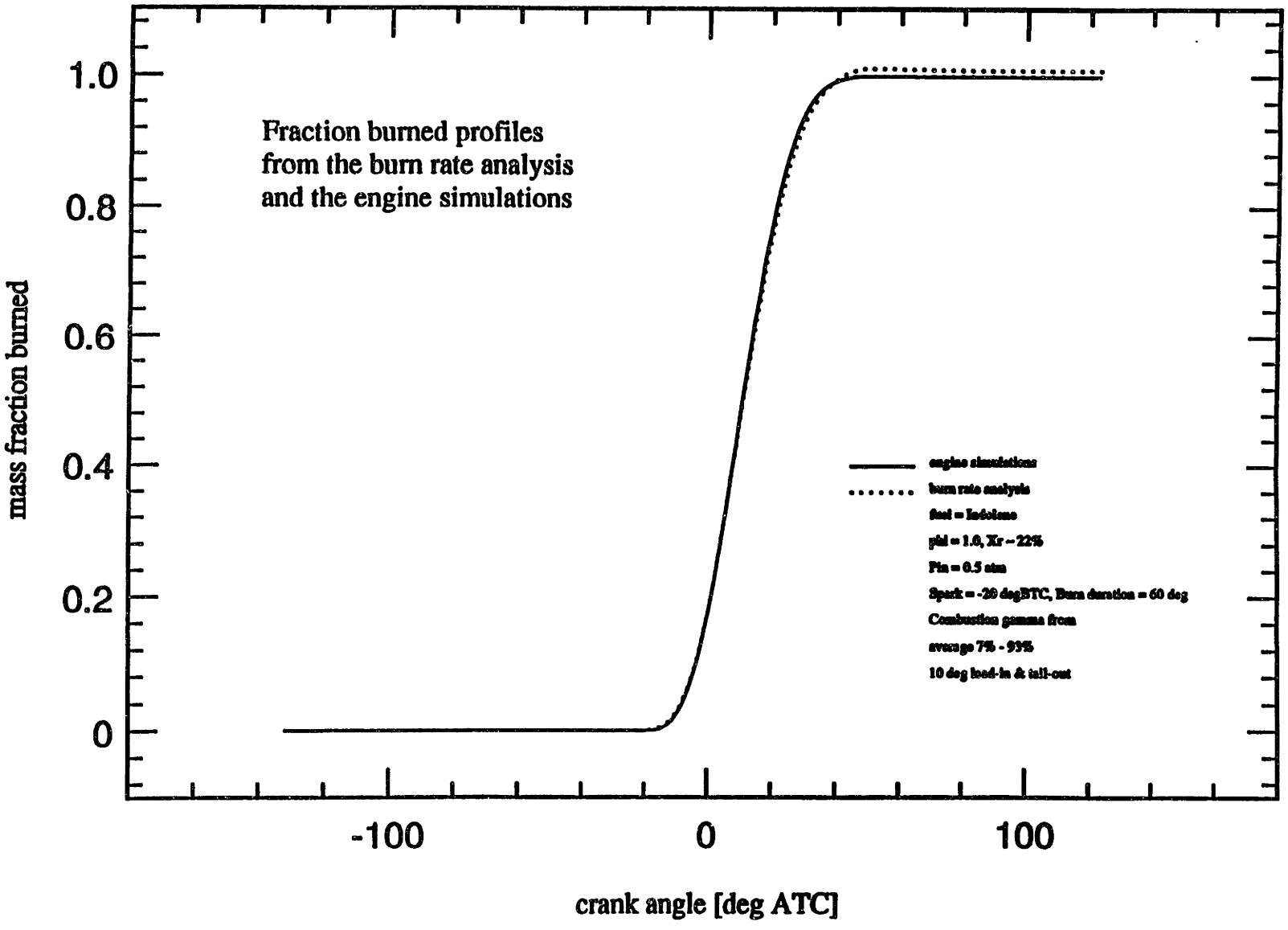

Figure 2-8. Comparison of fraction burned profiles from engine simulation and burn rate analysis.

CHAPTER 3 - AUXILIARY COMPUTATIONS

3.1 Introduction

In order to make the burn rate analysis package more useful to more engine developers and designers, additional calculations were added. Suggested by the engineers at Chrysler, these computations include the polytropic constants, blowdown and throttling energy losses, effective compression ratio, and the specific fuel consumption.

3.2 Polytropic Constants

Figure 3-1 shows the pressure-volume data from a firing engine on linear p-V and log p-log V scales. On the log p-log V diagram, the compression process and expansion process are straight lines. This is because both the compression of unburned mixture and the expansion of burned gases are close to adiabatic isentropic processes. For an isentropic process, $pV^{\gamma} = constant$ where γ is the ratio of specific heats. The compression and expansion processes are showed to be well fitted by a polytropic relation:

$$pV^{n} = constant \qquad (3.1)$$

where n is the polytropic constant. n has the value of 1.3 ± 0.05 for convention fuels. It is close to the value of γ for unburned mixture over the compression process, but is greater than γ for burned gases during expansion due to heat loss. The dotted lines in Figure 3-1 shows that the polytropic approximation fits the compression and expansion processes quite well.

To determine the value of n, least square straight lines are fitted through the compression and expansion processes on the log p-log V plot. The slopes of the lines are the polytropic constants. The main purpose of obtaining the polytropic constant for the experimental pressure-volume history is to check the pressure data. If the pressure data is erroneous, the polytropic constants will most likely to be very different from the average values.

3.3 Blowdown and Throttling Energy Losses

In practical engine operating cycles, there exist energy losses due to blowdown and throttling. Since valves never open and close at exactly top dead center (TDC) and bottom dead center (BDC), blowdown losses occur at the end of expansion and the beginning of exhaust while exhaust throttling loss may occur at the end of the exhaust stroke. Figure 3-2 shows the three possible areas of energy losses we had identified: the expansion blowdown, exhaust blowdown, and exhaust throttling losses.

To compute the expansion blowdown loss, the measured pressure-volume data is compared to the polytropic expansion. The polytropic expansion process is obtained by extrapolating the polytropic relation all the way to BDC. The area enclosed between the measured pressure history and the extrapolated pressure from the point they begin to differ to BDC is the desired expansion blowdown loss.

$$Loss_{blow} = \frac{\int_{p_{ext} \neq p_f}^{BDC} (p_{ext} - p_f) dV}{V_d} \qquad (3.2)$$

where p_{ext}, p_f = extrapolated and measured expansion pressure,

$Loss_{blow}$ = expansion blowdown loss in unit of pressure so it can be compared to the engine mean effective pressure.

When the piston reaches BDC during the exhaust process, the cylinder pressure is not close to the exhaust pressure. The cylinder pressure approaches the exhaust pressure after the piston has started moving upward. The time it took the pressure to reach the exhaust pressure from BDC is defined to be the exhaust blowdown loss. To calculate the amount of exhaust blowdown loss, the difference between the measured pressure data and the exhaust pressure is integrated starting BDC until the two pressures are equal. Since the exhaust pressure is not an input from the user, it has to be computed from the given pressure data. In order to avoid the effects of valve movement near TDC and BDC, exhaust pressure is taken to be the average of the measured exhaust pressure between

70% to 40% of the maximum volume (volume at BDC).

$$Loss_{exh} = \frac{\int_{pf=\bar{p}exh}^{BDC} (p_f - \bar{p}_{exh})dV}{V_d} \tag{3.3}$$

where $$\bar{p}_{exh} = \frac{\sum_{V=0.7V_{max}}^{V=0.4V_{max}} p_f}{n} \qquad (n = \text{\# of points})$$

In some operating conditions, throttling loss takes place at the end of the exhaust process and the beginning of the intake process when both the exhaust and intakes are opened. This loss is characterized by the "spike" near TDC of the exhaust stroke. The amount of exhaust throttling loss can be calculated by integrating the area between the measured exhaust pressure and the average exhaust pressure near BDC.

$$Loss_{thr} = \frac{\int_{TDC}^{Pf=\bar{p}exh} (p_f - \bar{p}_{exh})dV}{V_d} \tag{3.4}$$

Note all blowdown and throttling losses are expressed in the unit of pressure so that they can be compared to the engine mean effective pressure (*mep*).

3.4 Effective Compression Ratio

Another computation that was requested by the engineers at Chrysler is the effective compression ratio ($R_{c,eff}$). The regular compression ratio (R_c) is essentially the ratio of the maximum volume to the minimum. However, in operating engines the intake valves close after BDC and spark occurs before TDC. Therefore, R_c may not be a realistic representation of the ratio of compression. Instead of using the volume, pressure is used to evaluate $R_{c,eff}$.

$$R_{c,eff} = (\frac{p_{m,TDC}}{p_{f,BDC}})^{1/n_c} \tag{3.5}$$

where $p_{f,BDC}$ = pressure at BDC of compression stroke for normal firing cycle,

$p_{m,TDC}$ = motoring pressure at TDC of compression stroke,

n_c = compression polytropic constant.

The BDC firing pressure is readily available from the data whereas the TDC motoring pressure is obtained by extrapolating the compression pressure using the least-square fitted compression polytropic constant. The extrapolation is carried out by the polytropic relation Eq. (3.1). It starts from where the least-square fit ends, which should be a little before spark.

3.5 Specific Fuel Consumption

In order to learn more about the fuel efficiency of the engine, the specific fuel consumption (*sfc*) is also added to the analysis. The specific fuel consumption measures how efficiently an engine is using the fuel supplied to produce work. *sfc* is a function of intake fuel mass flow rate, and power output:

$$sfc = \frac{\dot{m}_f}{P} \tag{3.6}$$

where power output can be expressed in terms of the indicated mean effective pressure (*imep*), displacement volume, and engine speed.

$$P = \frac{(imep)V_d N}{n_R} \tag{3.7}$$

where n_R is the number of crank revolutions for each power stroke per cylinder (two for four-stroke cycles; one for two-stroke cycles). The mean effective pressure is calculated from integrating the *p-V* diagram. If only the compression, combustion and expansion processes are integrated, then it is the *gross* indicated mean effective pressure ($imep_g$). If the entire operating cycle including the exhaust and intake processes is integrated, then the *net* mean effective pressure is obtained ($imep_n$). In the burn rate analysis package, $imep_n$ is used to compute *P* and *sfc*. Therefore, the obtained value of *sfc* is the net indicated specific fuel consumption ($isfc_n$). However, *sfc* is by no mean limited to indicated

quantities. Depending on the form of power output that is used, one can obtain the *gross isfc* (*isfc*$_g$) and the *brake sfc* (*bsfc*). In order to compute these *sfc*'s, slight modifications will have to be made.

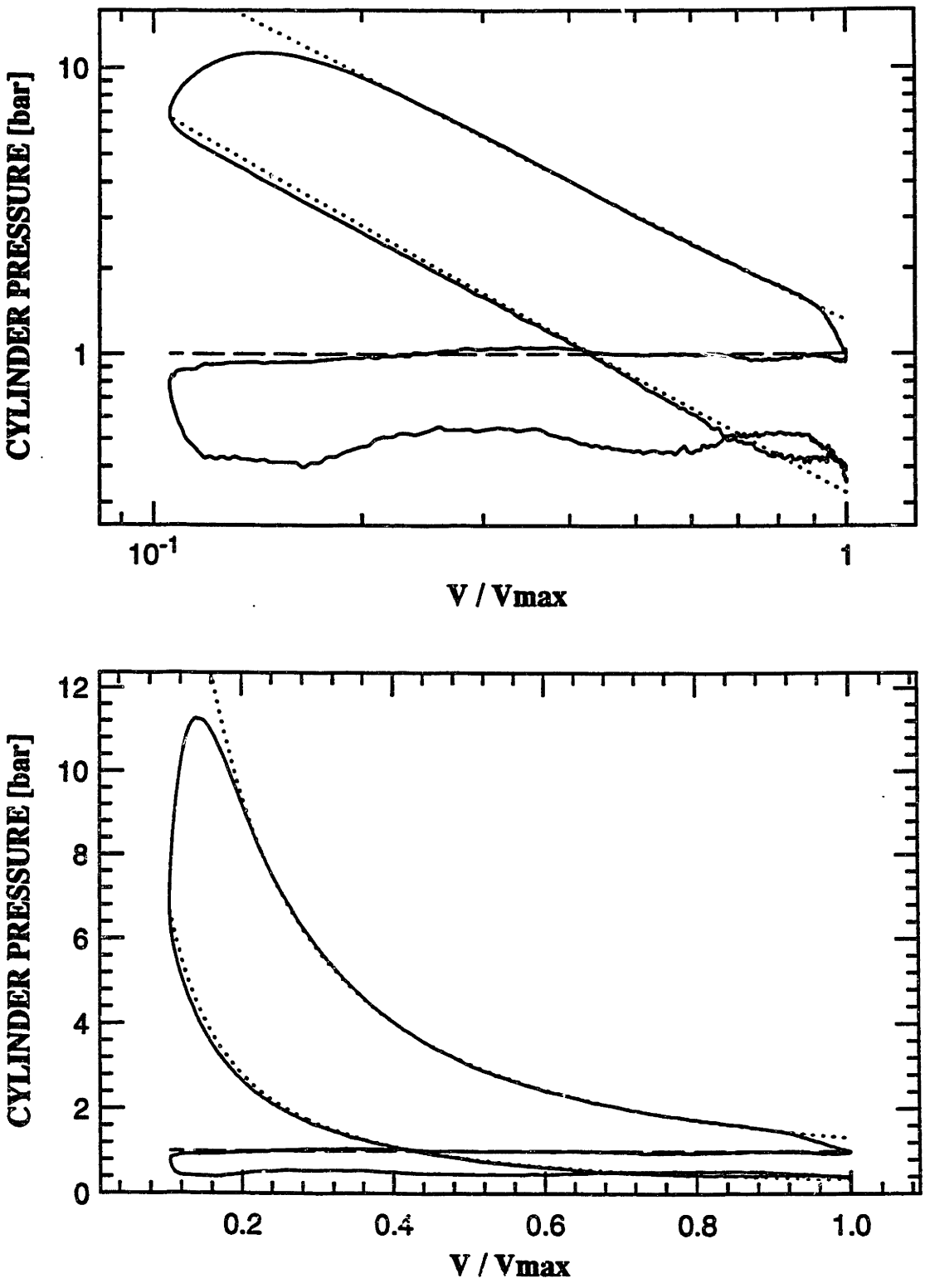

Figure 3-1. Pressure-volume history with approximated polytropic processes.

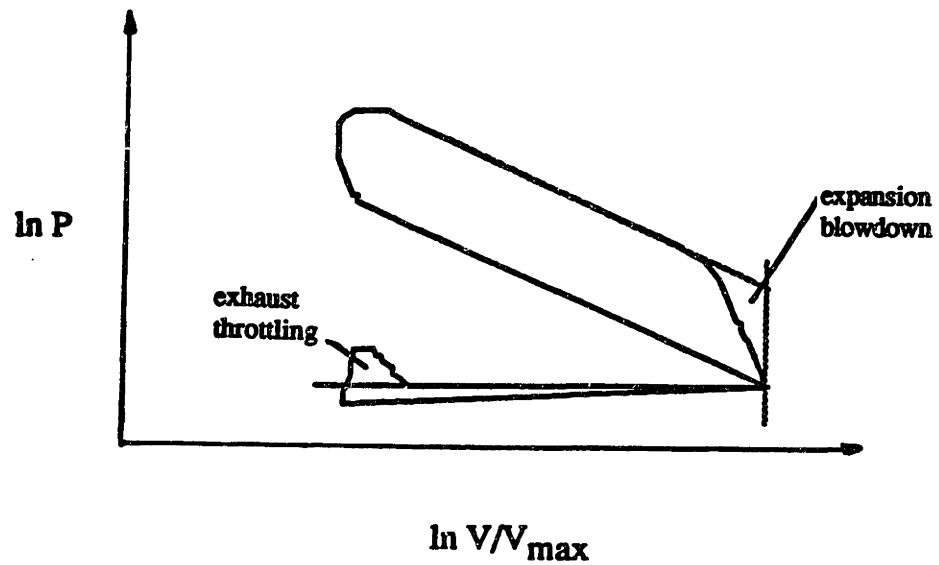

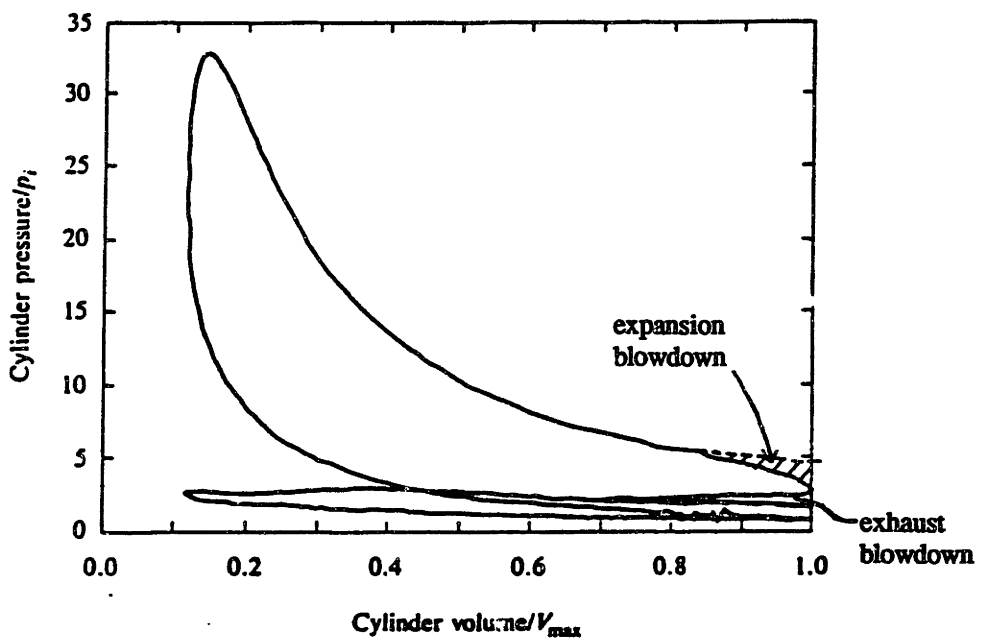

Figure 3-2. Possible areas of energy losses.

CHAPTER 4 - SENSITIVITY AND PARAMETRIC STUDIES

4.1 Introduction

Now that the framework of the burn rate model has been established, this chapter will investigate the sensitivities of several key variables and parameters. These variables include the wall temperature, heat transfer calibration constants, swirl ratio, motoring polytropic constant, initial mass, and the crevice volume. The first four quantities are mostly directly related to the heat transfer sub-model while the initial mass affects the overall burned fraction and the crevice volume obviously influences the crevice effect. Since some of these variables are not available explicitly, assumptions are made about them. In order to ensure that the assumptions are adequate. sensitivity tests are done to ensure that no large error in the analysis will result from expected uncertainties in these assumptions. By systematically adjusting the variables, the sensitivity of predictions to changes in these variables is determined.

4.2 Sources of Data

Sets of data taken at various engine operating conditions were used in the sensitivities and parametric studies. The Sloan Automotive Laboratory and Chrysler Corporation Powertrain Division were the sources of these data. The Sloan Lab. data were taken by Fox [7] and Min [9] on a single cylinder research engine. The engine is a four-stroke spark-ignition Ricardo Hydra Mark III with dual overhead cam. The spark plug of the engine is located near the center of a hemispherical combustion chamber. The engine geometry is described below:

bore, B = 85.7 mm,

stroke, L = 86.0 mm,

connecting rod, l = 157.9 mm,

clearance volume, V_{clear} = 68 cc,

IVO = 4 degBTC,

IVC = 132 degBTC,

EVO = 124 degATC,

EVC = 16 degATC.

The cylinder pressure data were taken with Kistler model 6121 pressure transducer coupled with Kistler model 5004 charge amplifier. A PC-based data-acquisition system was responsible for collecting the pressure data. The data were taken at a revolution of 2 crankangle degrees/sampling point, that is, 360 data points in one cycle of engine operation.

The Chrysler data were data by the engineers there with their 3.5L V6 production engine. It has the following geometry:

bore, B = 81.0 mm,

stroke, L = 96.0 mm,

connecting rod, l = 151.0 mm,

clearance volume, V_{clear} = 62.37 cc,

IVO = 8 degBTC,

IVC = 116 degBTC,

EVO = 122 degATC,

EVC = 14 degATC.

The data-acquisition system from DSP was used to collect the data. Only data from cylinder one was used for the burn rate analysis.

In order to assess the behavior of all the sub-models and the overall burn rate model, a wide variety of operating conditions were tested. Tables 4-1 and 4-2 list all the conditions tested both at the Sloan Lab. and Chrysler. In each condition, multiple cycles (at least 100) of pressure data were taken to ensure statistical validity.

4.3 Wall Temperature

In a firing engine, the distribution of the combustion chamber wall temperature is complicated. The wall temperature varies between different parts of the cylinder: piston crown, cylinder head, and cylinder liner. The wall temperature undergoes a small cyclical changes every cycle which is neglected. The wall temperature is controlled by engine speed, load, equivalence ratio, compression ratio, spark timing, charge motion, inlet temperature, wall material, and coolant temperature. It would require a too sophisticated a model for the burn rate analysis to predict the wall temperature. Therefore, the burn rate analysis assumes a constant wall temperature which is chosen based on the equivalence ratio only. Table 4-3 lists the criteria for choosing the wall temperature. In order to ensure the constant temperature assumption is adequate, a sensitivity test was done to check that reasonable variations in wall temperature has no drastic effect on the overall burn rate analysis.

Table 4-4 and Figure 4-1 show that the peak fraction burned and heat transfer changes little with wall temperature (< 1% for ΔT_w=100K) at operating conditions ranging from idle to WOT. The influence of wall temperature on heat transfer is larger at idle and part load than that of WOT. In addition, heat transfer per cycle is lower at high speed because of the shorter cycle time. Thus, changing of the wall temperature has less effect at high speed.

The sensitivity test shows that the heat transfer model and the overall analysis are insensitive to reasonable changes in the wall temperature. Hence, an approximate estimate of the wall temperature should be adequate.

4.4 Heat Transfer Calibration Constants

In the heat transfer model, two constants (c_1 and c_2) are included to calibrate the effect of heat transfer on the overall analysis and to balance the dimensions. These two constants are not physical quantities like wall temperature and may differ from engine to

engine. Therefore, c_1 and c_2 are calibrated with actual firing engine data. c_1 and c_2 are to be varied systematically from 0.7 to 1.3. The set of c_1, c_2 that gives the most consistent value for the peak fraction burned at different conditions is then chosen.

Table 4-5 and Figure 4-2 summarize the results of our parametric study. The results show that the combination of c_1=1 and c_2=1 gives more reasonable fraction burned values than other combinations most of the time. This conclusion agrees with the study done by Gatowski et al. in their original energy release analysis paper [2]. However, contrary to Gatowski's study, my results suggest that the analysis is quite sensitive to c_1 and c_2 especially at low speed. One possible source of differences could be the form of the convective heat transfer coefficient (h_c). In Gatwoski's paper, h_c has a constant coefficient of $131c_1$ and the bore has an exponent of 0.2 whereas h_c has a coefficient of c_1 and the bore is raised to a power of -0.2 in Woschni's correlation and the burn rate analysis. It is not completely clear how Gatowski obtained his correlation. This difference may also explain why Gatowski could vary c_1 from 0.75 to 2 and c_2 from 0 to 2 without causing major error in the analysis results.

4.5 Swirl Ratio

In the characteristic speed term of the heat transfer model, the effect of charge motion is included in the form of the mean swirl velocity. The swirl velocity is defined by the swirl ratio which is inputted by the user of the analysis. In most modern engine, there is some organized charge motion to enhance combustion speed; at the same time this increases heat transfer. Therefore, the swirl ratio can be an important parameter in the heat transfer model in the burn rate analysis. A sensitivity test was done to find out the significance of swirl ratio.

The swirl ratio does have a physical meaning; however, it is not measured during pressure data-acquisition. Thus, it is not always readily known by the user for data analysis. In the sensitivity study, the swirl ratio was varied from 0.0 to 1.5 which

corresponds to 4.4 m/s at 700 rpm and 37.7 m/s at 5000 rpm.

The results in Table 4-6 and Figure 4-3 show that the swirl ratio can have quite an effect on the heat transfer and the fraction burned. Changing R_{swirl} from 0.0 to 0.75 increased the peak fraction burned by about 5% at low speed and part-throttle conditions and about 2% at WOT. The effect R_{swirl} shows the same trend as that of wall temperature. It is more influential at low speed and load than at high speed and load because of the smaller heat transfer effect at high end conditions. Due to its significance, an accurate R_{swirl} will increase the confidence level of the burn rate analysis. R_{swirl} can usually be estimated by past or practical experience.

4.6 Motoring Polytropic Constant

In the heat transfer model (Chapter 2.2.1), the motoring pressure, that is the cylinder pressure without firing, is needed to determine the contribution of combustion to the characteristic velocity, Eq. (2.14). The polytropic relation, $pV^n = constant$, is used to estimate the motoring pressure (p_m).

$$p_m = p_{ivc}(\frac{V_{ivc}}{V})^n \qquad (4.1)$$

Since there is no exact value of n, an arbitrarily chosen constant n within the reasonable range would be used in the heat transfer model of the burn rate analysis. A sensitivity check was done to make sure that this assumption is acceptable, that is, changes in n do not cause big change in the burn rate analysis. Since n has the value of 1.30±0.05 for conventional fuels, it was varied from 1.25 to 1.35 during the sensitivity test.

Table 4-7 indicates that n_{motor} has little, if any, effects on the heat transfer and the peak fraction burned regardless of the operating conditions. Hence, using a constant n_{motor} would be adequate without leading to large error.

4.7 Initial Mass

In the burn rate analysis, the initial mass of mixture inside the cylinder is determined from the air mass flow rate, equivalence ratio, exhaust gas recirculation, and residual fraction. However, during experiment, the air mass flow rate is usually measured with a few percents of error due to the instruments and fluctuation of intake. In addition, the equivalence ratio is not exact either because the precise composition of gasoline is not known. The residual fraction is estimated by a model which can have an error of a few percents. As a result, the initial mass can be as much as five percents different from the exact mass inside the cylinder. Thus, a sensitivity check was done to see how significant this error could be.

In the sensitivity test, the air mass flow rate was varied ±5% from the measured rate; thus inducing a difference of about ±5% in total initial mass. Table 4-8 and Figures 4-4, 4-5 show that lowering and raising the initial mass by 5% can increase or decrease the peak burned fraction by 5 to 7%. The effect of varying the initial mass is closed to linear. Therefore, inaccuracy in the initial mass measurement can lead to a proportional error in the burned fraction results. One should be careful when measuring parameters that are directly related to the initial mass determination.

The peak fraction burned increases when the initial mass decreases because in order to produce the measured pressure history with less fuel, more portion of the fuel will have to be burned. The other side of this reasoning applies to increasing initial mass with lower fraction burned.

4.8 Crevice Volume

Crevice volume is the important parameter in the crevice effect model (Chapter 2.2.2). The model assumes a single aggregated crevice, that is, the crevice volume used in the calculations is the sum of all crevices in the chamber. The exact size of the total crevice is usually not known. Thus, it is customary to assume the crevice volume to be a

of the clearance volume.

The sensitivity check tested three crevice volume sizes: 0%, 1%, and 2% of the clearance volume. Table 4-9 and Figure 4-6 show that the variations of crevice volume has a minor effect on the mass fraction burned. Therefore, the assumption of constant crevice volume at about 1% of the clearance volume [9] should not lead to any major error.

The effect of the different crevice volume is the most obvious at the point of peak burning and near the end of combustion. At the point of peak burning, the pressure is high which pushes unburned mixture into the crevice. A bigger crevice means more gas would be pushed into the crevice and less gas left in the combustion chamber. Thus, a larger crevice volume shows a high peak burning rate. On the other hands, near the end of combustion, cylinder pressure drops and crevice gas returns to the chamber. A larger crevice would mean more unburned gas returns to the chamber at the end of combustion. That is why the burning rate is lower at end of combustion for larger crevice.

File ID	Spark Tim. [degBTC]	Pinlet [bar]	ϕ	Speed [rpm]	Fuel Type	EGR [%]
quench29	39 (MBT)	0.509	0.77	900	indolene	0.0
quench28	35 (MBT)	0.514	0.83	900	indolene	0.0
quench26	28 (MBT)	0.511	1.00	900	indolene	0.0
quench22	40 (MBT)	0.510	0.77	3000	indolene	0.0
quench21	38 (MBT)	0.510	0.83	3000	indolene	0.0
quench13	38 (MBT)	0.485	0.77	900	propane	0.0
quench59	38	0.500	0.77	900	propane	0.0
quench43	38	0.513	0.77	900	propane	0.0
quench11	39 (MBT)	0.514	0.77	3000	propane	0.0
quench35	38	0.514	0.77	3000	propane	0.0
quench30	30 (MBT)	0.521	1.00	900	propane	0.0
quench45	32 (MBT)	0.500	1.00	3000	propane	0.0
g91-11-3	16 (MBT)	1.000	0.94	900	indolene	0.0
g164-3-4	37 (MBT)	0.400	0.96	1600	indolene	0.0
g167-8-4	26 (MBT)	0.700	0.96	1600	indolene	0.0
g16-14-3	20 (MBT)	1.000	0.93	1600	indolene	0.0
g25-9-3	25 (MBT)	1.000	1.00	2500	indolene	0.0

Table 4-1. Sloan Lab. data operating conditions.

File ID	Spark Tim. [degBTC]	Pinlet [bar]	ϕ	Speed [rpm]	Fuel Type	EGR [%]
39_11	6	0.332	1.00	700	indolene	0.0
39_41	20	0.298	1.00	700	indolene	0.0
39_81	40	0.281	1.03	700	indolene	0.0
6_1-1	30 (MBT)	0.408	1.01	1600	indolene	0.0
6_2-1	39 (MBT)	0.408	1.01	3200	indolene	0.0
6_3-1	20	0.421	1.01	1600	indolene	0.0
6_4-1	5	0.506	1.02	1600	indolene	0.0
6_5-1	27 (MBT)	0.689	1.03	1600	indolene	0.0
6_6-1	33 (MBT)	0.646	1.02	3200	indolene	0.0
6_7-1	39 (MBT)	0.438	1.01	1600	indolene	5.4
41_11	12 (MBT)	1.005	1.18	1200	indolene	0.0
41_31	20 (MBT)	1.001	1.17	2000	indolene	0.0
41_51	19 (MBT)	0.985	1.17	2800	indolene	0.0
41_71	17 (MBT)	0.972	1.17	3600	indolene	0.0
41_91	24 (MBT)	0.971	1.17	4400	indolene	0.0
41111	24 (MBT)	0.957	1.16	5200	indolene	0.0
41131	27 (MBT)	0.947	1.17	6000	indolene	0.0

Table 4-2. Chrysler data operating conditions.

Equivalence ratio						Wall temp. [K]
		ϕ	<	0.833	=>	400
0.833	<	ϕ	<	0.900	=>	425
0.900	<	ϕ			=>	450

Table 4-3. Criteria used to determine wall temperature with equivalence ratio.

				Wall temperature					
				400 K		450 K		500 K	
Pinlet [bar]	Speed [rpm]	ϕ	File ID	Peak fct. brn.	Heat tfr. @EVO	Peak fct. brn.	Heat tfr. @EVO	Peak fct. brn.	Heat tfr. @EVO
0.298	700	1.01	39_41	0.8586	0.1143	0.8513	0.1074	0.8449	0.1002
0.408	1600	1.01	6_1-1	0.9834	0.1487	0.9765	0.1424	0.9695	0.1361
0.408	3200	1.01	6_2-1	0.9816	0.1068	0.9764	0.1029	0.9703	0.0977
1.000	1200	1.18	41_11	1.0592	0.1412	1.0555	0.1364	1.0519	0.1317
0.972	3600	1.17	41_71	1.0419	0.0788	1.0392	0.0761	1.0368	0.0735
0.947	6000	1.17	41131	0.9603	0.0641	0.9571	0.0617	0.9543	0.0594

Table 4-4. Effects of wall temperature on peak fraction burned and heat transfer.

Pinlet [bar]	Speed [rpm]	ϕ	File ID	c1	c2	Peak fct. brn.	Heat tfr. @EVO
0.298	700	1.01	39_41	0.7	0.7	0.8116	0.0662
				1.0	1.0	0.8513	0.1074
				1.3	1.3	0.8989	0.1564
				1.0	0.7	0.8378	0.0935
				1.0	1.3	0.8639	0.1209
				0.7	1.0	0.8210	0.0760
				1.3	1.0	0.8816	0.1389
0.408	1600	1.01	6_1-1	0.7	0.7	0.9179	0.0852
				1.0	1.0	0.9765	0.1424
				1.3	1.3	1.0452	0.2111
				1.0	0.7	0.9545	0.1213
				1.0	1.3	0.9968	0.1626
				0.7	1.0	0.9326	0.1000
				1.3	1.0	1.0189	0.1848
0.408	3200	1.01	6_2-1	0.7	0.7	0.9387	0.0644
				1.0	1.0	0.9764	0.1029
				1.3	1.3	1.0213	0.1476
				1.0	0.7	0.9649	0.0918
				1.0	1.3	0.9870	0.1137
				0.7	1.0	0.9464	0.0722
				1.3	1.0	1.0074	0.1336
1.000	1200	1.18	41_11	0.7	0.7	1.0239	0.0794
				1.0	1.0	1.0555	0.1364
				1.3	1.3	1.0979	0.2061
				1.0	0.7	1.0410	0.1130
				1.0	1.3	1.0691	0.1587
				0.7	1.0	1.0332	0.0957
				1.3	1.0	1.0786	0.1770
0.947	6000	1.17	41131	0.7	0.7	0.9448	0.0394
				1.0	1.0	0.9571	0.0617
				1.3	1.3	0.9716	0.0871
				1.0	0.7	0.9535	0.0562
				1.0	1.3	0.9606	0.0670
				0.7	1.0	0.9473	0.0433
				1.3	1.0	0.9670	0.0802

Table 4-5. Parametric study of heat transfer calibration constants.

				Swirl Ratio					
				0		0.75		1.5	
Pinlet [bar]	Speed [rpm]	ϕ	File ID	Peak fct. brn.	Heat tfr. @EVO	Peak fct. brn.	Heat tfr. @EVO	Peak fct. brn.	Heat tfr. @EVO
0.298	700	1.01	39_41	0.8513	0.1074	0.8807	0.1553	0.9262	0.2017
0.408	1600	1.01	6_1-1	0.9765	0.1424	1.0303	0.2002	1.0856	0.2547
0.408	3200	1.01	6_2-1	0.9764	0.1029	1.0280	0.1613	1.0818	0.2152
1.000	1200	1.18	41_11	1.0555	0.1364	1.0667	0.1787	1.0858	0.2191
0.972	3600	1.17	41_71	1.0392	0.0761	1.0490	0.1179	1.0686	0.1564
0.947	6000	1.17	41131	0.9571	0.0617	0.9646	0.1021	0.9824	0.1388

Table 4-6. Effects of swirl ratio on peak fraction burned and heat transfer.

				n(motor)					
				1.25		1.30		1.35	
Pinlet [bar]	Speed [rpm]	ϕ	File ID	Peak fct. brn.	Heat tfr. @EVO	Peak fct. brn.	Heat tfr. @EVO	Peak fct. brn.	Heat tfr. @EVO
0.298	700	1.01	39_41	0.8490	0.1024	0.8501	0.1037	0.8513	0.1074
0.408	1600	1.01	6_1-1	0.9689	0.1385	0.9767	0.1416	0.9765	0.1424
0.408	3200	1.01	6_2-1	0.9772	0.1030	0.9768	0.1026	0.9764	0.1029
1.000	1200	1.18	41_11	1.0549	0.1338	1.0552	0.1347	1.0555	0.1364
0.972	3600	1.17	41_71	1.0392	0.0754	1.0392	0.0756	1.0392	0.0761
0.947	6000	1.17	41131	0.9573	0.0616	0.9572	0.0616	0.9571	0.0617

Table 4-7. Effects of motoring polytropic constant on peak fraction burned and heat transfer.

File ID	Pin [bar]	Speed	ϕ	Lower by 5%		Measured Mass		Inc. by 5%	
				Peak fct. brn.	Heat tfr. @EVO	Peak fct. brn.	Heat tfr. @EVO	Peak fct. brn.	Heat tfr. @EVO
g164-3-4	0.4	1600	0.962	0.9889	0.1505	0.9372	0.1351	0.8864	0.1193
g167-8-4	0.7	1600	0.957	1.0744	0.1736	1.0116	0.1558	0.9649	0.1384
g91-11-3	1.0	900	0.943	0.9883	0.1753	0.9396	0.1559	0.8951	0.1382
g16-14-3	1.0	1600	0.926	0.9871	0.1262	0.9374	0.1131	0.8980	0.1005
quench28	0.51	900	0.833	1.1848	0.2397	1.1243	0.2190	1.0541	0.1905
quench21	0.51	3000	0.833	1.0060	0.0830	0.9587	0.0754	0.9048	0.0669
quench26	0.51	900	1.000	1.1931	0.2821	1.1206	0.2530	1.0623	0.2239

Table 4-8. Effects of varying initial mass on peak fraction burned and heat transfer.

Speed [rpm]	ϕ	Vcrev/ Vclear	Pinlet [bar]	File ID	Peak fct. brn.	Heat tfr. @EVO
900	0.94	0%	1.0	g91-11-3	0.9399	0.1533
900	0.94	1%	1.0	g91-11-3	0.9396	0.1559
900	0.94	2%	1.0	g91-11-3	0.9405	0.1585
1600	0.96	0%	0.4	g164-3-4	0.9301	0.1327
1600	0.96	1%	0.4	g164-3-5	0.9372	0.1351
1600	0.96	2%	0.4	g164-3-6	0.9472	0.1375
2500	1.00	0%	1.0	g25-9-3	0.8683	0.0812
2500	1.00	1%	1.0	g25-9-3	0.8705	0.0837
2500	1.00	2%	1.0	g25-9-3	0.8711	0.0852
900	0.77	0%	0.5	quench29	1.1033	0.1973
900	0.77	1%	0.5	quench29	1.1063	0.1997
900	0.77	2%	0.5	quench29	1.1093	0.2023
900	1.00	0%	0.5	quench26	1.1113	0.2486
900	1.00	1%	0.5	quench26	1.1206	0.2530
900	1.00	2%	0.5	quench26	1.1279	0.2576

Table 4-9. Effects of crevice volume on peak fraction burned and heat transfer.

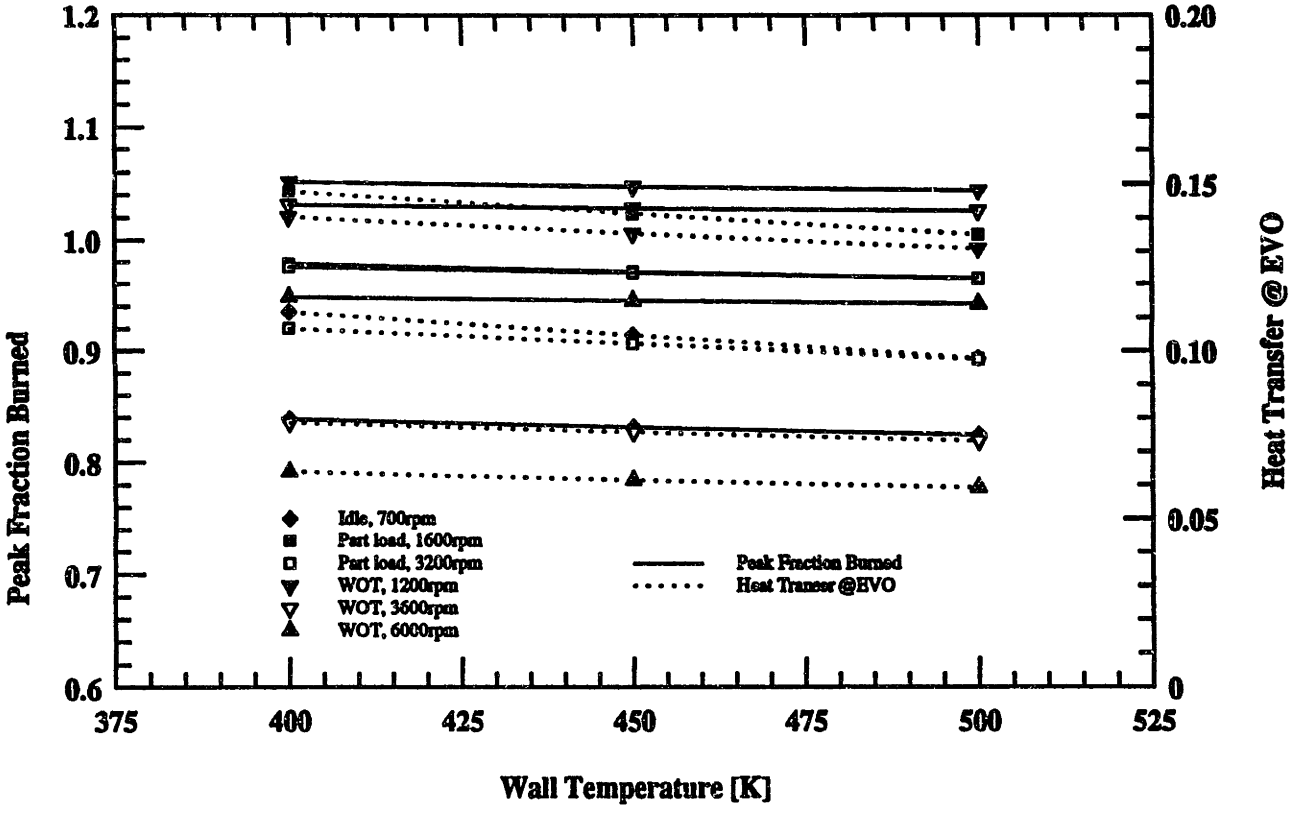

Figure 4-1. Effects of wall temperature on peak fraction burned and heat transfer.

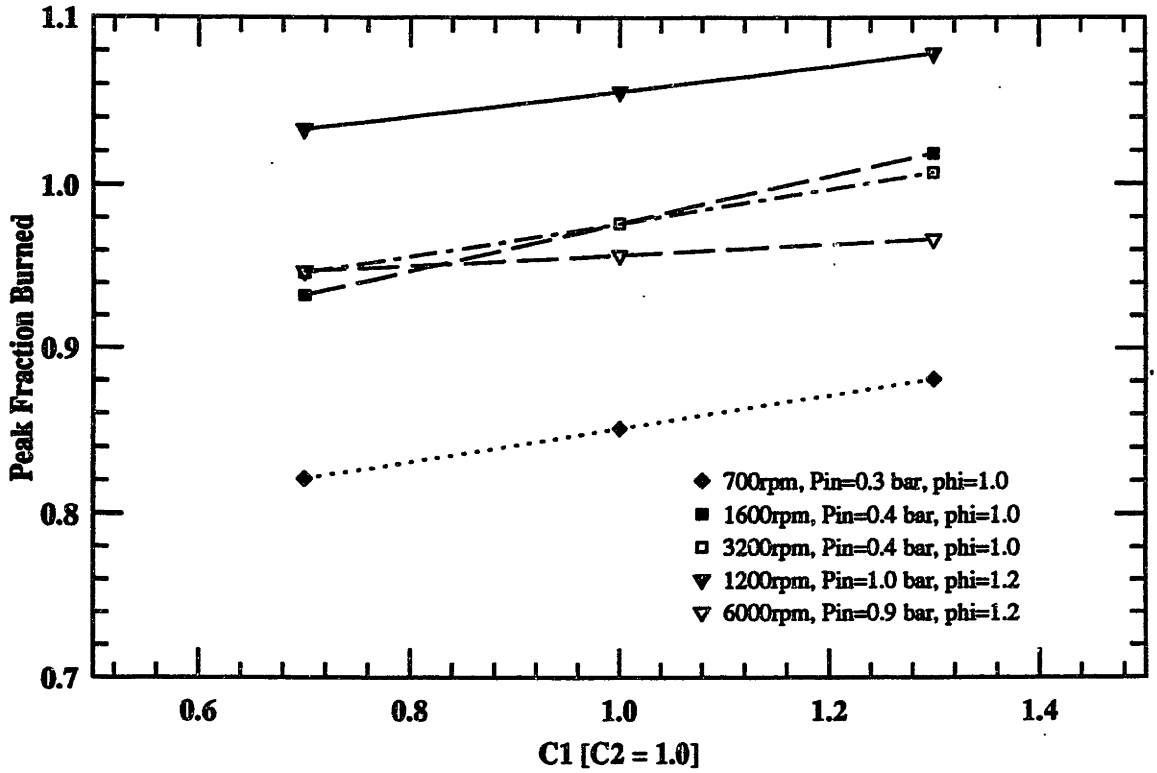

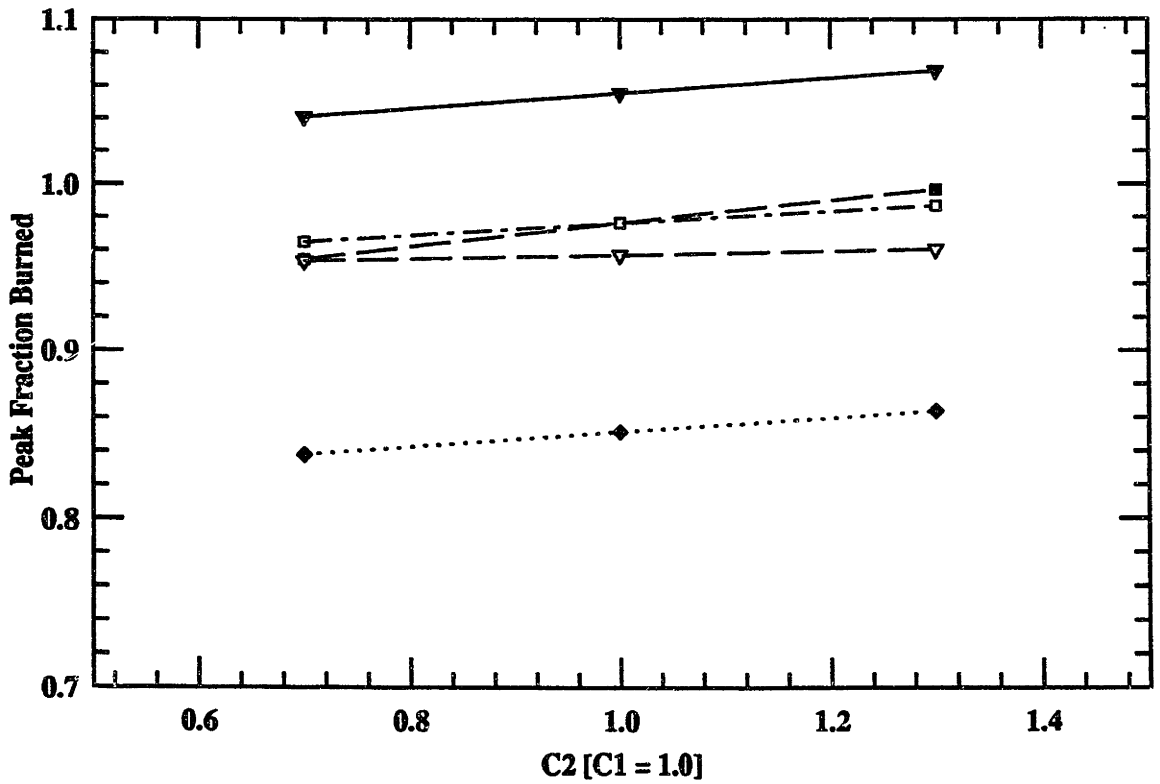

Figure 4-2. Effects of heat transfer calibration constants on peak fraction burned.

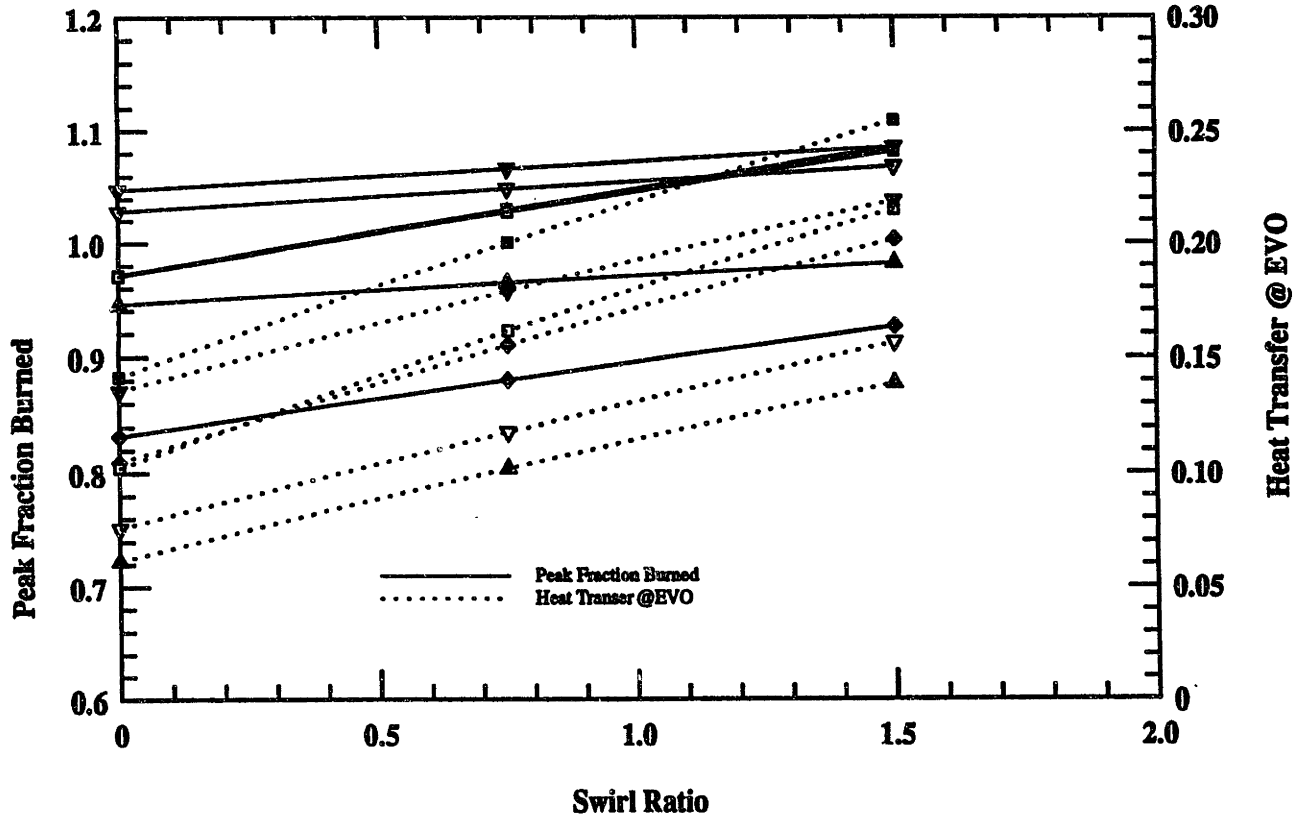

Figure 4-3. Effects of swirl ratio on peak fraction burned and heat transfer.

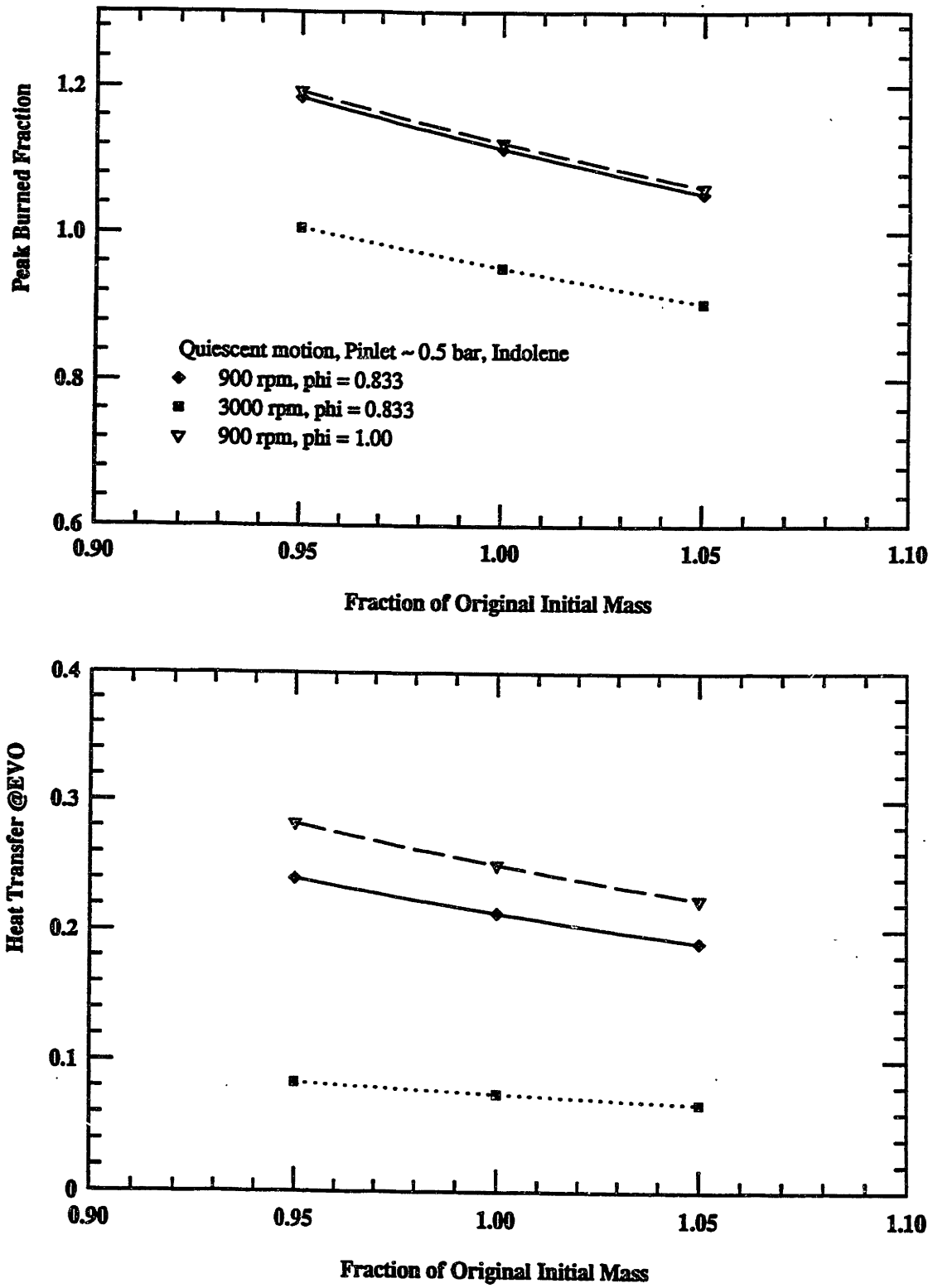

Figure 4-4. Effects of initial mass on peak fraction burned and heat transfer at different speeds.

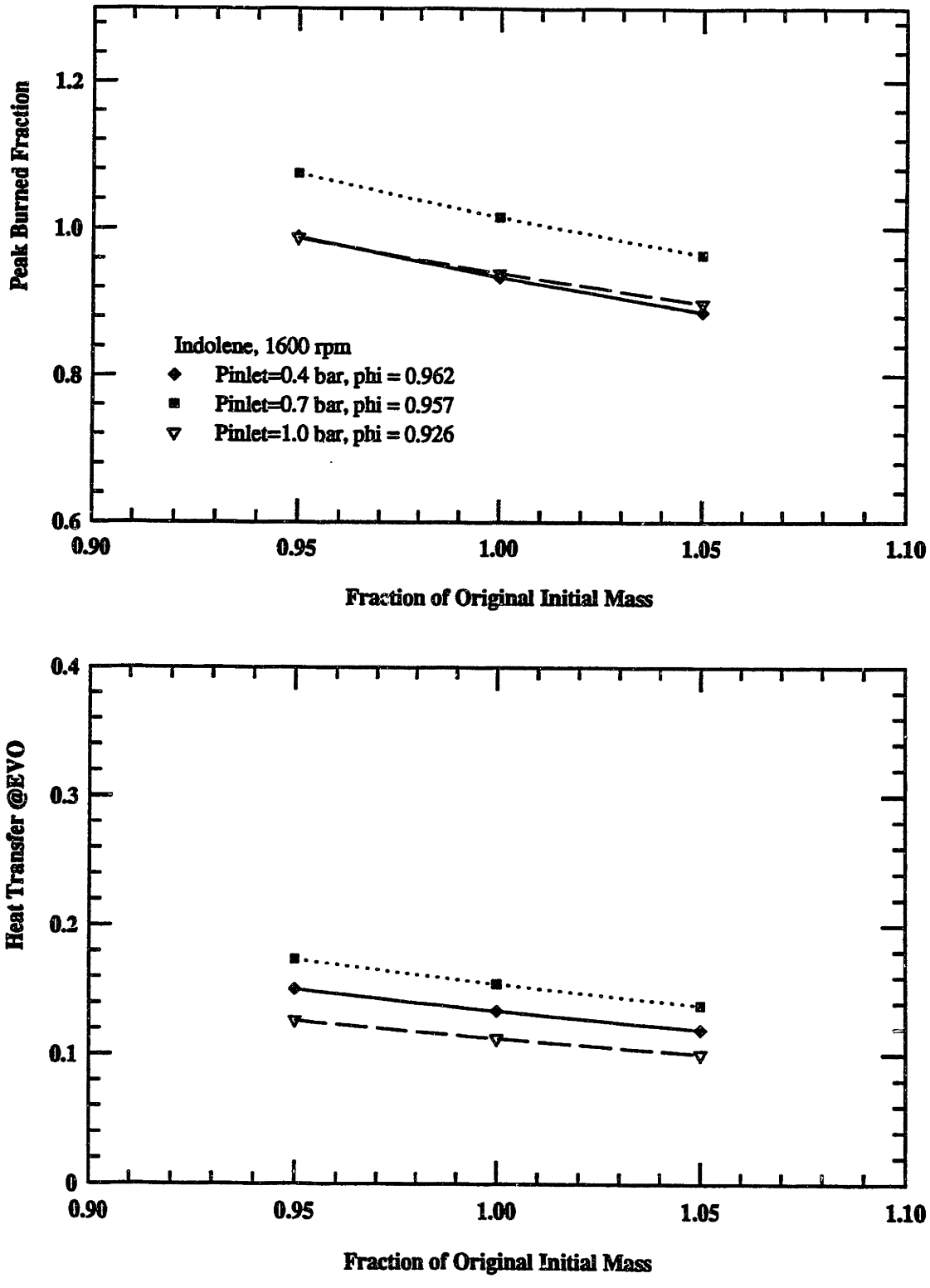

Figure 4-5. Effects of initial mass on peak fraction burned and heat transferat different loads.

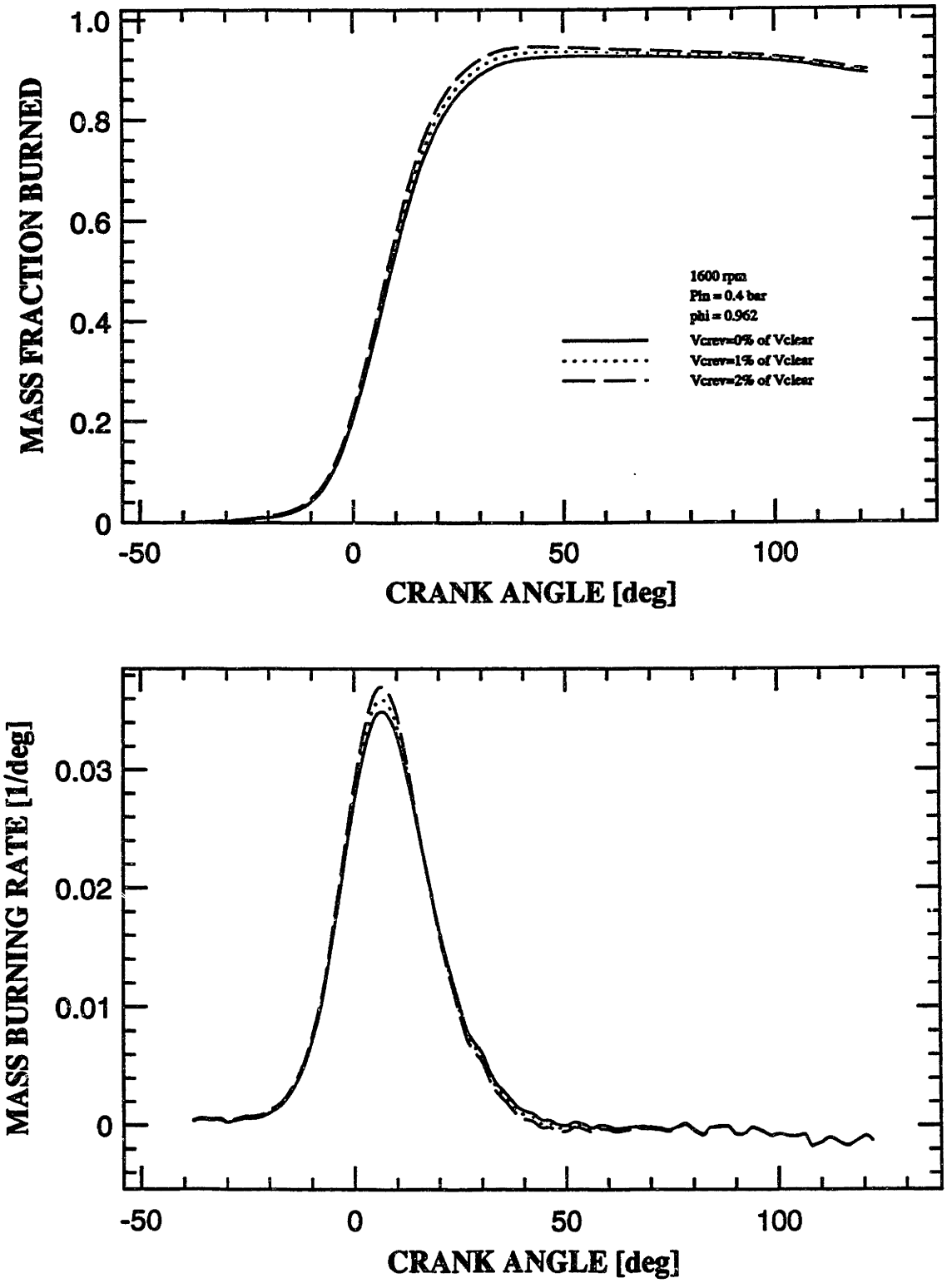

Figure 4-6. Effects of crevice volume on fraction burned and burning rate.

CHAPTER 5 - RESULTS AND DISCUSSION

5.1 Analysis of Data

The burn rate analysis was then tested with pressure data taken from actual firing engine. The conditions for these data were listed in Tables 4-1 and 4-2. This enables us to see how the analysis behaves over the entire range of operation and how compatible the analysis is with pressure data from different engines. These data were divided into three groups: idle, part-load, and wide open throttle (WOT). Within each group, operating parameters were changed to create different scenarios, for example, varying spark timing, speed, and amount of EGR. Analysis results from each group will be discussed in the following sections. The expected value of the maximum mass fraction burned under normal combustion conditions should be about 0.92 to 0.96. Complete combustion is not achieved because there exist unburned fuel in the crevices, quench layers on the cylinder walls, fuel absorption into the oil layer on cylinder liners, and combustion inefficiency. Therefore, the expected peak fraction burned of 0.92-0.96 will be used to compare against the calculated fraction burned from actual data.

5.1.1 Idle Cases

When operating at idle conditions, an engine produces just enough energy to overcome the friction and pumping losses of itself and to sustain its operation. No extra power is generated to carry load. In our analysis, three idle cases with different spark-timings were tested. All three cases were operated at stoichiometric, 700 rpm, and inlet pressure at about 0.3 bar, but with spark-timing of 6°, 20°, and 40° BTC.

The multiple-cycle plots of three idle cases are showed in Figures 5-1 to 5-3. The summaries in Table 5-1 and Figure 5-4 indicate combustion in these idle cases did not come close to complete burning. The closest value was given by the case of spark-timing at 40° BTC, but the result also showed some partial-burned and misfired cycles. The

multiple-cycle plots also show an irregular burning process with significant cycle-to-cycle variations. These phenomena were expected because of the low load condition. The existence of partial-burned and misfired cycles in the 40° BTC-spark-timing case could be due to the advanced timing. Pressure was not high enough at spark to ignite the charge or to sustain combustion even after ignition leading, therefore, to partial-burned and misfired cycles

.

5.1.2 Part Load Cases

An engine spends most of its time operating at part-load conditions when it is on the road. Thus, a number of part-load data were taken at different conditions. Firstly, a spark-sweep was done. Pressure data were taken at stoichiometric, 1600 rpm, and inlet pressure at about 0.4 bar, but with spark-timing of 5°, 20°, and 30° BTC. Figures 5-5 to 5-7 show the fraction burned profiles for these cases. The results in Table 5-2 and Figure 5-8 show that the combustion process reaches reasonable level except at the extremely retarded spark-timing (5° BTC). The multiple-cycle plots in Figures 5-5 and 5-6 show that the burning processes are more regular with less cycle-to-cycle variation at part load with logical spark-timings. At conditions with overly retarded spark-timing (5° BTC), cycle-to-cycle variation becomes prominent again. Increasing irregularity is expected at extreme conditions like this.

Then, data at two different loads at two speeds were analyzed. The operating conditions for these two sets of data are: stoichiometric, inlet pressure of 0.4 bar and 0.7 bar at 1600 rpm, and 0.4 bar and 0.65 bar at 3200 rpm. Figures 5-9 to 5-11 along with Figure 5-5 show the fraction burned and burning rate of five consecutive cycles for each of the conditions. The combined results are showed in Table 5-3 and Figure 5-12. At low load, the two speeds gave almost identical peak burned fractions, but the 1600 rpm had a slightly higher peak burned fraction at the higher load. Apart from the 1600 rpm high load, all other conditions show consistent peak fraction burned. Since the engine was

operated at part-load and MBT timing, cycle-to-cycle variations are less comparing to the idle cases.

Two more part-load cases involving EGR were provided by Chrysler. Both data were taken at 1600 rpm, stoichiometric, inlet pressure at 0.4 bar, MBT timing, and %EGR at 0% and 5.4%. The focus is to see the effect of EGR on the analysis. The results are showed in Table 5-4 and Figure 5-13. Both cases show reasonable level of fraction burned. The small amount of EGR does not appear to affect the analysis a great deal. The analysis should be able to handle data with moderate amount of EGR.

In addition to the Chrysler data, some part-load data were also taken from Fox [7] of the Sloan Lab. (Chapter 4.2). These data were taken at conditions ranging from lean to stoichiometric with speed at 900 or 3000 rpm. The burn rate analysis results are showed in Table 5-5 and Figure 5-14. The peak fraction burned is consistently higher at 900 rpm than that of 3000 rpm for both indolene and propane fuels. At the same speed, the fraction burned is relatively stable across the range of equivalence ratios although partial-burned cycles occur at low equivalence ratio (0.77). This is expected because the extremely lean mixture may cause problem at ignition and combustion. The consistency across the equivalence ratios shows that the burn rate analysis is adequate at different equivalence ratios. The effects of engine speed on the analysis may require further studies.

The second set of part-load data taken by Fox included three different charge motions: quiescent, swirl, and tumble. The fuel used was propane and the fuel-air ratio is 0.77. Results which are showed in Table 5-6 and Figure 5-15 display the similar trend as the previous set. The peak fraction burned is higher at low speed than at high speed. All fraction burned values at low speed are higher than 1.0. In terms of charge motion, the fraction burned increases from quiescent motion to swirl to tumble.

Keep in mind that the data with different charge motions were taken with propane fuel at very lean conditions. Comparing the Chrysler data to Sloan Lab. data, the Chrysler

data gave much more reasonable and consistent fraction burned values. This may indicate problems in the Sloan Lab. cylinder pressure data.

5.1.3 Wide Open Throttle Cases

After testing the analysis with idle and part-load data, WOT data from both Chrysler and Sloan Lab. were analyzed. In a road engine, WOT is usually accompanied by overfueling which means that the relative fuel-air ratio is rich ($\phi > 1.0$) to ensure maximum power output. The Chrysler WOT data were taken at equivalence ratio of 1.17.

Figures 5-16 to 5-18 show the multiple-cycle burn rate profiles for three of the Chrysler WOT cases. Table 5-7 and Figure 5-19 summarize the results of the WOT data with engine speed varying from 1200 rpm to 6000 rpm. Figure 5-19 displays the same trend that was observed with the part-load data. Fraction burned is higher at low speed than at high speed. However, in the part-load case, the fraction burned value reaches normal at about 3000 rpm whereas in the WOT case, the fraction burned would not fall below 1.0 until 4000 rpm. Thus, there may be additional factors affecting the WOT analysis.

One possibility is the thermal shock to the pressure transducer during pressure data measurement. The engine runs hotter and at higher pressure at WOT than at part-load. This higher temperature may cause drift to the transducer which leads to error in pressure data. According to Chrysler engineers, transducer thermal effect could exist in their data. The analysis of the Chrysler data also show a high level of cycle-to-cycle variations. The fraction burned and burning rate profiles both show a great deal of irregularity which may indicate noise in the pressure data. This could also contribute to error in the analysis.

The second set of WOT data were taken by Min [9] of the Sloan Lab. Instead of using rich mixture like Chrysler data, the Sloan Lab. data were taken at near stoichiometric conditions with speeds at 900 rpm, 1600 rpm, and 2500 rpm. Table 5-8

and Figure 5-20 show the analysis results. The peak fraction burned at 900 rpm and 1600 rpm are both reasonable while the value at 2500 rpm is too low.

Since the Chrysler WOT results display an over-sensitivity to low speed, an additional study was done to examine the influence the heat transfer model speed exponent, m, in Eq. (2.13) has on the overall analysis. The Chrysler 4400 rpm WOT data set was selected to be the baseline case because of its reasonable peak fraction burned. In both Woschni's and Gatowski's works, m was set to be 0.8. In our study, m was changed to 0.7 and 0.9. In order to keep the total heat transfer and fraction burned to be constants for the baseline case, the heat transfer calibration constant, c_1, was adjusted at the same time. The new combinations of m and c_1 were then used to analyze the 1200 rpm WOT data. Table 5-9 shows the combinations of m and c_1 used, and the results. The new speed exponent exhibits little effect on the fraction burned (<0.5%). This led us to conclude that the decrease of peak fraction burned from above 1.0 at low speed to below 1.0 at high speed is not primarily caused by the speed component in the heat transfer model.

Since the parameters in the analysis were unable to account for the discrepancies between the calculated and expected results, the quality of pressure data became a question. A sensitivity test was done to investigate the effects of uncertainty in pressure measurement on the burn rate analysis. Three cases were chosen for the test: one at part-load condition and two at WOT conditions. The original pressure data of these cases were scaled up and down by 5% to see the changes in the peak fraction burned results. Table 5-10 and Figure 5-21 summarize the outcome of the test. The burn rate analysis forms an almost one-to-one relation with the scaling. A change of 5% on the pressure data leads to a 5% - 6% variation in the peak fraction burned. Hence, the burn rate analysis is sensitive to errors in the pressure measurements. Errors in pressure data are potentially larger at WOT conditions than at moderate conditions due to the higher pressure transducer thermal loading. Therefore, the discrepancy in the analysis results of some of the cases could come from errors in the pressure data.

The table below summaries the sensitivity of the burn rate predictions to the key parameters:

Parameters	Changes to parameters	Resulting changes to peak fct. burned
wall temperature	±50 K	∓ 0.5%
swirl ratio	0 - 0.75	+ 2% - 5%
heat tfr. const., c1	±30% (c2=const)	± 1% - 4%
heat tfr. const., c2	±30% (c1=const)	± 1% - 2%
crevice volume	±1% of clear. vol.	± 0.5% - 1%
motoring poly. const.	1.30±0.05	± <1%
initial mass	±5%	∓ 4% - 6%
heat tfr. exponent	0.8±0.1	± <1%
inaccuracy in pressure	±5%	± 5% - 6%

Table 5-11. Summary of sensitivity of burn rate predictions to key parameters.

5.2 Results of Other Pressure-Related Calculations

In addition to the standard burn profile results, the analysis also incorporates several other pressure-related computations that were described in Chapter 3. Table 5-12 summaries some of the results obtained from the Chrysler data. The outcomes of these calculations suggest that there is a correlation between these results and the quality of the pressure data. For example, the data sets that give unusually large polytropic constants (>1.33) also have abnormal burning profiles or unexpected peak fraction burned. The average exhaust pressure for some of the WOT conditions are too low which suggest there is problem with the pressure measurement. Therefore, these calculations not only provide information about the combustion process but also serve as a check on the quality of the pressure measurements.

5.3 Summary and Conclusions

The motivation for this work was to develop and implement a robust and flexible burn rate analysis to replace the earlier Rassweiler and Withrow model for practical use in the industry. Based on the energy release approach, the overall burn rate analysis is comprised of several sub-models to account for the individual effect inside the combustion chamber which includes heat transfer, crevice, and residual gas fraction. Each of these sub-models was assessed and recalibrated, if needed. In addition, one of the major parameter used in the burn rate calculation, the ratio of specific heats, γ, was determined by matching the one-zone analysis to a more accurate two-zone simulation. The results of this matching process were shown to be satisfactory. Therefore, a number of γ's were generated at various initial burned gas fractions, equivalence ratios ranging from lean to rich, and fuel types including iso-octane, propane, methanol, and methanol-gasoline mixtures.

In order to make the analysis more complete for all users, additional pressure-related computations are included into the package. The complete burn rate analysis was implemented on PC based computers. Since the code used were FORTRAN 77, it could be transferred to other computing platforms without many alterations. Because of the simplicity of the one-zone model and the speed of modern computers, the program can analyze several hundreds continuous cycles in a minute. Its speed and flexibility should also allow the analysis to be directly connected to the data-acquisition systems for immediate post-processing of pressure data..

The conclusions of this work may be stated as follow:

1. The energy-release based burn rate analysis can provide more information about the combustion process. It includes the standard burn profile parameters, identifies partial burns, misfires, quantifies heat transfer, and crevice effects.

2. When used with pressure data at moderate engine operating conditions at which road engines operate most of the time, the burn rate analysis predicts burn profiles and maximum mass fraction burned which agree well with expected values.
3. The sensitivities of the burn rate predictions to some of the key parameters have been identified. The most important parameters are initial mass, accuracy of pressure data, and the swirl ratio. The heat transfer model variables are less significant. Less important still are the crevice volume, wall temperature and the motoring polytropic constant.
4. When the model predictions show discrepancy between the calculated peak mass fraction burned and the expected value of this parameter, the problems are most likely to be caused by inaccuracies with the cylinder pressure. The quality of pressure data appears to be worst at WOT possibly due to the high thermal loading on the pressure transducer.

Spark Tim. [degBTC]	Pinlet [bar]	File ID	Peak fct. brn.	Standard deviation	Heat tfr. @EVO	Standard deviation
6	0.332	39_11	0.8728	0.0433	0.0868	0.0122
20	0.298	39_41	0.8513	0.0723	0.1074	0.0243
40	0.281	39_81	0.9228	0.0667	0.2038	0.0482 *

* This data set contained misfired and partial-burned cycles which were not included in the averaging.

Table 5-1. Results of Chrysler idle conditions at various spark-timing.
Speed=700 rpm, Phi=1.0, fuel=indolene.
Average over 100 cycles.

Spark Tim. [degBTC]	Pinlet [bar]	File ID	Peak fct. brn.	Standard deviation	Heat tfr. @EVO	Standard deviation
30	0.408	6_1-1	0.9765	0.0138	0.1424	0.0107
20	0.421	6_3-1	0.9867	0.0128	0.1152	0.0078
5	0.506	6_4-1	0.9783	0.0133	0.0726	0.0048

Table 5-2. Results of Chrysler part-load conditions at various spark-timings.
Speed=1600 rpm, Phi=1.0, fuel=indolene.
Averaged over 100 cycles.

Speed [rpm]	Pinlet [bar]	File ID	Peak fct. brn.	Standard deviation	Heat tfr. @EVO	Standard deviation
1600	0.408	6_1-1	0.9765	0.0138	0.1424	0.0107
1600	0.689	6_5-1	1.0156	0.0130	0.1562	0.0089
3200	0.408	6_2-1	0.9764	0.0162	0.1029	0.0084
3200	0.646	6_6-1	0.9762	0.0326	0.1015	0.0072

Table 5-3. Results of Chrysler part-load conditions at two loads and speeds.
Phi=1.0, fuel=indolene, MBT timing.
Averaged over 100 cycles.

EGR [%]	Pinlet [bar]	File ID	Peak fct. brn.	Standard deviation	Heat tfr. @EVO	Standard deviation
0	0.408	6_1-1	0.9765	0.0138	0.1424	0.0107
5.4	0.438	6_7-1	0.9772	0.0153	0.1522	0.0119

Table 5-4. Results of Chrysler part-load conditions with and without EGR.
Phi=1.0, fuel=indolene, MBT timing.
Averaged over 100 cycles.

Speed [rpm]	φ	Fuel type	Pinlet [bar]	File ID	Peak fct. brn.	Standard deviation	Heat tfr. @EVO	Standard deviation
900	0.77	indolene	0.509	quench29	1.1428	0.0774	0.1997	0.0522 *
900	0.83	indolene	0.514	quench28	1.1243	0.0277	0.2190	0.0388
900	1.00	indolene	0.511	quench26	1.1206	0.0109	0.2530	0.0217
3000	0.77	indolene	0.510	quench22	0.9353	0.0835	0.0681	0.0155 *
3000	0.83	indolene	0.510	quench21	0.9587	0.0181	0.7540	0.0106
900	0.77	propane	0.485	quench13	1.1063	0.0168	0.2399	0.0289
900	1.00	propane	0.521	quench30	1.1287	0.0128	0.3348	0.0217
3000	0.77	propane	0.514	quench11	0.9292	0.0140	0.0855	0.0087
3000	1.00	propane	0.500	quench45	0.8954	0.0091	0.0885	0.0054

* This data set contained misfired and partial-burned cycles which were not included in the averaging.

Table 5-5. Results of Sloan Lab. part-load conditions at twospeeds and various equivalence ratios. MBT timing. Averaged over 500 cycles.

Speed [rpm]	Charge motion	Pinlet [bar]	File ID	Peak fct. brn.	Standard deviation	Heat tfr. @EVO	Standard deviation
900	quiescent	0.485	quench13	1.1063	0.0168	0.2399	0.0289
900	swirl	0.500	quench59	1.2106	0.0186	0.3457	0.0301
900	tumble	0.513	quench43	1.2774	0.0392	0.3668	0.0424
3000	quiescent	0.514	quench11	0.9292	0.0140	0.0855	0.0087
3000	tumble	0.514	quench35	1.0069	0.0113	0.1237	0.0127

Table 5-6. Results of Sloan Lab. part-load conditions with various charge motion.
Phi=0.77, fuel=propane, MBT timing.
Averaged over 500 cycles.

Speed [rpm]	Pinlet [bar]	ϕ	File ID	Peak fct. brn.	Standard deviation	Heat tfr. @EVO	Standard deviation
1200	1.005	1.178	41_11	1.0555	0.0083	0.1364	0.0054
2000	1.001	1.174	41_31	1.0789	0.0088	0.1232	0.0058
2800	0.985	1.165	41_51	1.0341	0.0055	0.0872	0.0044
3600	0.972	1.165	41_71	1.0392	0.0062	0.0761	0.0028
4400	0.971	1.171	41_91	0.9877	0.0067	0.0718	0.0025
5200	0.957	1.164	41111	0.9641	0.0060	0.0621	0.0028
6000	0.947	1.168	41131	0.9571	0.0085	0.0617	0.0026

Table 5-7. Results of Chrysler WOT conditions at various speeds.
MBT timing, fuel=indolene.
Averaged over 100 cycles.

Speed [rpm]	Pinlet [bar]	ϕ	File ID	Peak fct. brn.	Standard deviation	Heat tfr. @EVO	Standard deviation
900	1.000	0.943	g91-11-3	0.9396	0.0118	0.1559	0.0089
1600	1.000	0.926	g16-14-3	0.9374	0.0131	0.1131	0.0081
2500	1.000	1.000	g25-9-3	0.8705	0.0143	0.0837	0.0062

Table 5-8. Results of Sloan Lab. WOT conditions at various speeds.
MBT timing, fuel=indolene.
Averaged over 500 cycles.

Speed [rpm]	Pinlet [bar]	ϕ	File ID	c1	c2	Heat tfr. exponent	Peak fct. brn.	Heat tfr. @EVO
4400	0.971	1.17	41_91	1	1	0.8	0.9877	0.0718
4400	0.971	1.17	41_91	1.3	1	0.9	0.9892	0.0705
4400	0.971	1.17	41_91	0.75	1	0.7	0.9853	0.0715
1200	1.005	1.18	41_11	1	1	0.8	1.0555	0.1364
1200	1.005	1.18	41_11	1.3	1	0.9	1.0527	0.1239
1200	1.005	1.18	41_11	0.75	1	0.7	1.0567	0.1475

Table 5-9. Sensitivity of burn rate analysis to heat transfer exponent.
Averaged over 100 cycles.

				Pressure trace lowered by 5%		With measured pressure trace		Pressure trace raised by 5 %	
Pinlet [bar]	Speed [rpm]	ϕ	File ID	Peak fct. brn.	Heat tfr. @EVO	Peak fct. brn.	Heat tfr. @EVO	Peak fct. brn.	Heat tfr. @EVO
0.408	1600	1.01	6_1-1	0.9295	0.1275	0.9765	0.1424	1.0225	0.1580
1.005	1200	1.18	41_11	0.9991	0.1223	1.0555	0.1364	1.1122	0.1513
0.971	4400	1.17	41_91	0.9366	0.0650	0.9877	0.0718	1.0388	0.0789

Table 5-10. Sensitivity of burn rate analysis to uncertainity in pressure data.
Averaged over 100 cycles.

Type of conditions	File ID*	Polytropic const. ** compr.	exp.	Eff. Rc	Energy losses exp. blow. [bar]	exh. blow. [bar]	exh. thr. [bar]	Mean exh. prs. [bar]	isfc [g/kW hr]
idle	39_11	1.26	1.36	10.12	0.0365	0.0000	0.0000	1.000	1089.1
idle	39_41	1.29	1.45	9.99	0.0087	0.0000	0.0000	1.013	1055.2
idle	39_81	1.28	1.43	9.53	-0.0095	0.0000	0.0000	0.981	767.1
part-load	6_1-1	1.27	1.27	10.40	0.0302	0.0000	0.0000	1.036	296.8
part-load	6_2-1	1.39	1.24	10.02	0.0289	0.0000	0.0000	1.074	283.0
part-load	6_3-1	1.28	1.28	10.19	0.0381	0.0000	0.0000	1.031	300.8
part-load	6_4-1	1.25	1.29	9.96	0.0555	0.0000	0.0000	1.035	360.5
part-load	6_5-1	1.29	1.26	10.12	0.0584	8.19E-06	0.0000	1.020	247.6
part-load	6_6-1	1.36	1.24	10.61	0.0446	0.0267	0.0000	1.105	247.5
part-load	6_7-1	1.30	1.27	10.22	0.0333	0.0000	0.0000	1.004	291.7
part-load	6_8-1	1.29	1.28	10.10	0.0453	0.0000	0.0000	1.006	309.1
WOT	41_11	1.30	1.47	10.59	0.1610	0.0000	0.0193	0.409	268.6
WOT	41_31	1.39	1.39	10.38	0.1380	0.0041	0.0587	0.384	242.9
WOT	41_51	1.36	1.50	11.04	0.1130	0.0163	0.0111	0.158	260.8
WOT	41_71	1.34	1.50	12.10	0.0944	0.0240	0.0000	0.347	266.0
WOT	41_91	1.32	1.51	11.85	0.0481	0.0196	0.0000	0.825	285.8
WOT	41111	1.34	1.51	12.33	0.0255	0.0353	0.0000	0.960	296.1
WOT	41131	1.36	1.46	11.90	-0.0117	0.0576	0.0701	1.250	313.5

* For operating conditions of these pressure data, see Table 4-2.

** For detail definitions of all the calculated quantities, see Chapter 3.

Table 5-12. Results of additional pressure-related calculations.

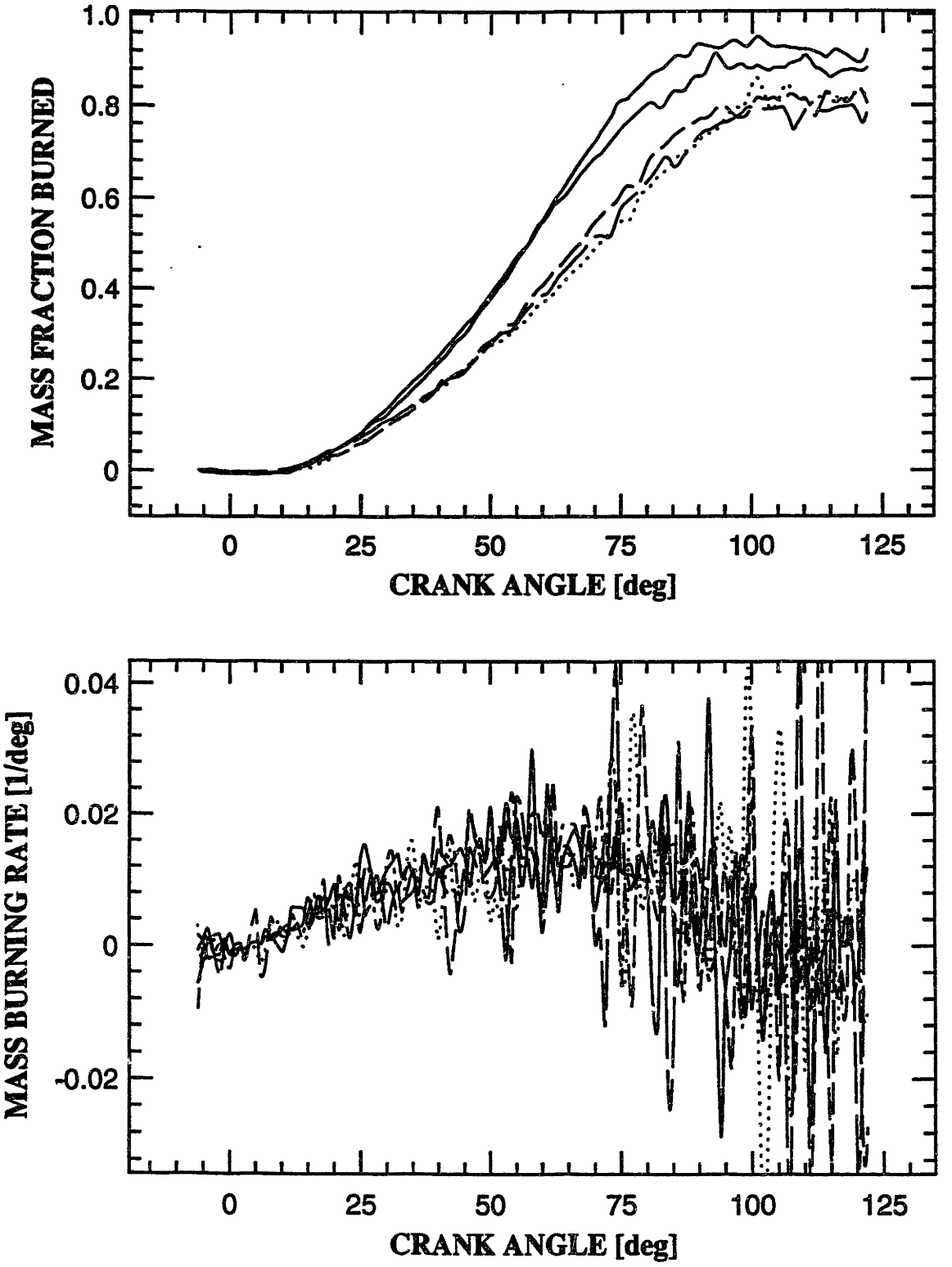

Figure 5-1. Mulitple-cycle burn rate plot for idle data 39_11, P_{in}=0.3 bar, 700 rpm, ϕ=1.0, 6°BTC spark, indolene.

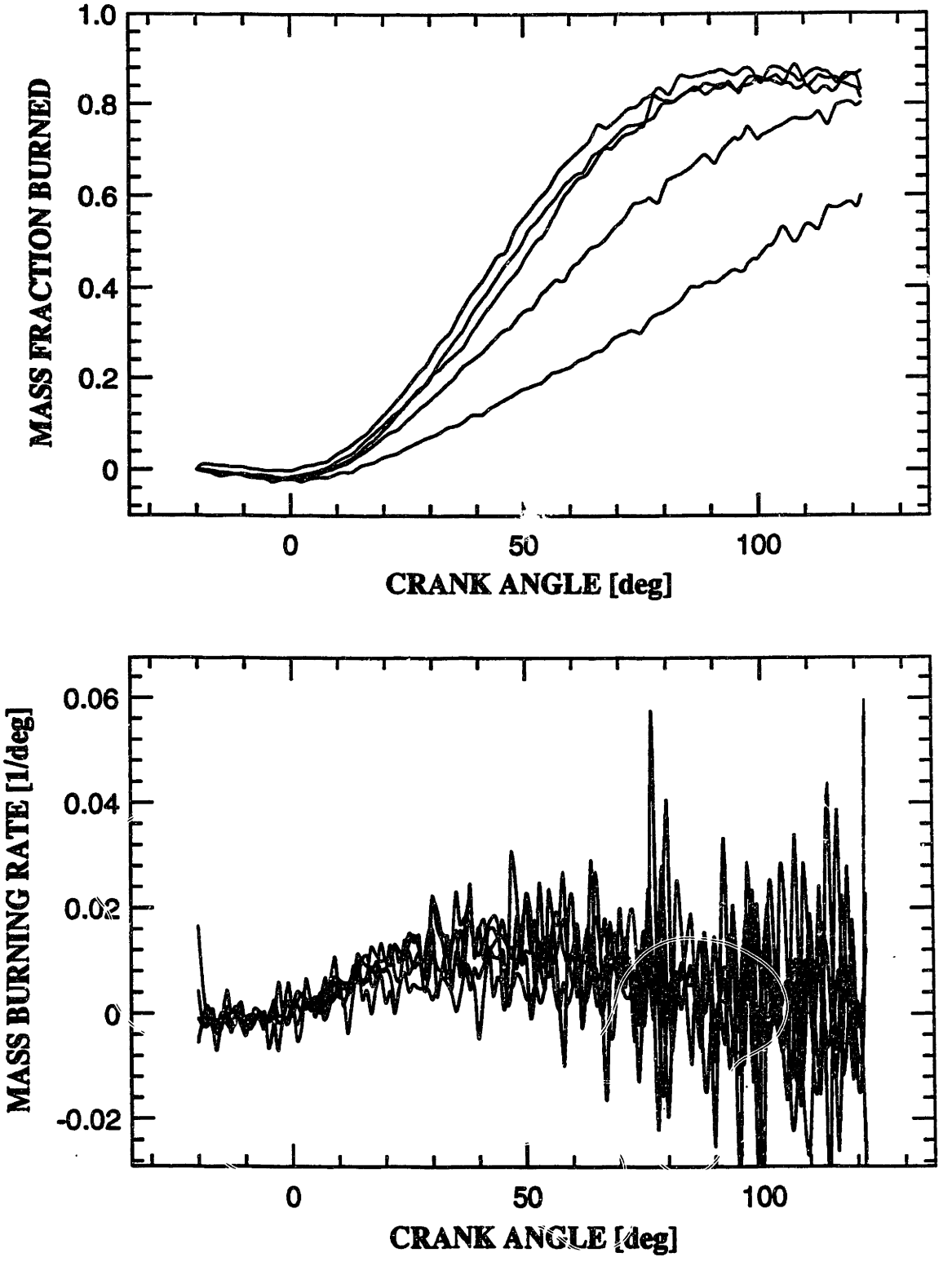

Figure 5-2. Mulitple-cycle burn rate plot for idle data 39_41, P_{in}=0.3 bar, 700 rpm, ϕ=1.0, 20°BTC spark, indolene.

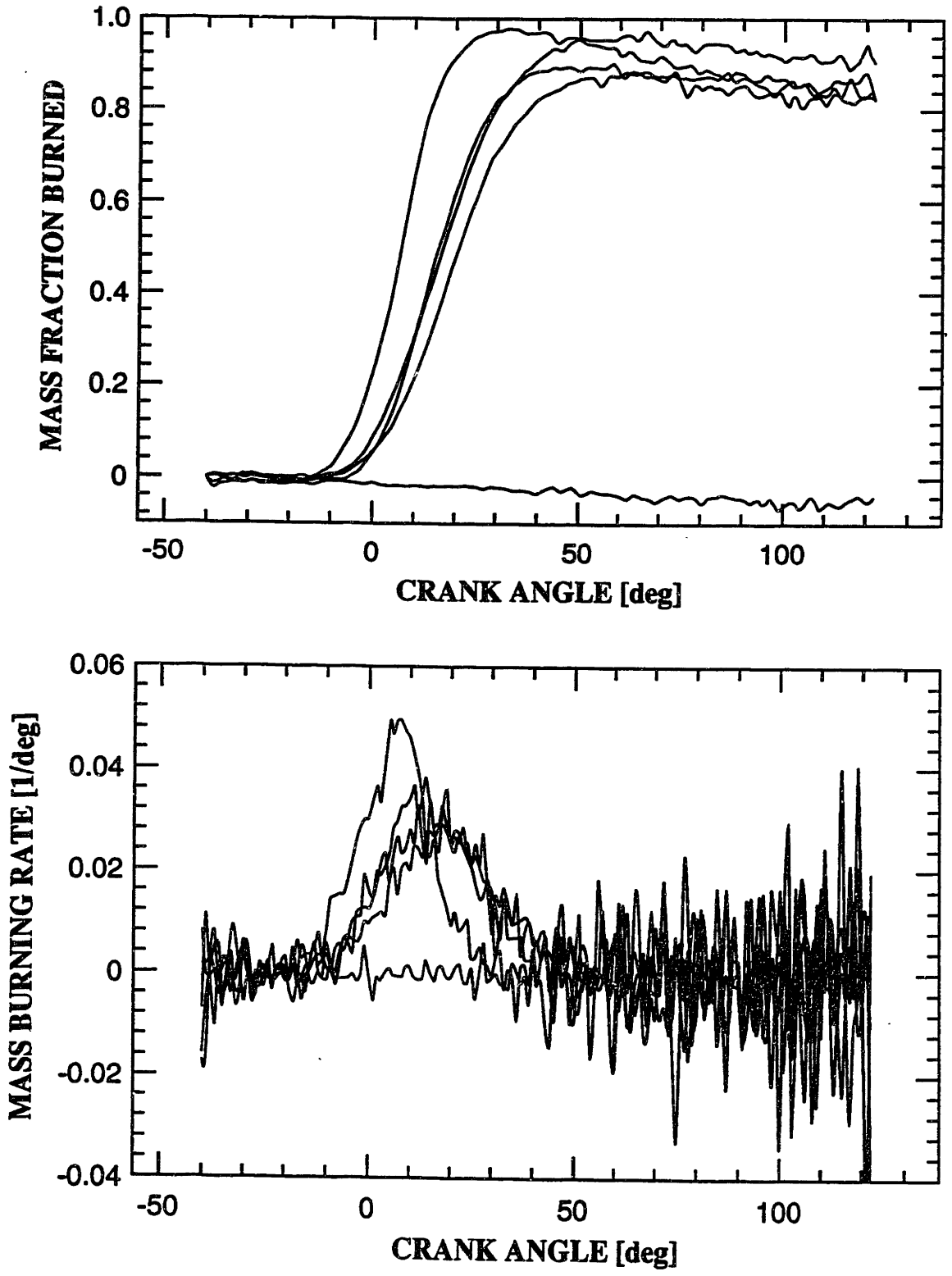

Figure 5-3. Mulitple-cycle burn rate plot for idle data 39_81, P_{in}=0.3 bar, 700 rpm, ϕ=1.0, 40^{o}BTC spark, indolene.

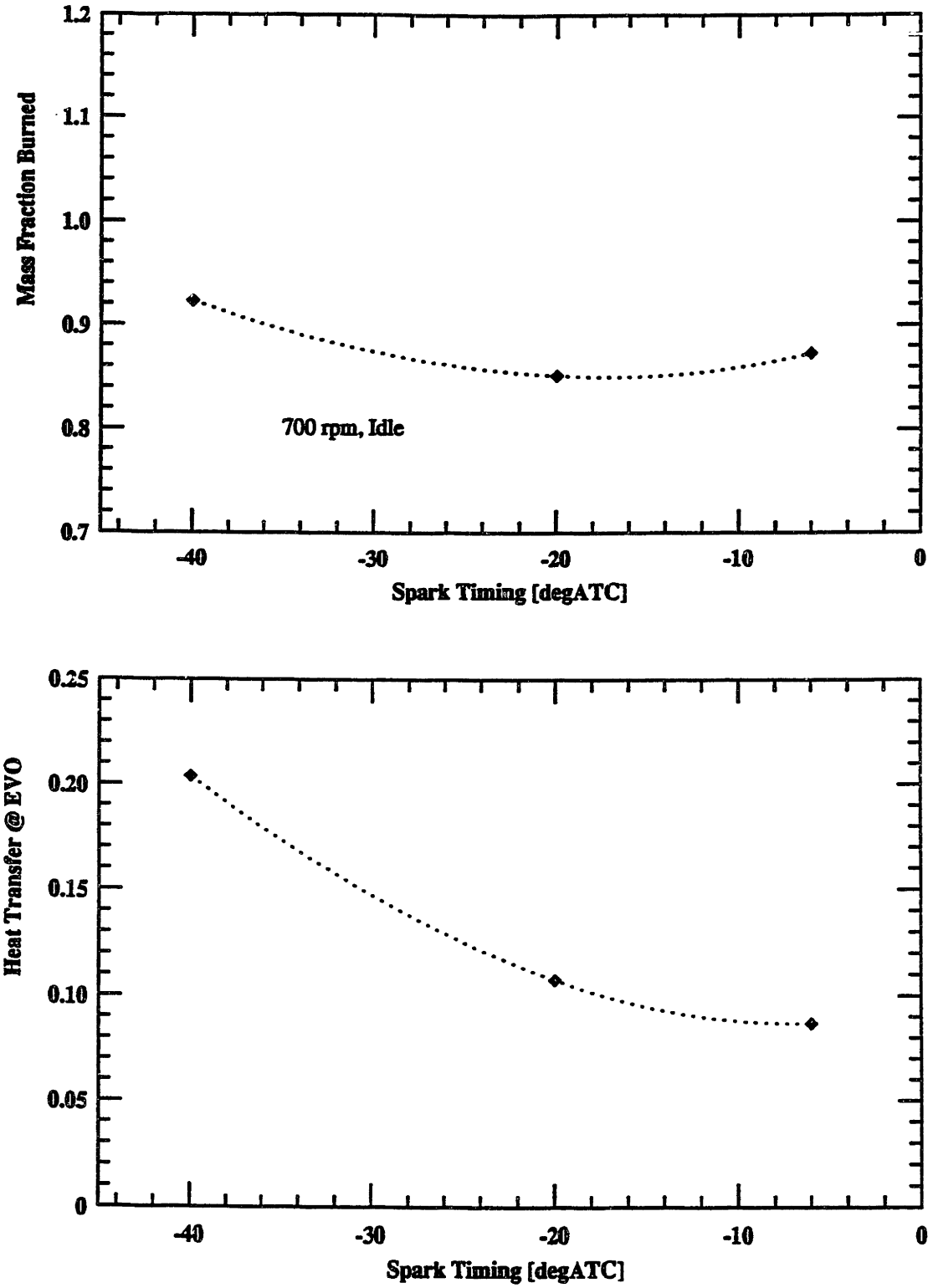

Figure 5-4. Result of Chrysler idle conditions as a function of spark-timing.

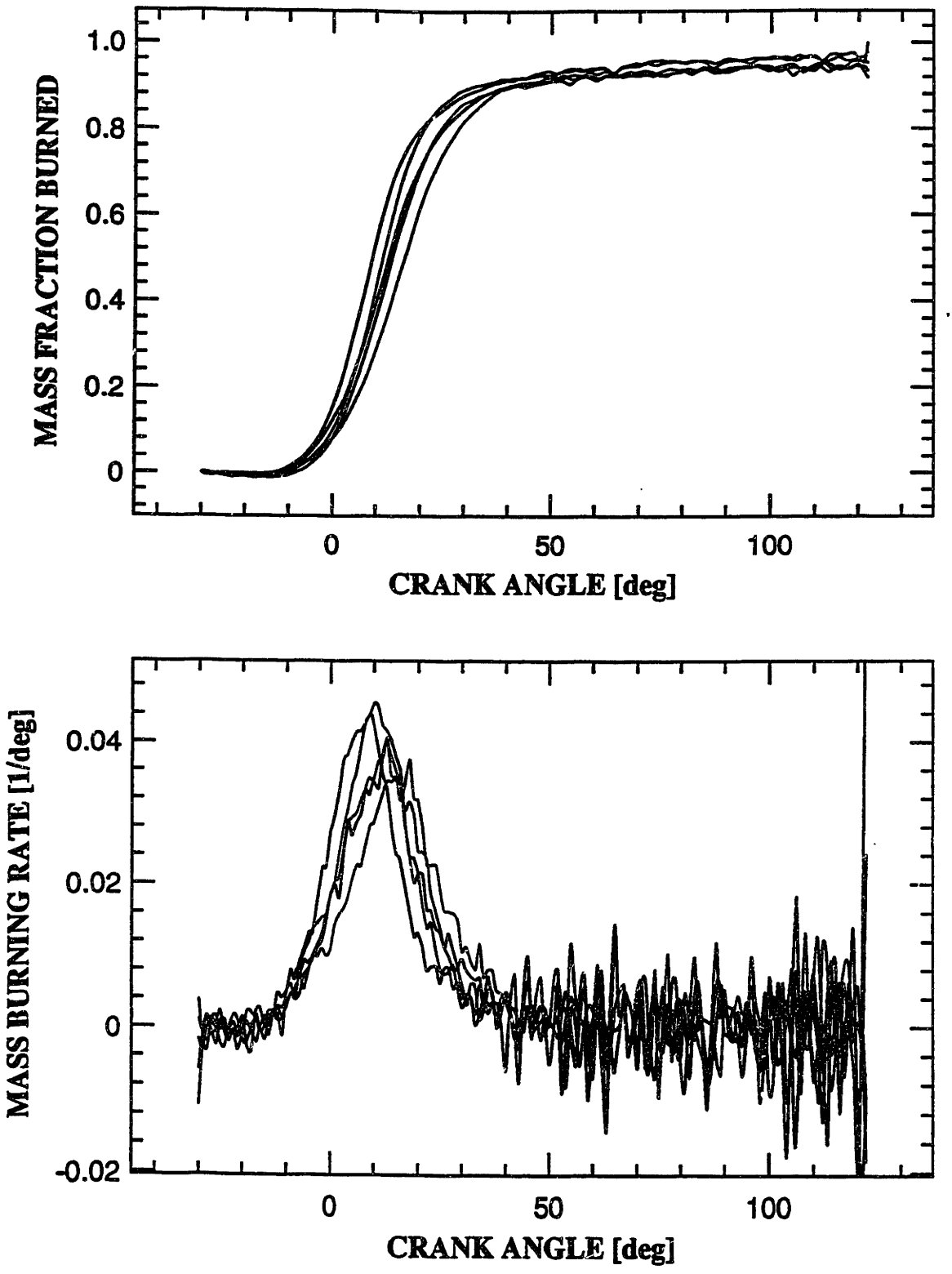

Figure 5-5. Multiple-cycle burn rate plot for part-load data 6_1-1, P_{in}=0.4 bar, 1600 rpm, ϕ=1.0, 30^{o}BTC spark, indolene.

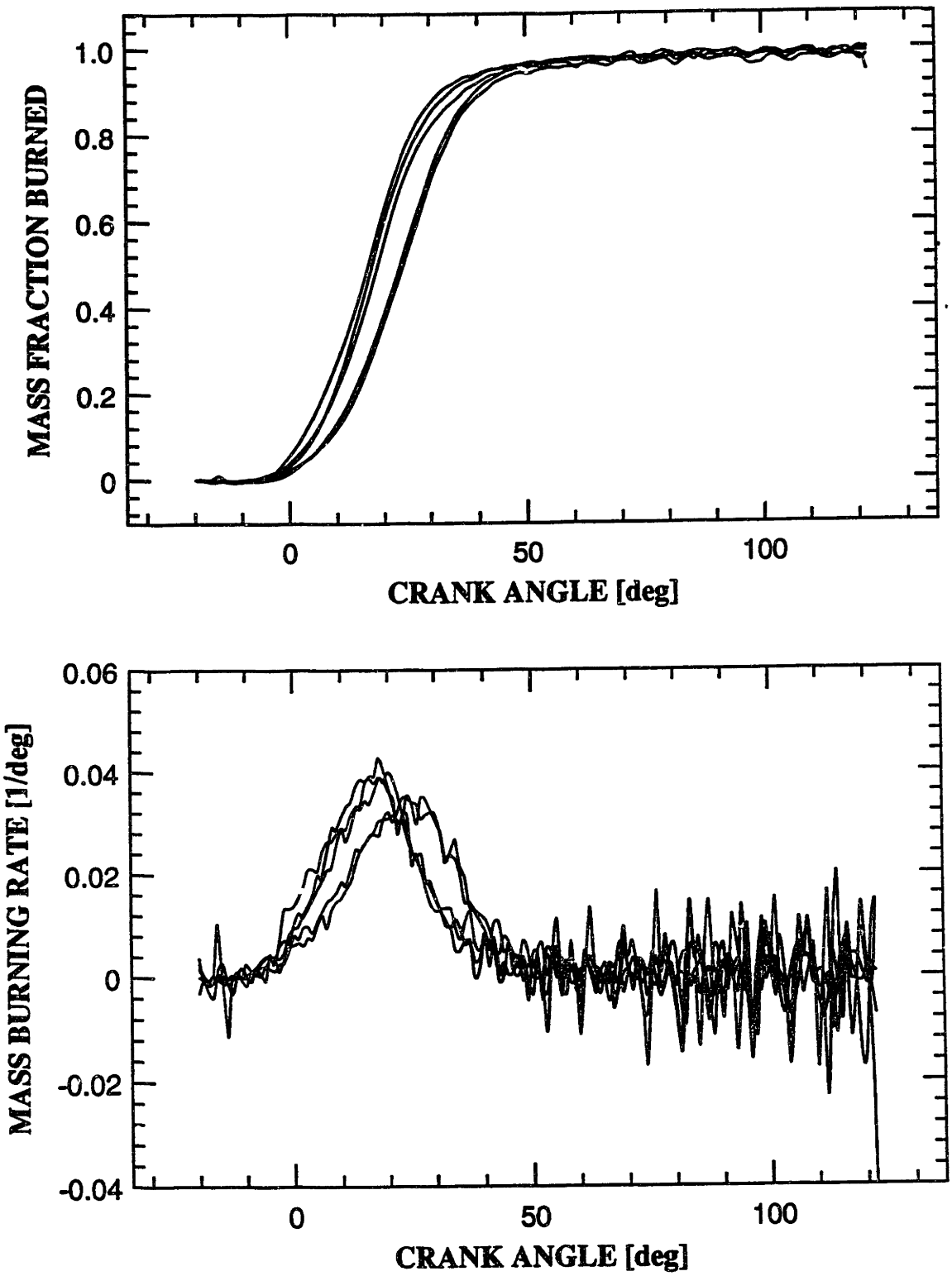

Figure 5-6. Multiple-cycle burn rate plot for part-load data 6_3-1, P_{in}=0.4 bar, 1600 rpm, ϕ=1.0, 20^{o}BTC spark, indolene.

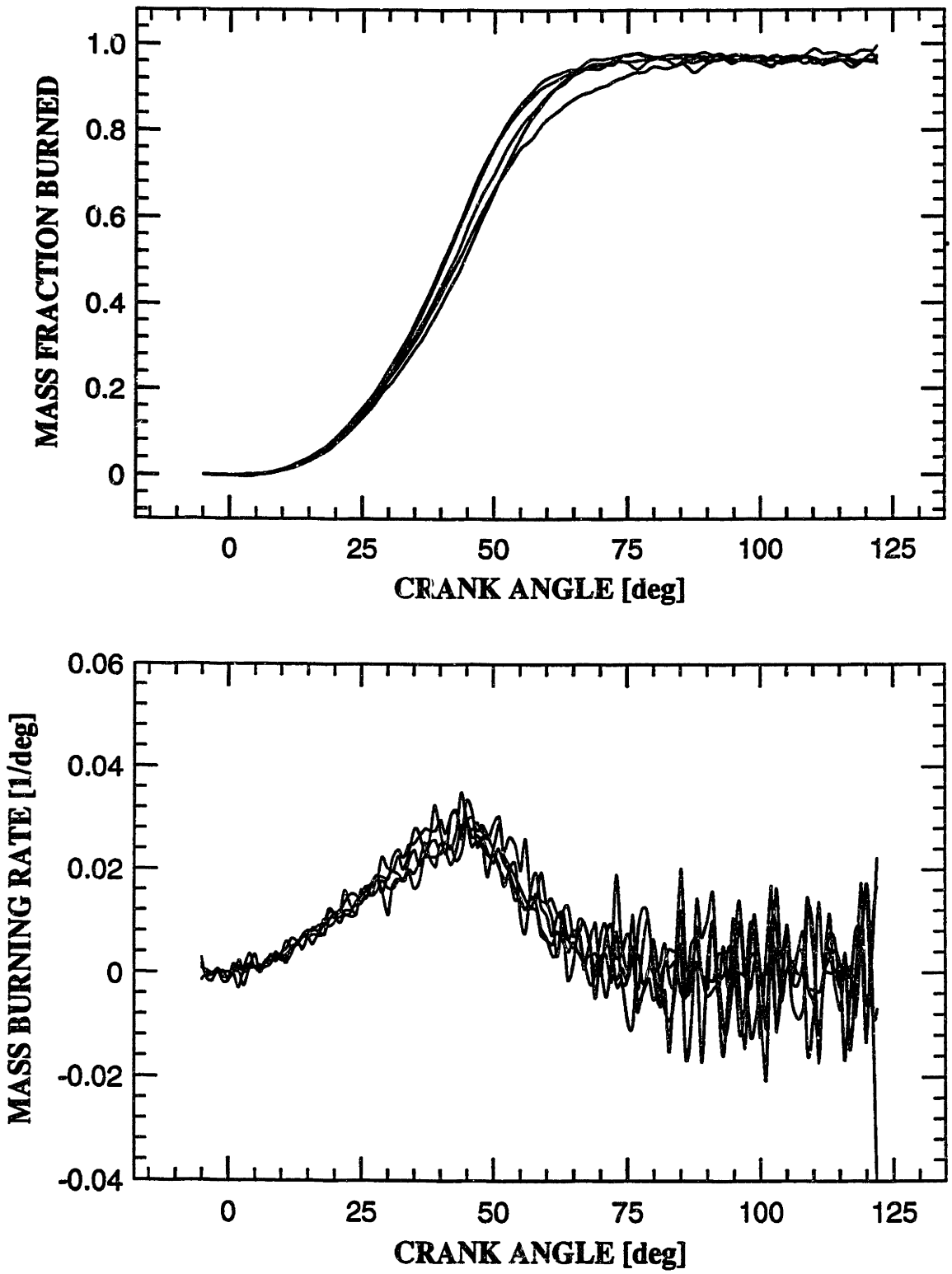

Figure 5-7. Multiple-cycle burn rate plot for part-load data 6_4-1, P_{in}=0.5 bar, 1600 rpm, ϕ=1.0, 5^{o}BTC spark, indolene.

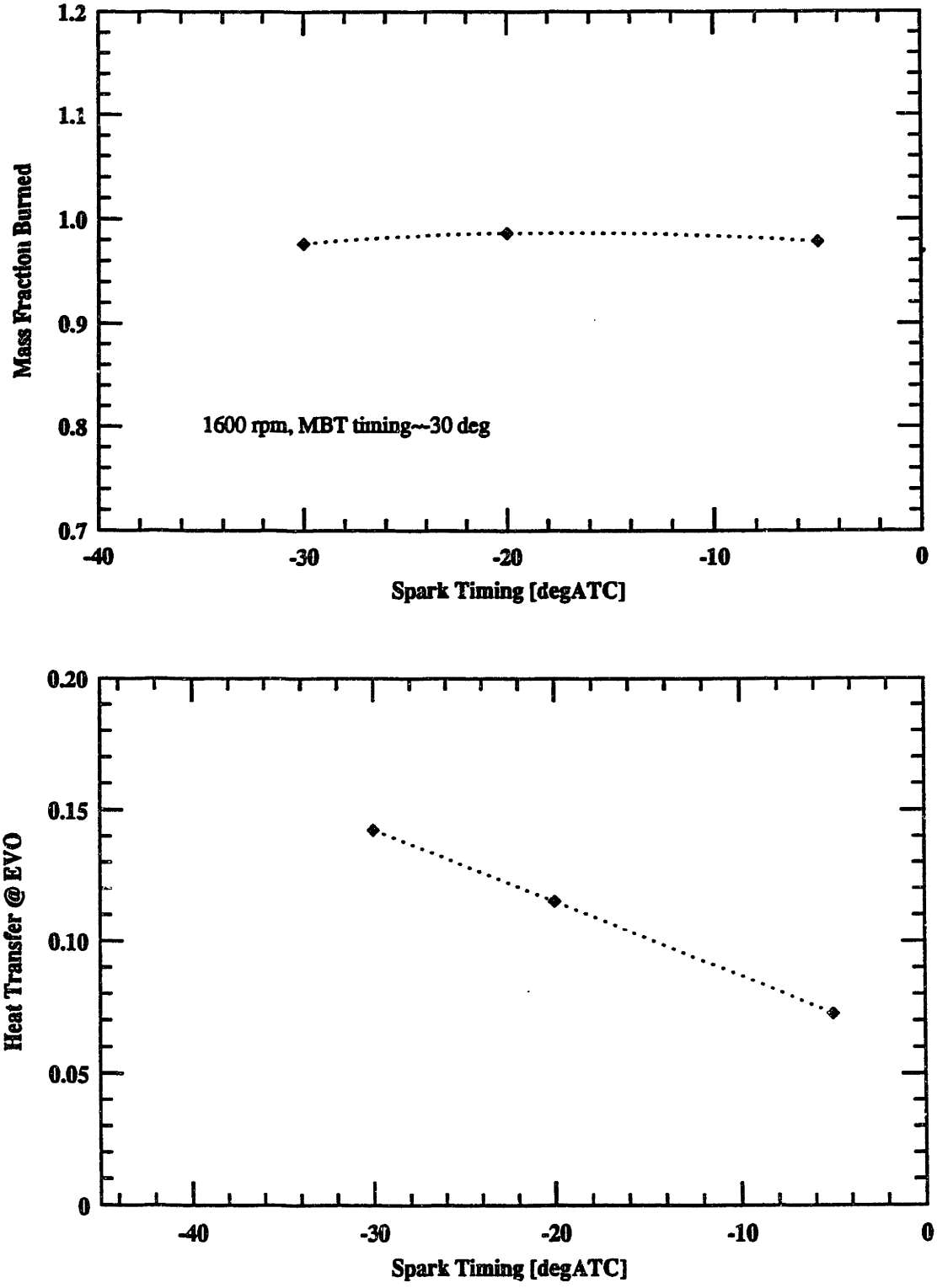

Figure 5-8. Result of Chrysler part-load conditions as a function of spark-timing.

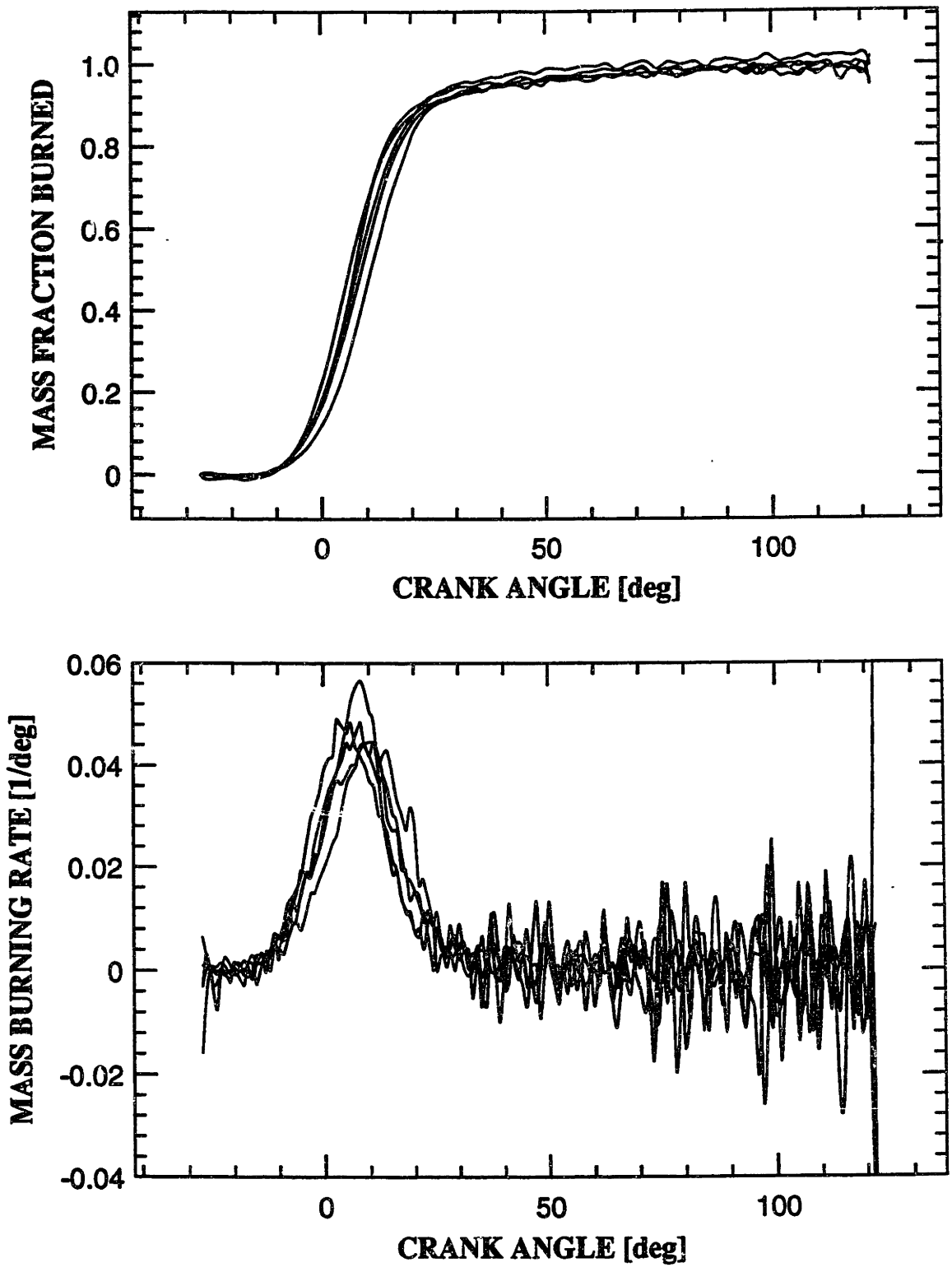

Figure 5-9. Multiple-cycle burn rate plot for part-load data 6_5-1, P_{in}=0.7 bar, 1600 rpm, ϕ=1.0, 27°BTC spark, indolene.

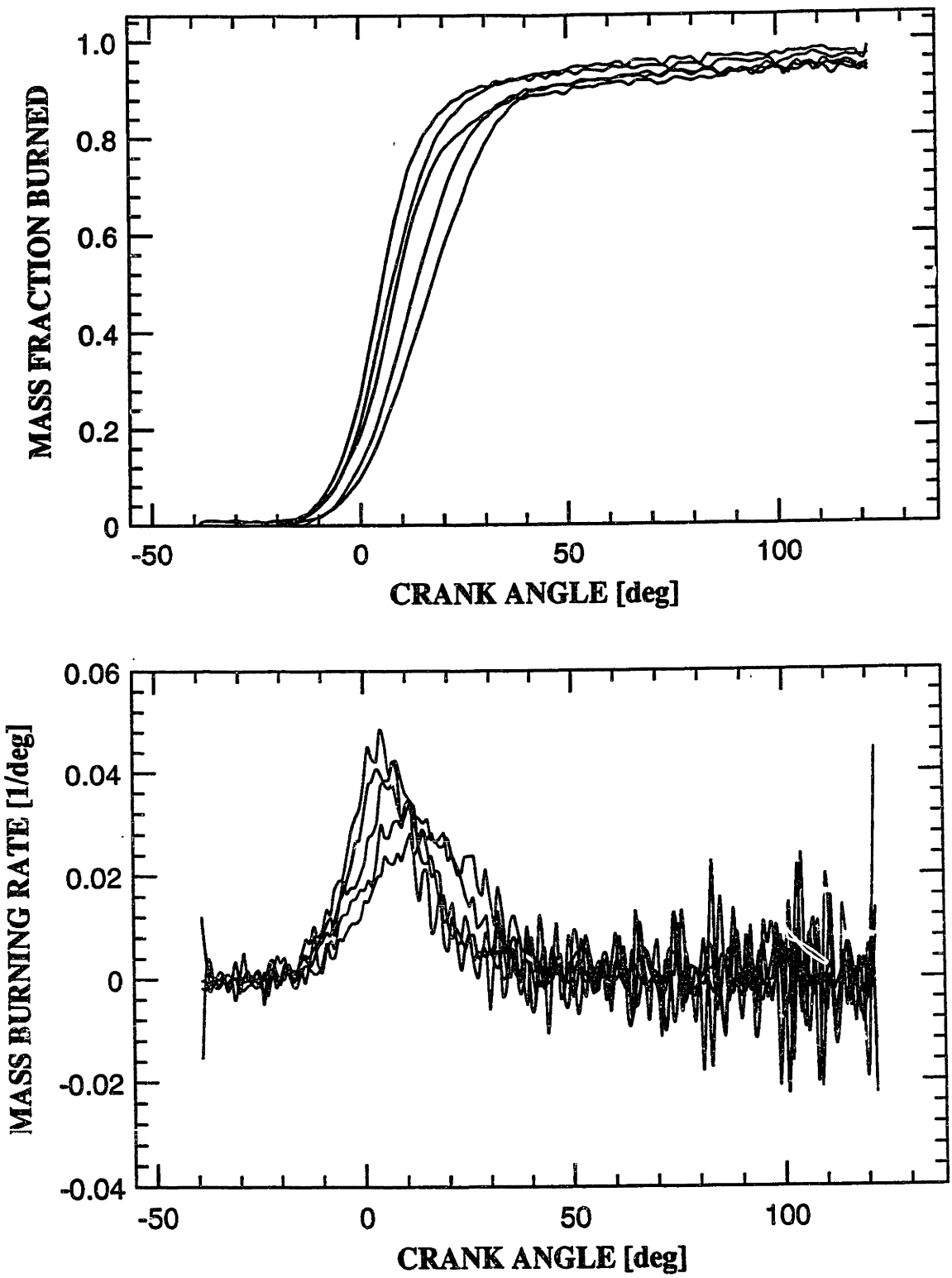

Figure 5-10. Multiple-cycle burn rate plot for part-load data 6_2-1, P_{in}=0.4 bar, 3200 rpm, ϕ=1.0, 39^{o}BTC spark, indolene.

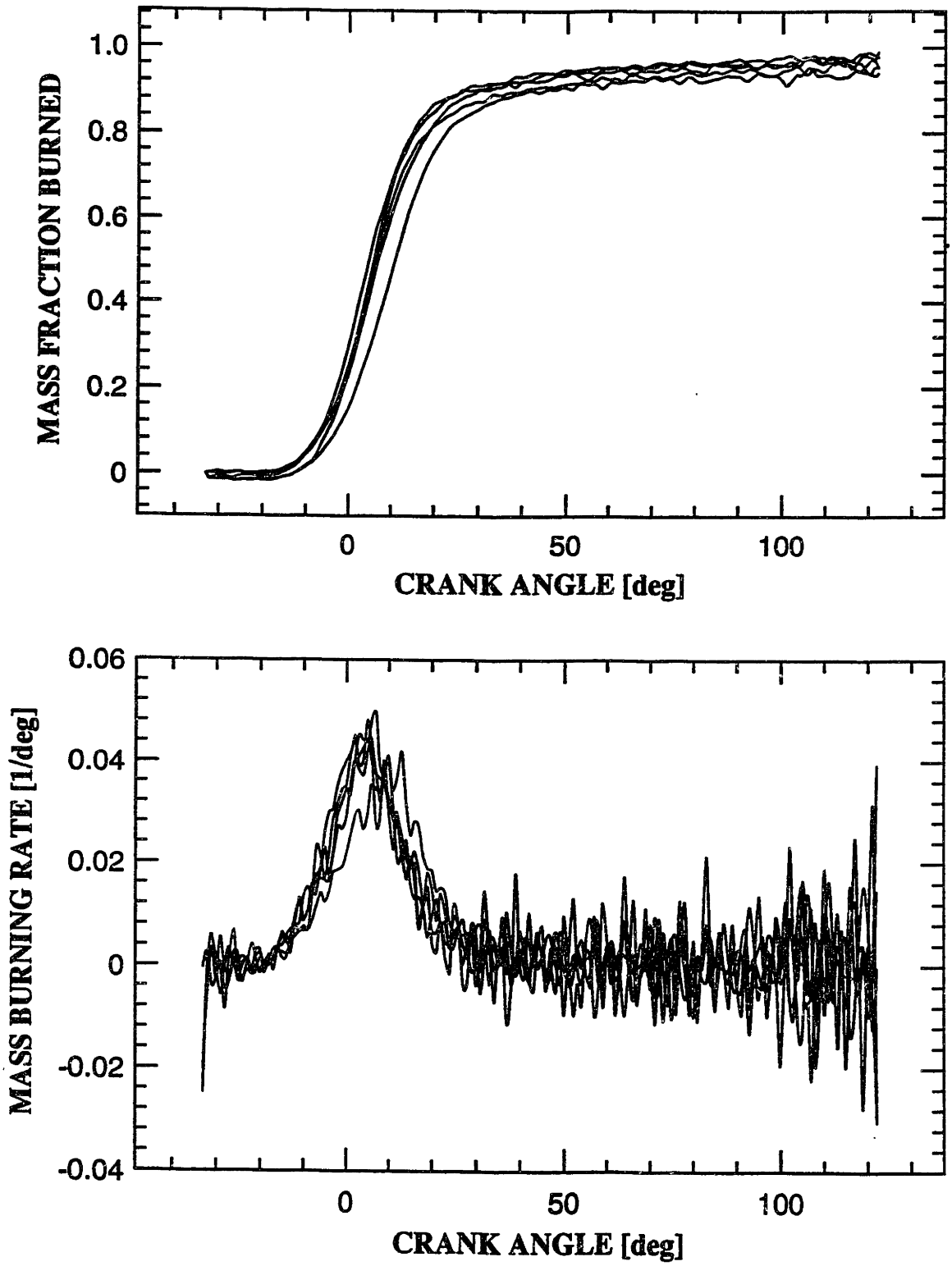

Figure 5-11. Multiple-cycle burn rate plot for part-load data 6_6-1, P_{in}=0.6 bar, 3200 rpm, ϕ=1.0, 33°BTC spark, indolene.

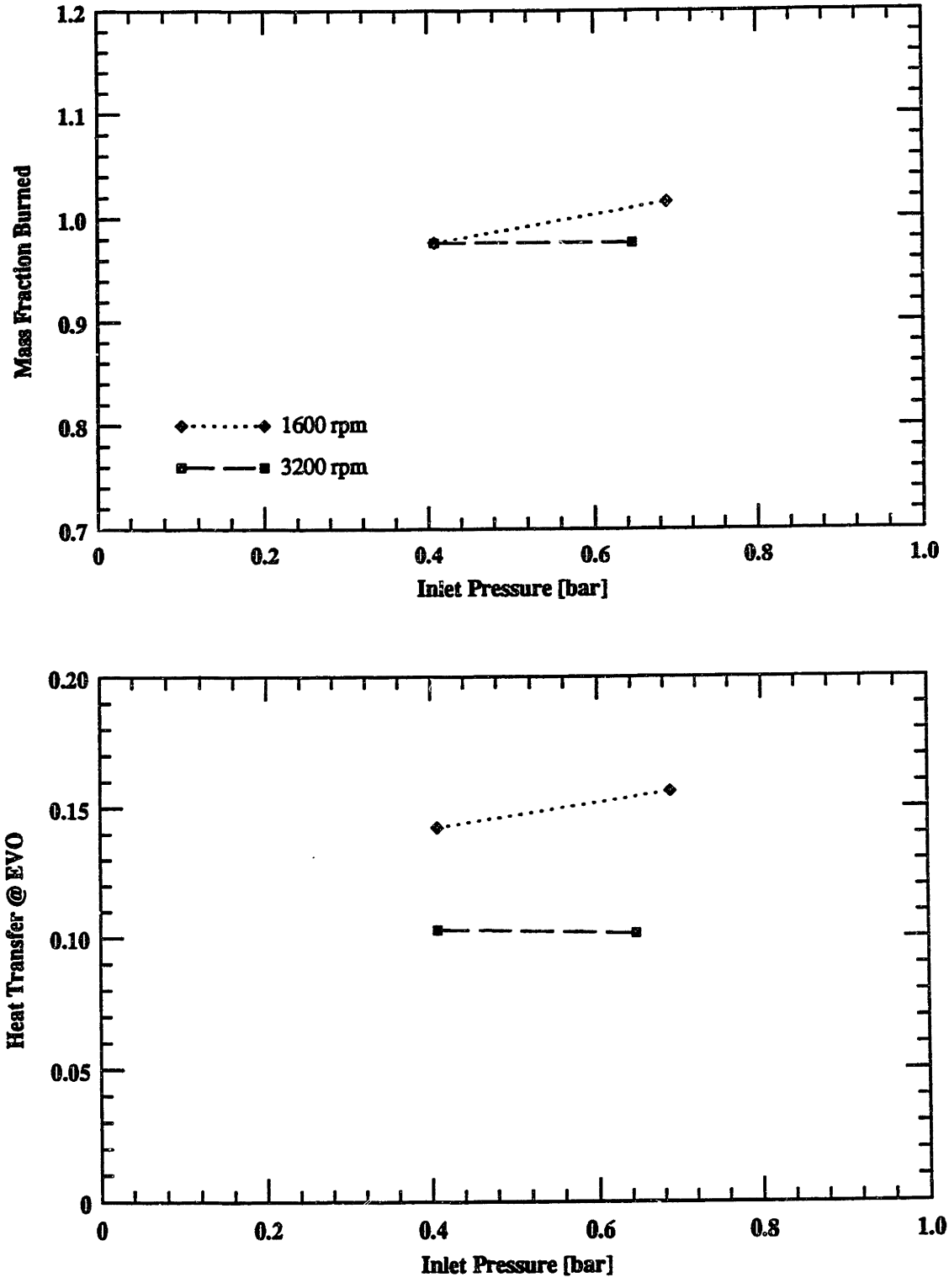

Figure 5-12. Result of Chrysler part-load conditions as a function of load.

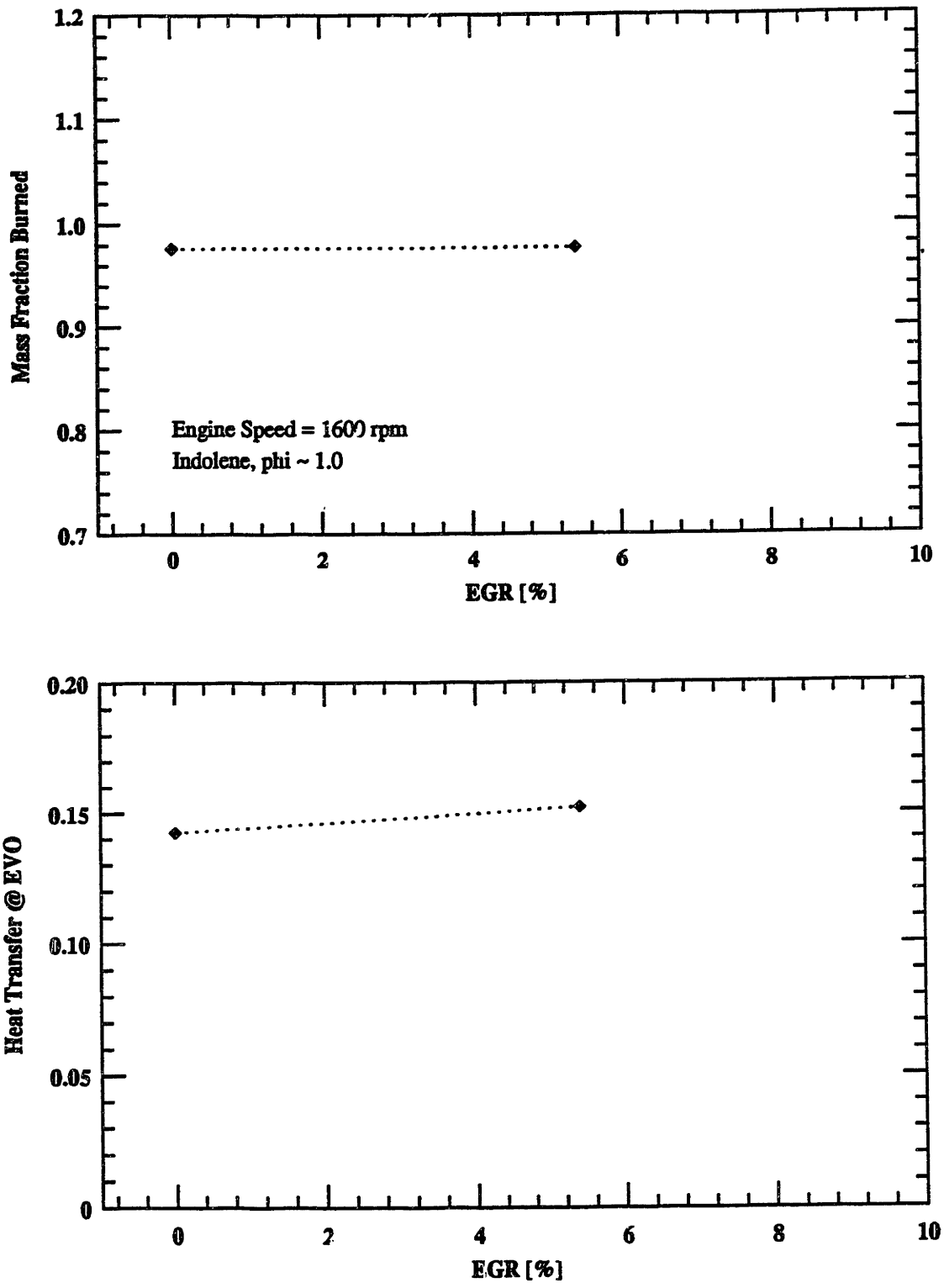

Figure 5-13. Result of Chrysler part-load conditions as a function of EGR%.

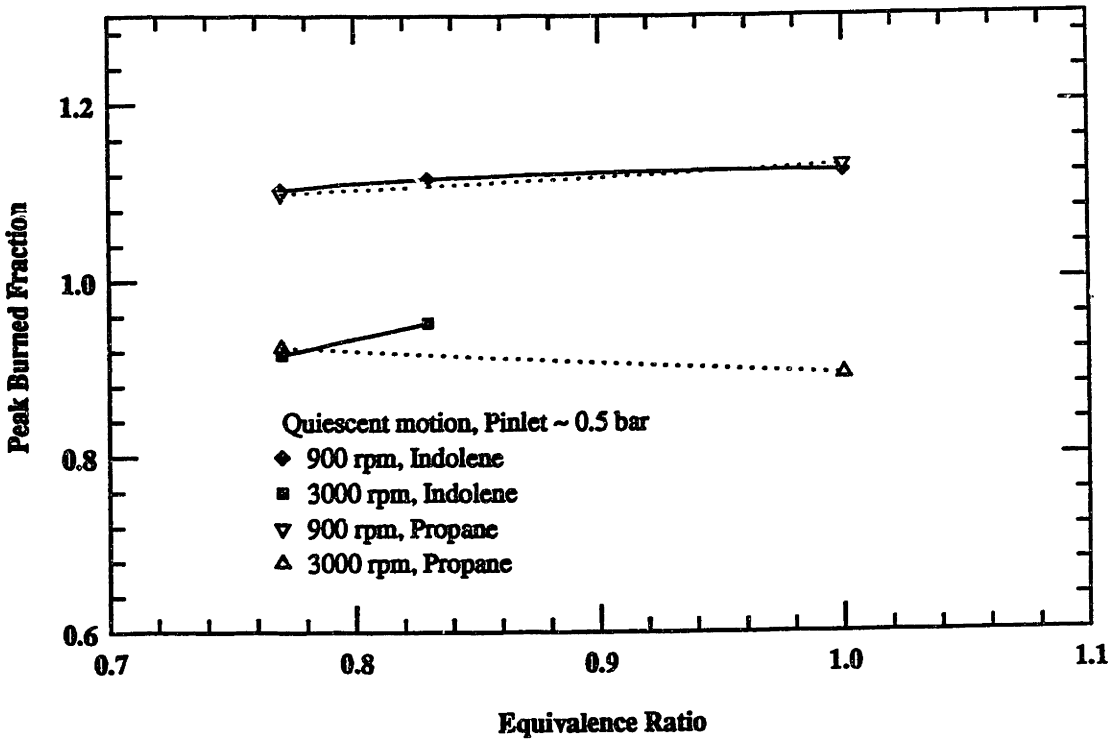

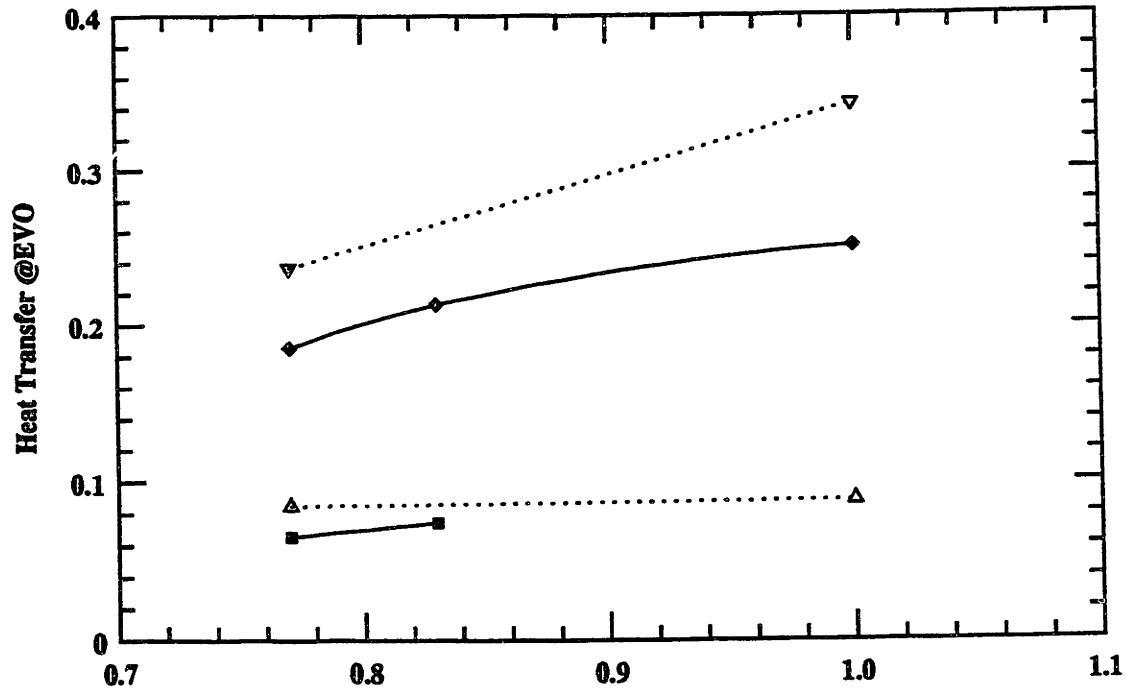

Figure 5-14. Result of Sloan Lab. part-load conditions as a function of equivalence ratio.

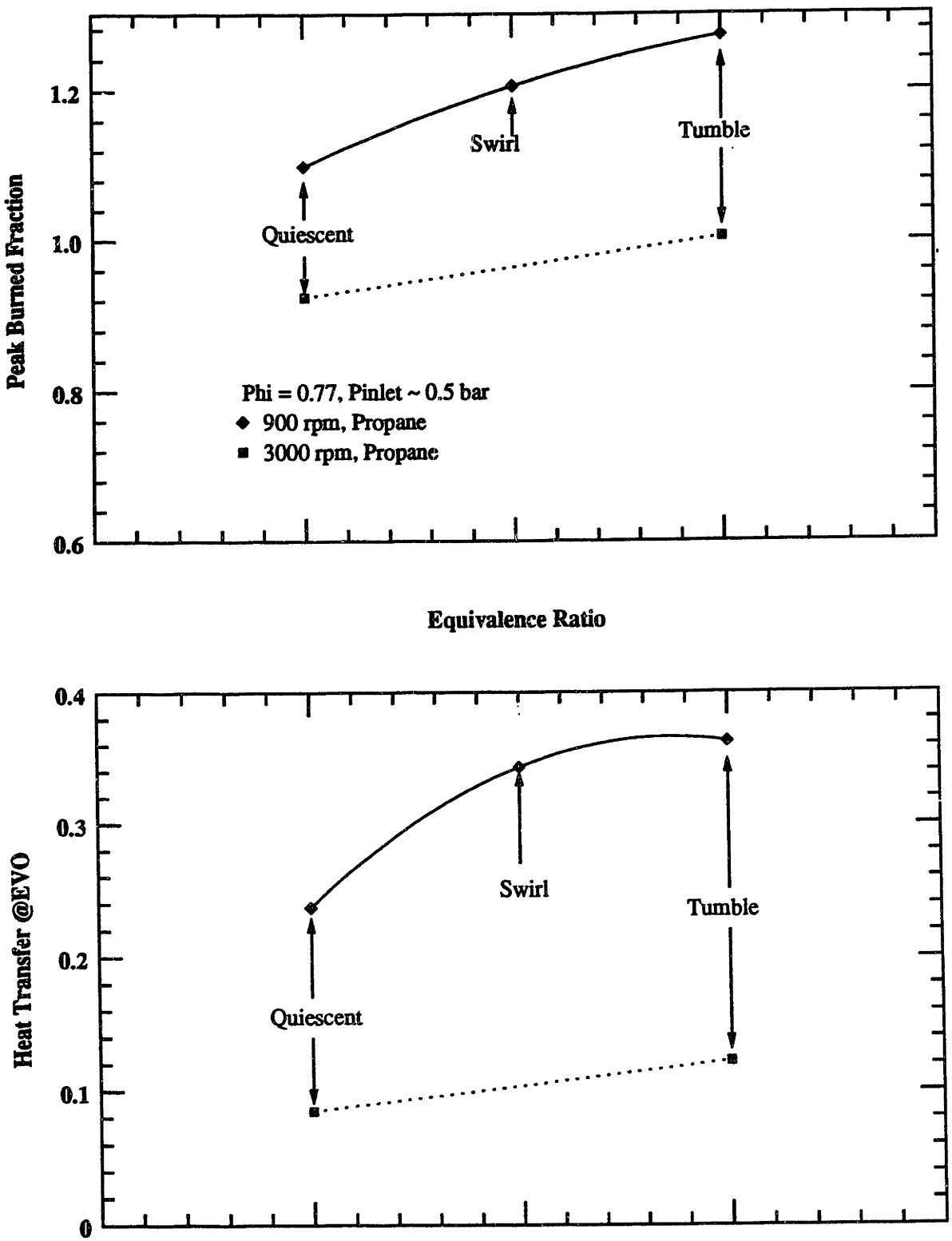

Figure 5-15. Result of Sloan Lab. part-load conditions as a function of charge motion.

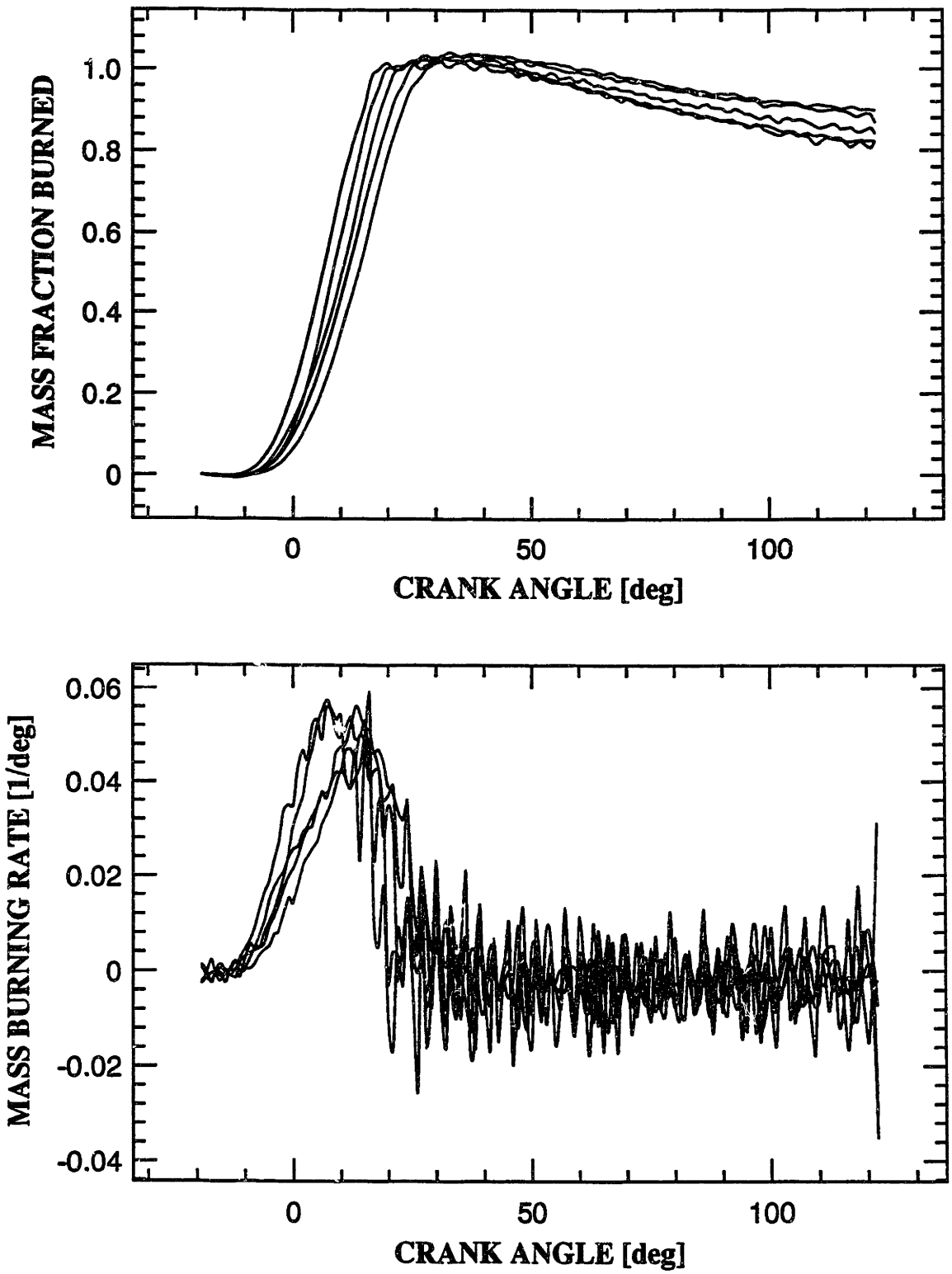

Figure 5-17. Multiple-cycle burn rate plot for part-load data 41_51, P_{in}=1.0 bar, 2800 rpm, ϕ=1.2, 19°BTC spark, indolene.

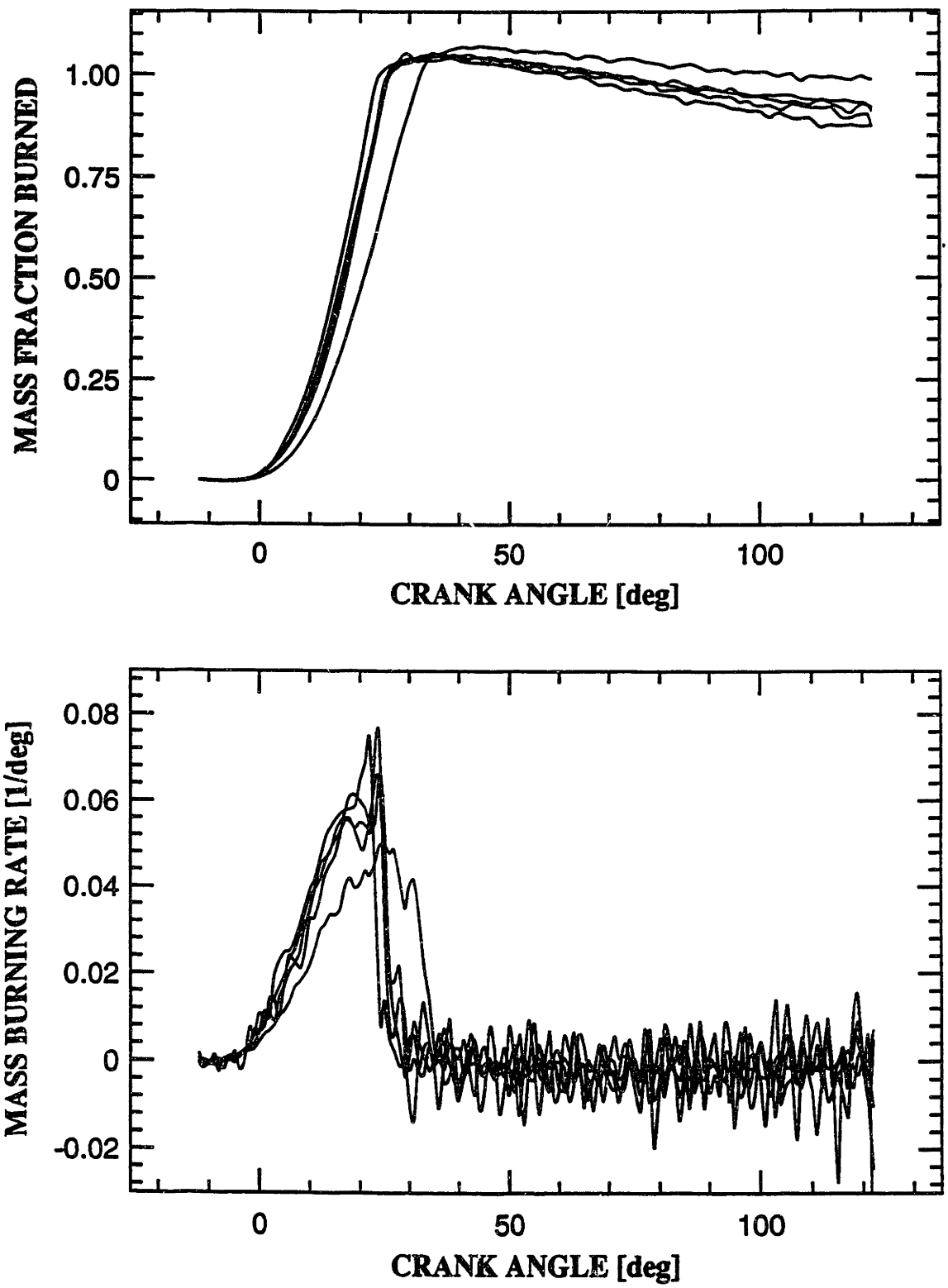

Figure 5-16. Multiple-cycle burn rate plot for part-load data 41_11, P_{in}=1.0 bar, 1200 rpm, ϕ=1.2, 12^{o}BTC spark, indolene.

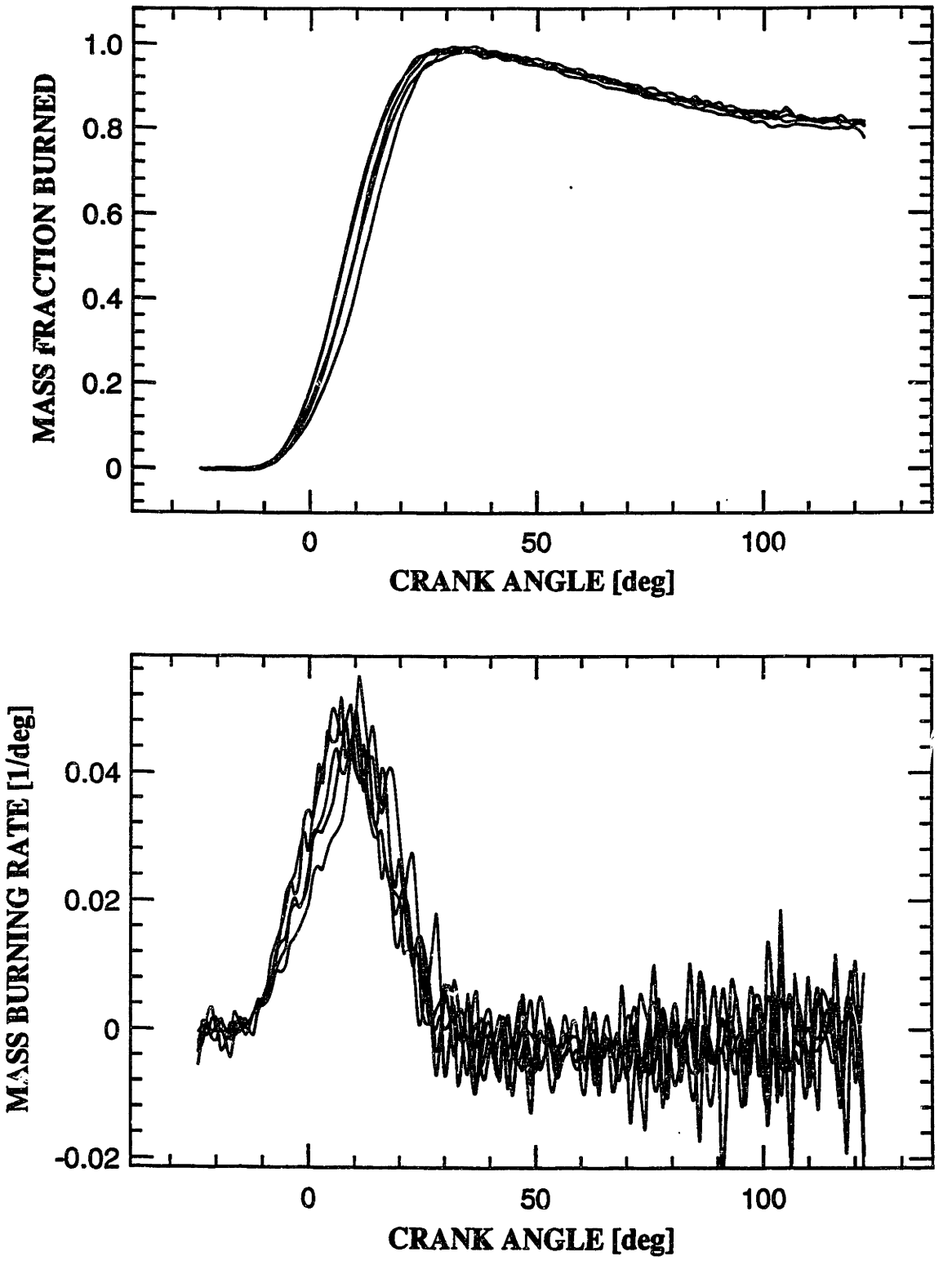

Figure 5-18. Multiple-cycle burn rate plot for part-load data 41_91, P_{in}=1.0 bar, 4400 rpm, ϕ=1.2, 24°BTC spark, indolene.

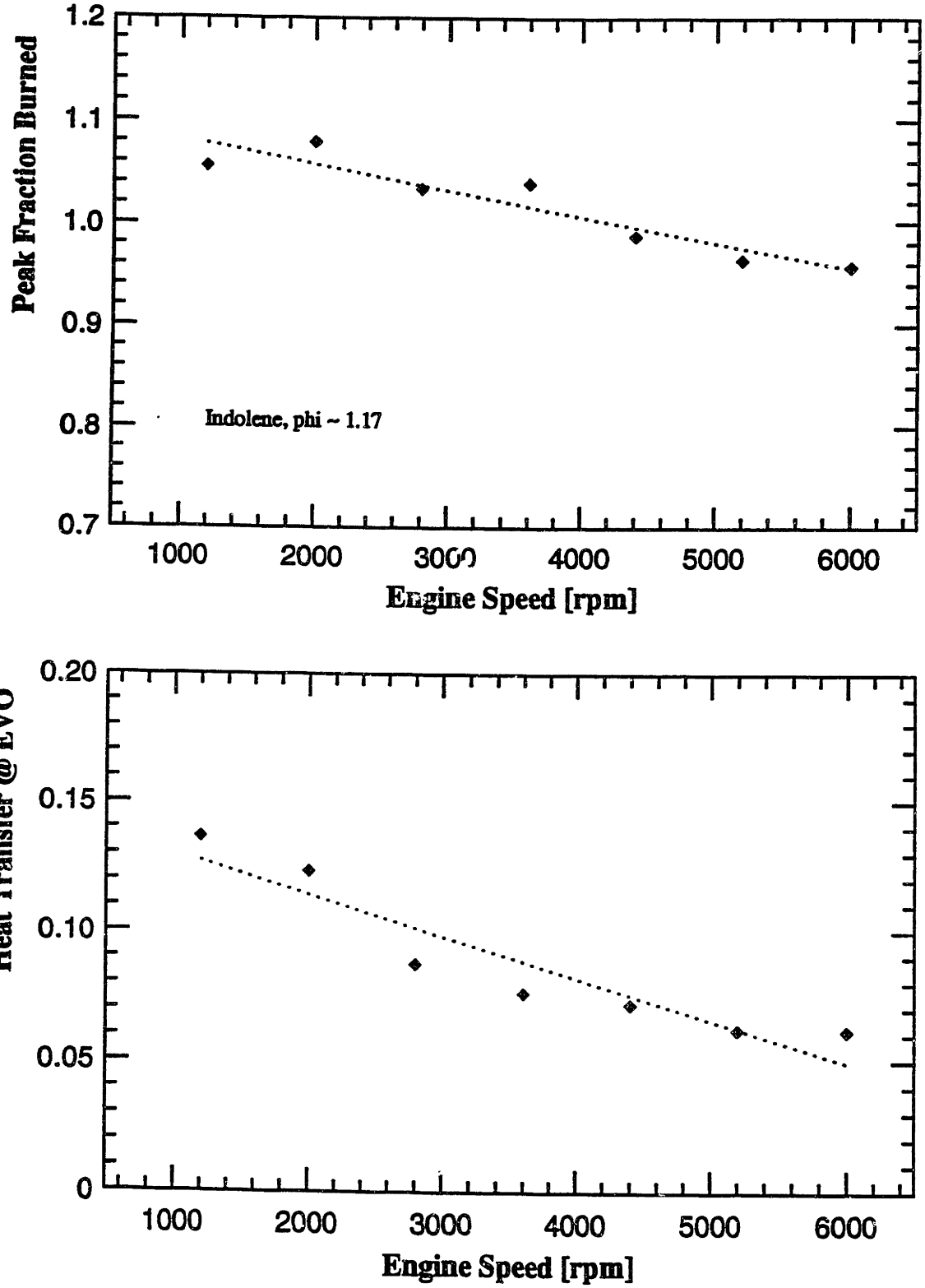

Figure 5-19. Result of Chrysler WOT conditions as a function of speed.

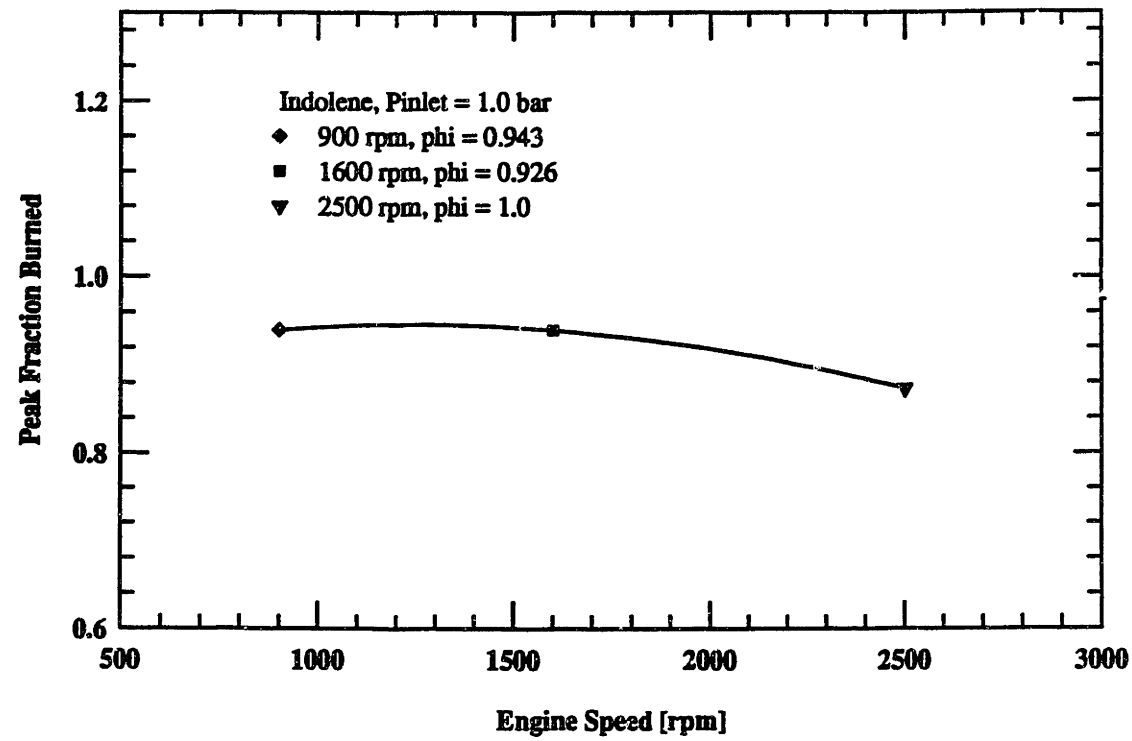

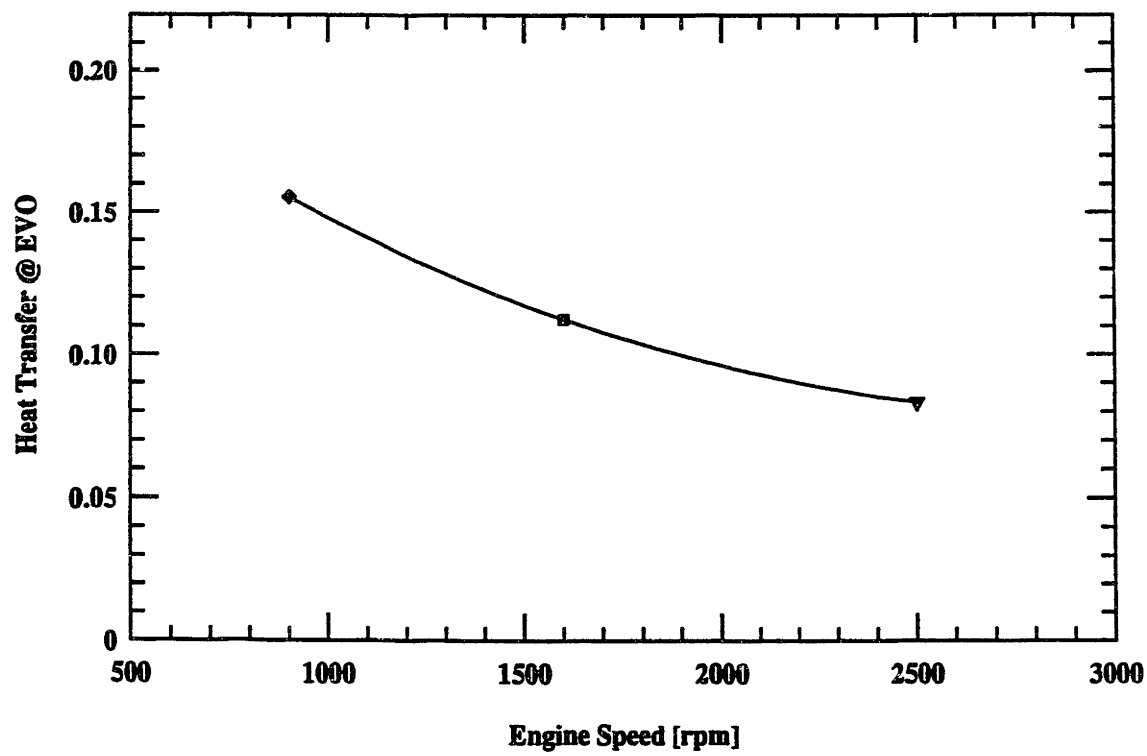

Figure 5-20. Result of Sloan Lab. WOT conditions as a function of speed.

REFERENCES

1. Rassweiler, G. M., and Withrow, L., "*Motion Pictures of Engine Flames Correlated with Pressure Cards*," SAE paper 670931, 1967.

2. Gatowski, J. A., Balles, E. N., Chun, K. M., Nelson, F. E., Ekchian, J. A., and Heywood, J. B., "*Heat Release Analysis of Engine Pressure Data*," SAE paper 841359, 1984.

3. Chun, K. M., and Heywood, J. B., "*Estimating Heat-Release and Mass-of-Mixture Burned from Spark-Ignition Engine Pressure Data*," Combust. Sci. Technol. vol. 54, pp. 133-144, 1987.

4. Sztenderowicz, M. L., and Heywood, J. B., "*Cycle-to-Cycle IMEP Fluctuations in a Stoichiometrically-Fueled S. I. Engine at Low Speed and Load*," SAE paper 902143, 1990.

5. Woschni, G., "*Universally Applicable Equation for the Instantaneous Heat Transfer Coefficient in the Internal Combustion Engine*," SAE paper 670931, 1967.

6. Kaplan, J. A., "*Modeling the Spark Ignition Engine Warm-up Process to Predict Component Temperatures*," M.S. thesis, Department of Mechanical Engineering, MIT, 1990.

7. Fox, J. W., "*Effects of Fuel Injection Strategy on HC Emissions During SI Engine Start-Up*," M.S. Thesis, Department of Mechanical Engineering, MIT 1992.

8. Poulos, S. G., and Heywood, J. B., "*The Effect of Chamber Geometry on Spark-Ignition Engine*," SAE paper 830587, 1983.

9. Min, K. D., Research Data and Notes. Department of Mechanical Engineering, MIT, 1992.

10. Heywood, J. B., Internal Combustion Engine Fundamentals, McGraw-Hill, Inc., New York, 1988.

11. Grimm, B. M., and Johnson, R. T., "*Review of Simple Heat Release Computations*," SAE paper 900445, 1990.

12. Amann, C. A., "*Cylinder-Pressure Measurement and Its Use in Engine Research*," SAE paper 852067, 1985.

13. Shayler, P. J., Wiseman, M. W., and Ma, T., "*Improving the Determination of Mass Fraction Burnt*," SAE paper 900351, 1990.

14. Ramos, J. I., Internal Combustion Engine Modeling, Hemisphere, New York, 1989.

15. Automotive Handbook, 2nd. edition, Bosch, Stuttgart, 1986.

16. Lancaster, D. R., Krieger, R. B., and Lienesch, J. H., "*Measurement and Analysis of Engine Pressure Data*," SAE paper 750026, 1975.

17. Hobenberg, G. F., "*Advanced Approaches for Heat Transfer Calculations*," SAE paper 790825, SAE Trans., vol. 88, 1979.